MAREES TERRESTRES

BULLETIN D'INFORMATIONS

1 1 6

31 JUILLET 1993

Association Internationale de Géodésie

Commission Permanente des Marées Terrestres

Editeur Prof. Paul MELCHIOR
Observatoire Royal de Belgique
Avenue Circulaire 3
1180 Bruxelles

BIM 116

31 juillet 1993

Special Issue

Meeting of the three Working Groups of the Permanent Commission on Earth Tides

Bonn, october 1992

Part II

Table des matières

Study of the Extensometric Records of the Pannonian Basin in the Non-Tidal Frequency Domain.

Varga T.
Eötvös Lorand Geophysical Institute of Hungary
Budapest

Latynina L.A.
Institute of the Physics of the Earth
Russian Academy of Sciences
Moscow

Brimich L.
Geophysical Institute of the
Slovak Academy of Science
Bratislava

Mentes GY., Katona GY, Varga P.
Geodetic and Geophysical Research Institute
of the Hungarian Academy of Sciences
Sopron

Introduction

It is usually supposed that local observations of the recent crustal movements, like the strainmeter observations suffer in their interpretation from local influences (cavity and topography effects, influence of hydrological and meteorological processes) and it is not clear yet whether the non-tidal part of the extensometer records — the "drift" of the instruments — has some geological signicance or they are determined by instrumental effects alone combined with the influence of very local effects of minor interest.A network of extensometers (consisting at present of five stations in three countries) (Fig.1) has been set up in the Pannonian Basin to investigate local measurements of relative deformations in monitoring of the recent tectonical activity of a known tectonic unit.

Description of the extensometer stations

The extensometric stations of the studied region were mounted – expect Pécs – during the eighties and all of them are equipped with similar quartzglass-tube strainmeters, with the same calibration units. The instruments have either photoelectric (Beregovo, Vyhné) or capacitive (Budapest, Sopron, Pécs) sensor systems which allow a relative resolution of 10^{-10}. All stations are under the Earth surface at the depths of 40-50 m or deeper. Exception is Beregovo which operates at a distance 20 m from the surface. The diurnal temperature variations are less as 0.05C°, while the annual ones are less than 0.5C°.

As example the ground-plans of stations Budapest and Sopron are shown on Figs.2 and 3. The most important parameters of the equipments installed at different stations are listed in Table I. Two of the observatories (Beregovo and Budapest) are equipped with two extensometers (Beregovo I and II, Budapest I and II).

Table I does not contain the observatory operating in Pécs because it was mounted during 1991 and at the present time there are no records with lengths sufficient for the present study.

Wath concerns the geological circumstances of the stations Beregovo and Budapest are situated in the sedimentary part of the Pannonian Basin, while Vyhné

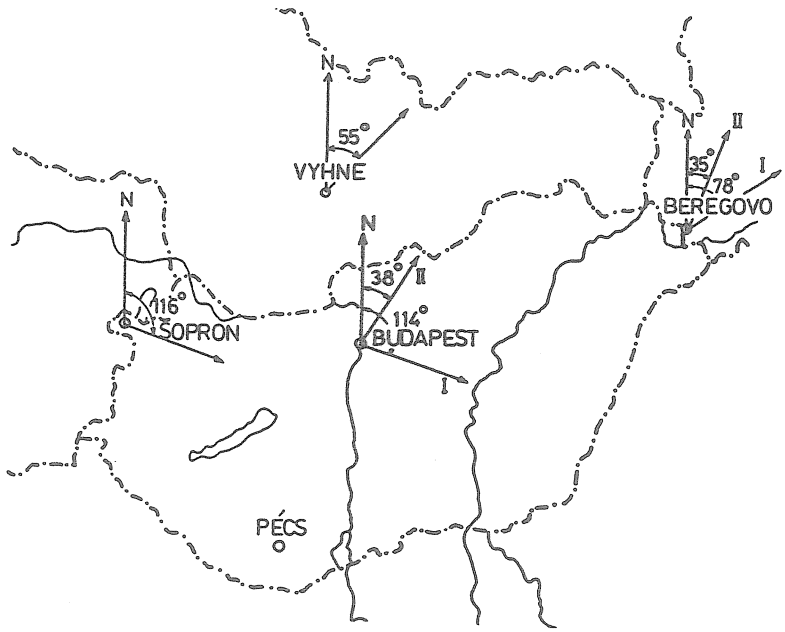

Figure 1. The extensometer network of the Pannonian Basin

Table I. Quartzglass-tube extensometers of the observatories of the Pannonian Basin used in present study

Instrument	Azimuth	Length of the instrument (in m)	Drift in micron·a^{-1} (and relative·a^{-1})		Reference
Beregovo I	73$^-$	27.5	2.05	($7.45\cdot10^{-8}$)	Latynina et al., 1992
Beregovo II	37$^-$	11.4	40.0	($3.51\cdot10^{-6}$)	Latynina et al., 1992
Vyhné	55$^-$	20.5	2.0	($1.05\cdot10^{-7}$)	Brimich et al., 1988
Budapest I	114$^-$	21.3	2.5	($1.17\cdot10^{-7}$)	Varga T. et al., 1991
Budapest II	38$^-$	13.8	30.0	($7.17\cdot10^{-6}$)	Varga T. et al., 1991
Sopron	116$^-$	22.0	1.0	($4.54\cdot10^{-8}$)	Mentes, 1991

and Sopron are close to the margin of the area and they are connected to the Alpic–Carpathian range. The Pannonian Basin itself is charecterised by a thin crust (25km), by a pronouncedly high heat flow [(80–130)mW·m^{-2}] and temperature gradient (less than 50C$^-$/km^{-1}) with low density upper mantle and with moderate seismicity in the inner part of the depression (one I$_-$=4 MSK intensity earthquake pro year, I$_-$=8 MSK intensity earthquakes occurs twice in the cen-

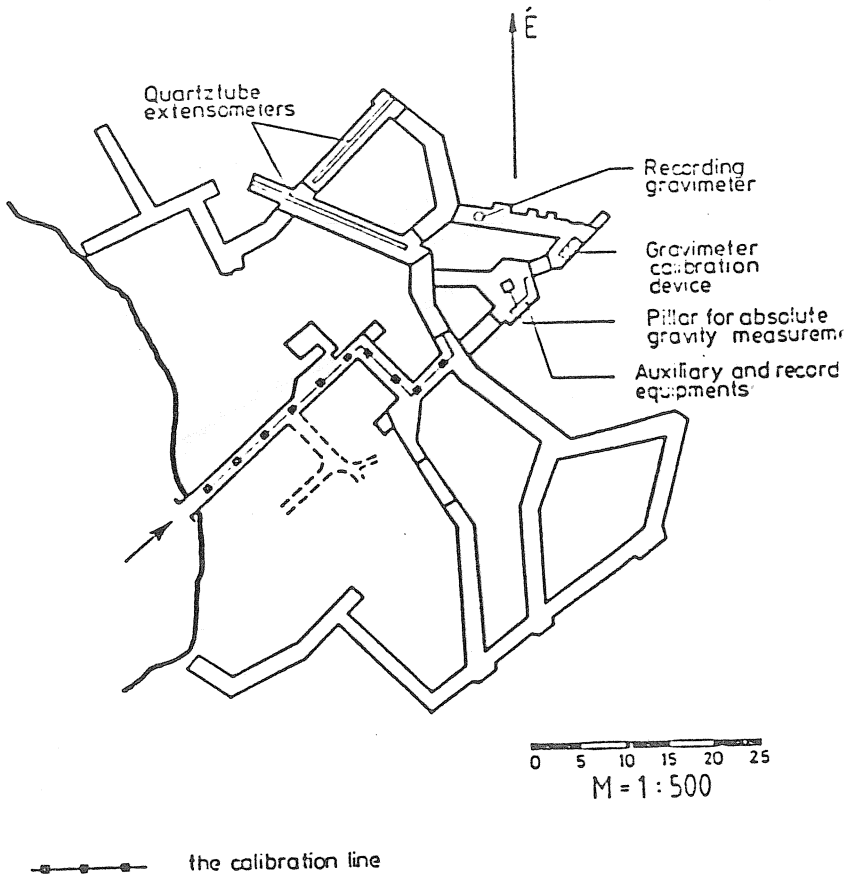

Figure 2. Scheme of the Budapest Observatoy

tury). It is worth mentioning that the earthquake activity of the margins is about 10 times higher than of the seismicity of the central parts.

Data used for the study of the records in non–tidal domain

As it was mentioned before the stations of the Pannonian Basin have been operated since the eighties. There was a considerable data set collected rist of all at stations Beregovo, Budapest and Vyhné. The deformation measurements in Sopron began at the end of the previous decade. To have a homogeneous data set for the present study recorded with the above mentioned similar equipments basicall the interval 1990–1991 was selected. During this time the recording conditions were stable and measurements at different stations were carried out under very similar conditions. The mean annual drift of 28 extensometers installed at different places of the world is $2.1 \cdot 10^{-6}$ a^{-1} (Varga P, 1984). In a comparison with this value it is concluded that two instruments (Table I) have rates similar to the mean annual values (Beregovo II, Budapest II) and four are characterized with significantly lower drift values (Beregovo I, Vyhné, Budapest I and Sopron).

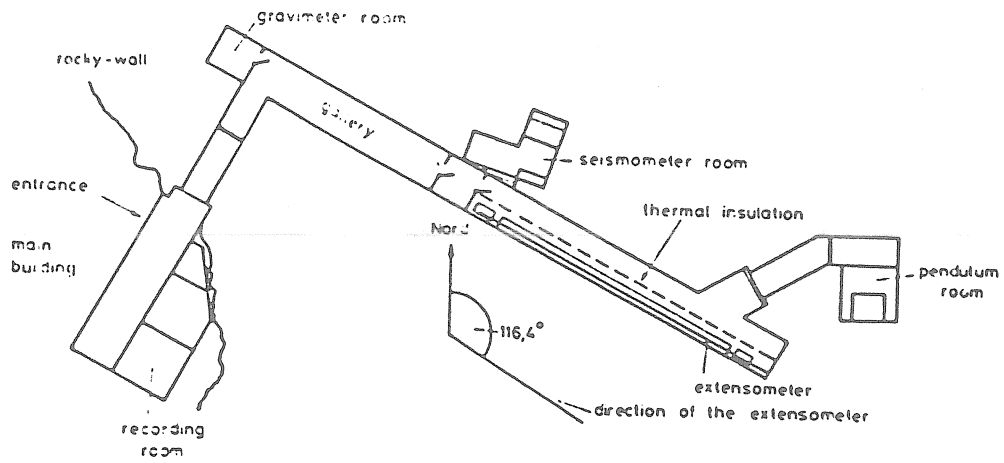

Figure 3. Scheme of the Sopron Observatoy

It should be mentioned that during the studied interval (1990–1991) there were no important changes in recording conditions. The temperature of the galleries, where the instruments were installed, was stable and remained constant. The calibration of the equipments was carried out regularly (usually once per day), and there were no significant changes in the scale of the observations.

Analysis of the recorded data based on the hourly values obtained with six extensometers (Table I) and expressed in micrometers. Because of technical reasons different data sets were at disposal in case of different stations. The two extensometers of the Budapest Observatory were in function without interruptions during the whole interval from 01.01.1991 till 31.12.1992. In Vyhné there was an interruption of records during 1991 and to have a similar amount of data to Beregovo and to Budapest records of this station were used from 10.07.1989 till 10.11.1991. Data recorded in Sopron appeared in course of 1990 unstable therefore the first half year 1992 was included into this investigation, too. Two questions are to be answered about extensometric data for the study of the tectonocs among others:

a) Are there similarities between the records of different stations after the removal of the lunisolar effect?

b) Does the non–tidal part of the record (i.e.the drift of the records) contain beside the instrumental effects external (e.g. geological, hydrological, meteorological) components too?

To answer these questions, the records of six extensometers, recording at four diffeent locations in two different frequency bands were investigated:

1. "Long period band" where periods than longer as 240 hours

2. "Short period band" where 48 hours $\leq T \leq$ 240 hours

"Long period band"

Temporal variations in this band are similar in case of stations in the Basin itself (Beregovo, Budapest) (Fig.4) and for the observatories which are nearer to the margin of the depression (Vyhné, Sopron) (Fig.5)

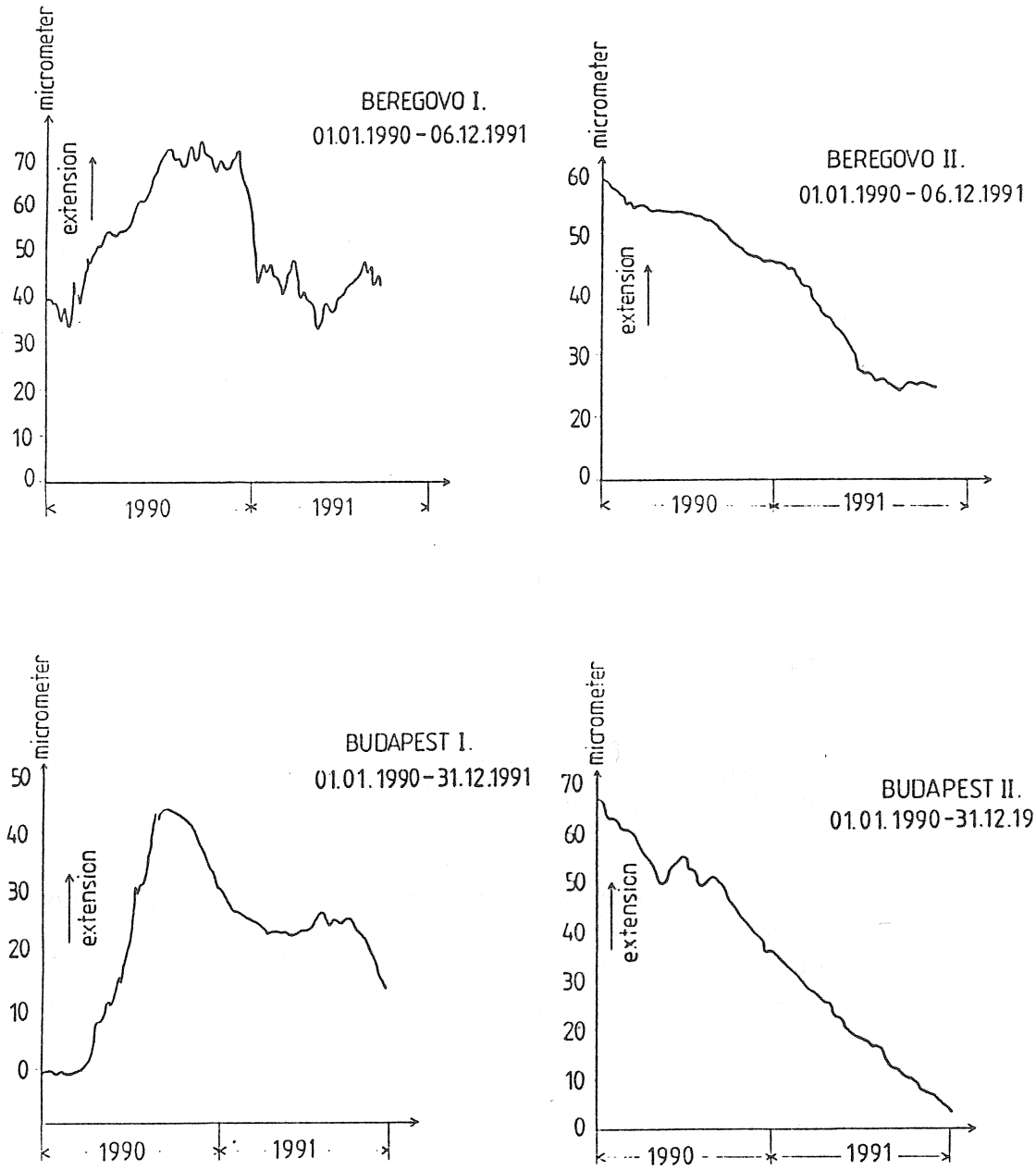

Figure 4. Long-term variations recorded at Beregovo and at Budapest Observatories

In case of Beregovo and Budapest the equuipments oriented nearly to north

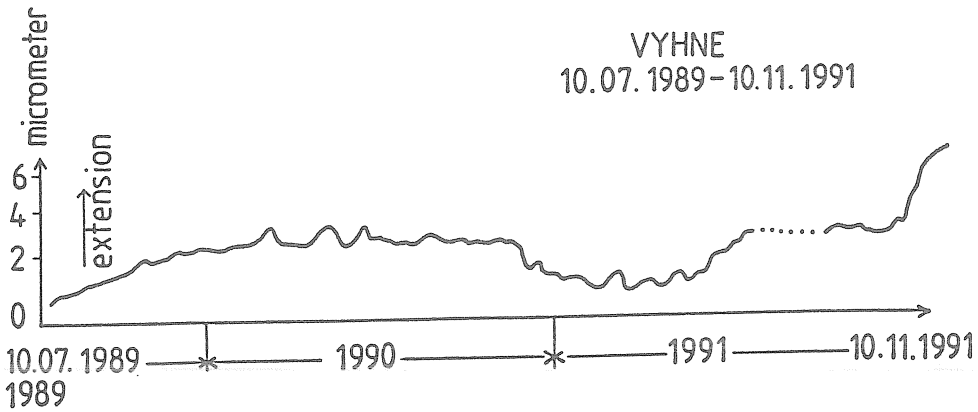

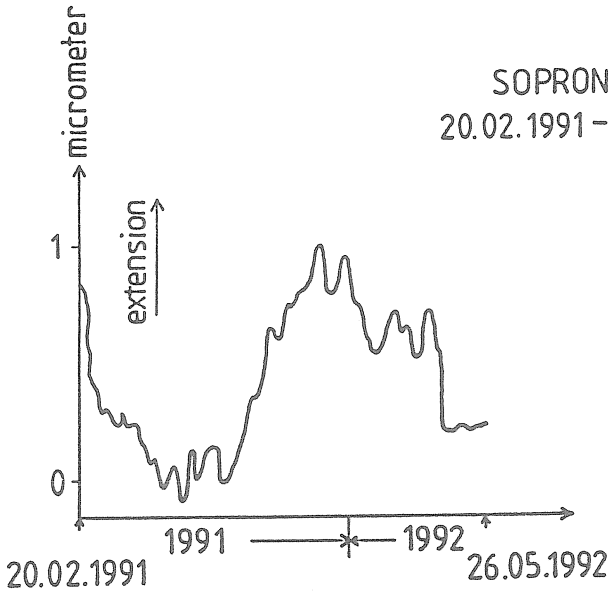

(BeregovoII, Budapest II) have an expressed compressional character. In this direction a compression of 20 micrometer/a ($1.9 \cdot 10^{-7}$/a) was detected at Beregovo, while in Budapest 35 micrometer/a ($2.5 \cdot 10^{-7}$/a). In other azimuths similarly to Vyhné and Sopron no long-term variations greater than as some micrometers were observed ($10^{-9}/a - 10^{-8}/a$) except the annual wave which has bigger amplitudes in the middle of the Pannonian Basin as near to its margins:

Beregovo	1.8	micrometer	=	$6.5 \cdot 10^{-8}$
Budapest	1.2	micrometer	=	$5.6 \cdot 10^{-8}$
Vyhné	~ 1	micrometer	=	$4.9 \cdot 10^{-9}$
Sopron	~ 1	micrometer	=	$4.5 \cdot 10^{-9}$

It is important to mention here that long-term features of extensometric records of 1990-1991 are valid for longer intervals, too. For example the different behaviour of two extensometers of Beregovo and Budapest in two different

azimuths has been reflected in the records since the middle of eighties. Nevertheless the stations were previously newer compared.

"Short period band"

The spectral features at this frequency band were compared for different monthly records first between the instruments installed at the same station (see two examples of this type of spectra on Fig.6) and afterwards the spectra of instruments installed at different sites (Fig.7).

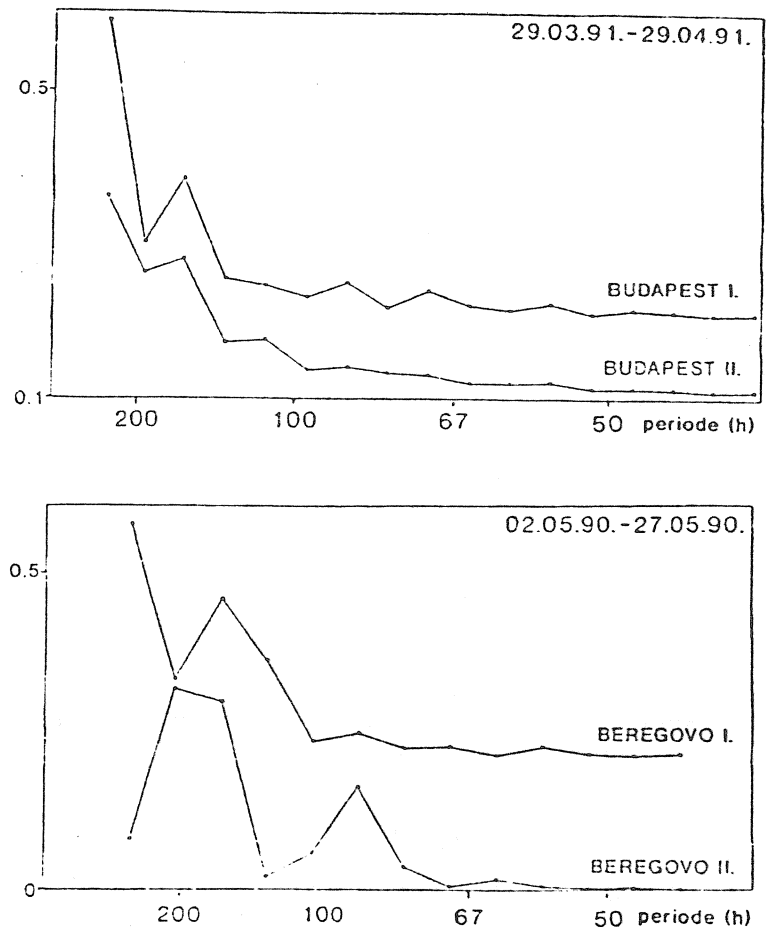

Figure 6. Short-term variations: a) results obtained at Budapest Observatory; b) results obtained at Beregovo Observatory

Spectra of the instuments of the same station but indifferent azimuths correlate much better the spectra of records obtained at different stations. Furthermore the similarity between Budapest and Vyhné is stronger between Budapest and Sopron or between Vyhné and Sopron.

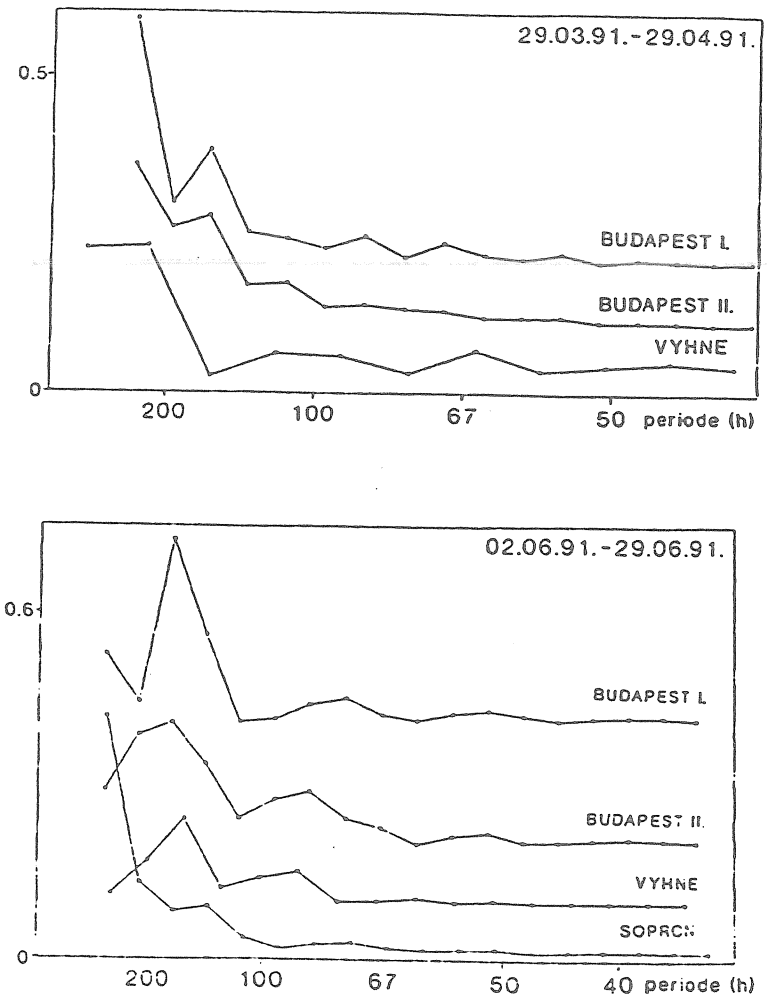

Figure 7. Comparison of short-term variations: a) between Budapest I, II and Vyhné; b) between Budapest I, II, Vyhné and Sopron

Conclusions

The use of extensometric data is usual in active tectonic areas (e.g. California, Middle Asia) to investigate recent crustal movements, tectonic activity and even for earthquake perediction (Groten, 1991). Every conclusion concerning recent geological activity must be done, howewer, with careful verification, because of the strong influence of very local factors (e.g. those which were mentioned in the Introduction). The network of strainmeters described in this paper is placed in the relative "quite" (or stable) area. The interpretation of the the long-period, non-tidal, extensometric data in this case is an even more complicated problem due to the reduced scale of the variations. Nevertheless, we found some qualitative features of the records obtained at four observatories located at different geological conditions and relatively far from each other.

On the basis of the "Long period band" data we concluded that only oriented near to the N-S direction — in azimuths 37°N and 38°N — strainmeters observed real long-term strain variations of compressional type. This phenomenon coincides with the main feature of the Europen recent stress field (Zoback et al.,1992). Of course this similarity is not yet well established in the extensometric network described in this paper due to the small number of the strainmeters and due to the possible strong and not accurately enough known local distrubances. For the further investigation of the problem the data of the Pécs observatory are strougly needed, together with the analysis of in situ and borehole stress orientation data obtained in the Pannonian Basin in the course of last years.

In other than nearly N-S direction the long period changes are characterised by much smaller.

The annual wave — possibly of thermoelastic origin—has much smaller amplitude at the margins of the Pannonian Basin (Vyhné, Sopron) than at its deeper parts (Beregovo, Budapest).

The study of the "Short period band" shows that the regionality of the deformations is limited at higher frequencies (Fig.7), but the spectra of data obtained with equipments at the same stations with different orientations are similar to each other (Figs.6 and 7). It seems that in this case the presence of local tectonical and hydrological processes together with meteorological ones is mastly felt. Due to short record-lengths (of about one month) used for calculation of the spectra of the "short period band" does an allow the exact separation of two — long and short periodic — frequency bands.

As far as the two questions formulated above are concerned there are some similarities in the records of different observatories which can be connected — in principle — to real external (geological, hydrological, meteorological) processes. The nature and the regionality of these correlations are still, howewer, doubtful and need further investigations.

References

LATYNINA L A, JURKIEVICH O I, BAJSAROVICH I M, (1992): Results of deformometric measurements in the vicinity of Beregovo. *Geophysical Journal*, 14, No.2 pp. 63-67 (in Russian).

VARGA P, VARGA T, (1991): A study of the nature of the drift curves recorded with different quartz tube extensometers. *B.I.M.* 111, pp. 8027-8030.

MENTES GY, (1991): Installation of a quartz tube extensometer at the Sopron Observatory. *B.I.M.* 111, pp. 7936-7939.

BRIMICH L, HVOZDARA M, (1988): Long-periodic thermoelestic deformations and their influence on the extensometric and tidal measurements. *B.I.M.* 101, pp. 7075-7087.

VARGA P (1984): Long - term variations recorded by extensometers. *Journal of Geophysics*, 55, No.1 pp. 68-72.

ZOBACK M L (1992): First- and second-order patterns of stress in the litosphere: The world stress map project. *Journal of Geophysical Research* vol.97, No.B8, pp.11703-11728.

GROTEN E (1991): Geodetic techniques applied to the detection and monitoring of recent crustal movements. *Journal of Geodynamics* 14, No 1-4, pp. 1-7.

On the Time Variations of the Sensitivity.

C. De Toro, A.P. Venedikov, R. Vieira
Instituto de Astronomia y Geodesia
Madrid
Spain

1. Introduction.

It is a well known and evident fact that the variations of the sensitivity can be manifested as variations of the tidal amplitudes. Here we shall use this and develop a technique for the determination of the sensitivity/amplitude variations before the tidal analysis. We shall namely use the filtered numbers computed for the analysis and an amplitude factor δ determined through them.

In another paper we intend to develop a method for analysis where the sensitivity/amplitude variations can be incorporated in the observational equations.

Let us note that the pure amplitude variations are interesting as possible earthquake and volcano precursors. Our study is orientated towards this heavy problem. First of all we have to be able to establish the total sensitivity/amplitude variations. Only after that, through a comparison with the calibration data, it could be possible to separate the amplitude variations.

2. Normalized tidal parameters.

The basic equation for the Earth tide data is

$$(1) \qquad g(t) = \sum_{j=1}^{m} \delta_j h_j \cos(\phi_j + \omega_j t + \kappa_j) + D(t) + \varepsilon(t), \quad t \in (a,b).$$

Here $g(t)$ is the ordinate at time t of the observed tidal phenomena, h_j, ϕ_j and ω_j are the theoretical elements of the j-th tide, δ_j and κ_j are the Earth tidal parameters, $D(t)$ is the drift and $\varepsilon(t)$ is the noise, i.e. the observational error at time t. The expression $t \in (a,b)$ means that we dispose by a record of $g(t)$ in a time interval (a,b).

The equation (1) can be written for a set of values $t\in(a,b)$, for example every hour, so that (1) is in fact a system of equations. The object of the tidal analysis is to solve this system and find the estimates $\tilde{\delta}_j$ and $\tilde{\kappa}_j$ of δ_j and κ_j respectively.

We shall suppose that this is done, i.e. $\tilde{\delta}_j$ and $\tilde{\kappa}_j$ are obtained by using one or another method of analysis.

Let us see what will happen if we replace

$$(2) \qquad h_j \text{ by } \tilde{h}_j = \tilde{\delta}_j h_j \quad \text{and} \quad \phi_j \text{ by } \tilde{\Phi}_j = \phi_j + \tilde{\kappa}_j.$$

The equations (1) then become

$$(3) \qquad g(t) = \sum_{j=1}^{m} \delta_{Nj} \tilde{h}_j \cos(\tilde{\Phi}_j + \omega_j t + \kappa_{Nj}) + D(t) + \varepsilon(t), \qquad t \in (a,b)$$

with new unknowns denoted here by δ_{Nj} and κ_{Nj}. We shall call them "normalized parameters" because they have the following properties.

If we solve the system (3) in the same way as (1), i.e. by applying the same method of analysis on the same data for $t\in(a,b)$, we shall get identically the estimates

$$(4) \qquad \tilde{\delta}_{N1} = \tilde{\delta}_{N2} = \ldots = \tilde{\delta}_{Nm} = 1 \quad \text{and} \quad \tilde{\kappa}_{N1} = \tilde{\kappa}_{N2} = \ldots = \tilde{\kappa}_{Nm} = 0.$$

On the basis of this the equations (3) can be replaced by

$$(5) \qquad g(t) = \delta_N \sum_{j=1}^{m} \tilde{h}_j \cos(\tilde{\Phi}_j + \omega_j t + \kappa_N) + D(t) + \varepsilon(t), \qquad t \in (a,b).$$

If we apply once again the same method for analysis for $t\in(a,b)$ we shall get as estimates of δ_N and κ_n

$$(6) \qquad \tilde{\delta}_N = 1 \quad \text{and} \quad \tilde{\kappa}_N = 0.$$

The properties (4) and (6) of the normalized parameters will be accomplished independently on the properties of the noise and the drift, even if there are some systematic errors. However, if we analyze another

time interval, for example a subinterval (a_i, b_i) with a central epoch t_i, we shall get an estimate $\tilde{\delta}_N = \tilde{\delta}_N(t_i)$ generally depending on the time due to the noise and all possible errors. If (a_i, b_i) are n subintervals of (a,b) with central epochs t_i, $i = 1,2,\ldots n$, the empirically obtained function $\tilde{\delta}_N(t_i)$ can be used for studying some systematic errors in particular an error coming from a sensitivity/amplitude variation.

If there is a constant error in the calibration it will not affect the values of the normalized parameter $\tilde{\delta}_N(t_i)$. But, if the calibration coefficient is variable and the variations are not introduced correctly, these kind of systematic errors can be studied through $\tilde{\delta}_N(t_i)$.

For example let $C(t_1) < C(t_2)$ are the true values of the calibration coefficients at time t_1 and t_2 respectively. If the difference between $C(t_1)$ and $C(t_2)$ is not taken into account, the expected values of δ_N will be $\delta_N(t_2) < \delta_N(t_1)$ instead of $\delta_N(t_2) = \delta_N(t_1) = 1$.

This could be used for studying the sensitivity/amplitude variations through a processing of calibrated data. However, as it will be discussed in the next paragraph, more information about the sensitivity can be obtained if we process the data before the calibration.

3. Analysis of raw data.

Let $y(t)$, $t \in (a,b)$, are the raw (non-calibrated) data of a tidal record, i.e. $y(t)$ are ordinates in some conventional units, like *mm* or *mV*, while $g(t)$ are expressed in tidal units, e.g. *μgal*. The relation between $y(t)$ and $g(t)$ is

$$(7) \qquad g(t) = C(t).y(t) \quad \text{or} \quad y(t) = R(t).g(t), \quad R(t) = 1/C(t),$$

where $C(t)$ is the calibration coefficient at time t. The coefficient $R(t)$ can be called a response coefficient. It describes how the initial input geophysical signal $g(t)$ is transformed by the instrumentation into the output $y(t)$, namely

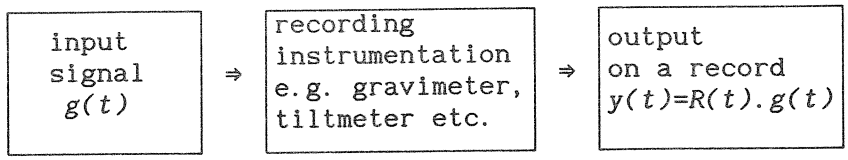

The coefficients C and R are considered as functions of t as there can be variations in the sensitivity or the amplitudes. They can be represented as

$$(8) \qquad R(t) = R_0 + \Delta R(t) \quad \text{and} \quad C(t) = C_0 + \Delta C(t)$$

where R_0 and C_0 are some constants.

By using (1) we get the equation

$$(9) \qquad y(t) = \sum_{j=1}^{m} d_j(t) h_j \cos(\phi_j + \omega_j t + k_j) + D(t) + \varepsilon(t), \quad t \in (a,b)$$

where $D(t)$ and $\varepsilon(t)$ are now the drift and the noise in the units of $y(t)$. The amplitude factor δ_j in (1) is here replaced by

$$(10) \qquad d_j(t) = \delta_j R(t)$$

while the phase shift remains the same.

We can apply the analysis on the raw data $y(t)$ in the same way as on $g(t)$ for $t \in (a,b)$, by using the equations (9) instead of (1). Then we shall get some estimates $\tilde{d}_j$ as amplitude factors which are a kind of a mean value of $d_j(t)$. It seems very natural to define the constants R_0 and C_0 in relation with $\tilde{d}_j$ as it follows

$$(11) \qquad \tilde{d}_j = \delta_j R_0 = \delta_j / C_0$$

This is not perfectly correct because R_0 and C_0 thus defined are not just the same for $j = 1,2,\ldots m$. However, it can be shown that (11) is justified when $R(t)$ is a linear function, i.e. the error in this expression is of a second order. Then, as we do not pretend for a very high precision, we can afford us to use it.

If we replace similarly to (2)

(12) $$h_j \text{ by } \tilde{h}_j = \tilde{d}_j h_j \quad \text{and} \quad \phi_j \text{ by } \tilde{\Phi}_j = \phi_j + \tilde{k}_j$$

the equations (9) become, like (3),

(13) $$y(t) = \sum_{j=1}^{m} d_{Nj}(t)\tilde{h}_j \cos\,(\Phi_j + \omega_j t + k_{Nj}) + D(t) + \varepsilon(t), \quad t\in(a,b)$$

where

(14) $$d_{Nj}(t) = d_j(t)/\tilde{d}_j.$$

Now, if we accept (11) and apply here (10), we get

(15) $$d_{Nj}(t) = \frac{\delta_j R(t)}{\delta_j R_0} = \frac{R(t)}{R_0} = \frac{C_0}{C(t)} = \delta_N(t)$$

where $\delta_N(t)$ is a normalized amplitude factor which depends on t but which does not depend on the index j. That is why we can replace (13) through

(16) $$y(t) = \delta_N(t) \sum_{j=1}^{m} \tilde{h}_j \cos\,(\tilde{\Phi}_j + \omega_j t + k_N) + D(t) + \varepsilon(t).$$

If we analyze, again in the same way, the data $y(t)$ for $t\in(a,b)$ we shall get an estimate of the normalized parameter

(17) $$\tilde{\delta}_N(t_0) = 1,$$

related to the central epoch t_0 of (a,b). If we process the intervals (a_i,b_i) we shall get estimates $\tilde{\delta}_N(t_i)$ depending on t.

According to (15) $\tilde{\delta}_N(t_i)$ will be related with the calibration coefficients. Something more, from here we get a rather strong result that we can compute the calibration coefficient $C(t)$, as well as the

response coefficient $R(t)$ at time t through

$$C(t) = C_0/\tilde{\delta}_N(t), \quad R(t) = R_0\tilde{\delta}_N(t) = \tilde{\delta}_N(t)/C_0 \tag{18}$$

provided we know C_0. Actually, C_0 is not known but we can use, as an approximation, a mean value of the calibration coefficients. Then (18) can be used, with much precaution, to check up some values of $C(t)$ and their relative variations.

4. Determination of the normalized tidal parameters from very short time intervals.

The replacement of the equations (1) by (5) as well as (9) by (16) has the following important advantage. Through this we take into account the differences within the tidal parameters for the different tidal waves. The consequences are: (i) we have only one couple of unknowns, namely δ_N and κ_N and (ii) we can estimate such a limited number of unknowns from very short tidal records.

If the method for analysis (Venedikov, 1966, Melchior and Venedikov, 1968, Venedikov, 1984, see also Melchior, 1978) is used, the original record is first subdivided into intervals of 48 hours or another length of this order, then these intervals are filtered. As the intervals (a_i, b_i) used above we can take just these filtered intervals.

For such an interval, for a given tidal group, for example for SD, we obtain one couple of filtered numbers, $U(t_i)$ and $V(t_i)$, by applying respectively an even and an odd filter. The equations (1) are transformed in the following way:

$$\begin{aligned} U(t) &= \sum_{j=1}^{m} \delta_j c_j h_j \cos(\phi_j + \omega_j t + \kappa_j) + \varepsilon_1(t), \\ V(t) &= \sum_{j=1}^{m} \delta_j s_j h_j \sin(\phi_j + \omega_j t + \kappa_j) + \varepsilon_2(t) \end{aligned} \tag{19}$$

The effect of the filters is: the drift is eliminated, the noise is transformed into $\varepsilon_1(t)$ and $\varepsilon_2(t)$ and the tides are multiplied by the

amplifying factors of the filters c_j and s_j.

Without repeating the details, by using the normalization already described, we can get the following equations

$$U(t) = \delta_N(t) \sum_{j=1}^{m} c_j \tilde{h}_j \cos(\tilde{\Phi}_j + \omega_j t + \kappa_N) + \varepsilon_1(t) \quad \text{and}$$

(20)

$$V(t) = \delta_N(t) \sum_{j=1}^{m} s_j \tilde{h}_j \sin(\tilde{\Phi}_j + \omega_j t + \kappa_N) + \varepsilon_2(t).$$

For a given fixed $t = t_i$, i.e. for a given interval (a_i, b_i), the system (20) of two equations can be easily solved and we can get the value $\tilde{\delta}_N(t_i)$, of course with a corresponding influence of the noise.

If $U(t)$ and $V(t)$ are filtered numbers obtained from the raw data $y(t)$ we can relate $\tilde{\delta}_N(t_i)$ with $C(t_i)$ or $R(t_i)$ through (18).

5. A regression analysis of the normalized parameters with the use of calibration data (linear interpolation).

Let the calibrations are made at the epochs $\tau = \tau_1, \tau_2, \ldots \tau_\nu$ and the observed values of the calibration coefficients are $c(\tau_1)$, $c(\tau_2)$ $\ldots c(\tau_\nu)$. We shall consider the widely spread practice to make a linear interpolation between every two consecutive calibrations. According to it, the calibration coefficient at time t, say $c(t)$, is computed after

$$c(t) = c(\tau_k) + a_{k+1}(t-\tau_k), \quad \text{if} \quad \tau_k \le t \le \tau_{k+1}. \tag{21}$$

where the coefficients a_k are computed after

$$a_1 = c(\tau_1)$$

$$a_k = \left(c(\tau_k) - c(\tau_{k-1})\right) / (\tau_k - \tau_{k-1}), k = 2, \ldots \nu \tag{22}$$

When this expression is used this has the meaning, that for the observations $c(\tau_k)$, $k = 1,2,\ldots\nu$, we accept the equations

$$
\begin{aligned}
& c(\tau_1) = a_1 \\
& c(\tau_2) = a_1 + a_2(\tau_2-\tau_1) \\
(23) \qquad & c(\tau_3) = a_1 + a_2(\tau_2-\tau_1) + a_3(\tau_3-\tau_2) \\
& \quad . \quad . \quad . \quad . \quad . \quad . \quad . \quad . \quad . \quad . \quad . \quad . \quad . \\
& c(\tau_\nu) = a_1 + a_2(\tau_2-\tau_1) + a_3(\tau_3-\tau_2) + \ldots + a_\nu(\tau_\nu-\tau_{\nu-1})
\end{aligned}
$$

This as a system of ν equations with the same number ν of unknowns, the coefficients a_k. The solution of the system is namely (22).

There is no room for any statistical processing of (23), for example for the Method of the Least Squares, because the number of the equations (23) is just equal of the number of the unknowns. For this reason we cannot estimate the precision of a_k. Actually, as we have zero degrees of freedom, the estimates a_k have indefinite intervals of confidence. Something more, any error in a_k is directly transferred as a systematic error onto the data.

These weaknesses of the scheme can be partly reduced if we use our normalized parameters and the equations (18). This can be done in the following way.

We shall introduce a variable

$$
(24) \qquad x(t_i) = C_o/\delta_N(t_i), \quad i=1,2,\ldots n.
$$

Then, according to (18) and (21), we shall have the observational equations for x

$$
\begin{aligned}
& x(t) = a_1 + a_2(t-\tau_1), \quad \text{for } \tau_1 \le t \le \tau_2 \\
& x(t) = a_1 + a_2(\tau_2-\tau_1) + a_3(t-\tau_2), \quad \text{for } \tau_2 \le t \le \tau_3 \\
(25) \qquad & \quad . \quad . \quad . \quad . \quad . \quad . \quad . \quad . \quad . \quad . \quad . \quad . \quad . \\
& x(t) = a_1 + a_2(\tau_2-\tau_1) + a_3(\tau_3-\tau_2) + \ldots + a_\nu(t-\tau_{\nu-1}), \\
& \qquad\qquad \text{for } \tau_{\nu-1} \le t \le \tau_\nu, \\
& \qquad\qquad t = t_i, \; i = 1,2,\ldots n
\end{aligned}
$$

If there are discontinues changes in $C(t)$, there are further

complications in the scheme which is without this not very comfortable for computations. Let us suppose that such a change we have after τ_ν, i.e. we have new sensitivity and new calibrations made at time $\tau_{\nu+1}$, $\tau_{\nu+2}, \ldots \tau_{\nu+\mu}$. Then for $\tau_{\nu+1}$ we must introduce a new calibration constant at the place of a_1 and write new equations, independent from the equations (25), like

$$x(t) = a_{\nu+1} + a_{\nu+2}(\tau_{\nu+2}-\tau_{\nu+1}) + \ldots + a_{\nu+k}(t-\tau_{\nu+k-1}), \tag{26}$$

$$\text{for } \tau_{\nu+k-1} \leq t \leq \tau_{\nu+k}.$$

If there is another change of the sensitivity we must create another new system of equations, like (26), and so on. What is interesting, through (25) or (25), (26) and all other equations like (26), we can determine the coefficients a_k, $k = 1, \ldots \nu$ or $k = 1, \ldots \nu, \ldots \nu + \mu$ etc. Then, on the basis of the expressions (21) through (23) we can compute the calibration coefficient $C(t)$ at any time t. And all this without using the observed calibration coefficients $c(\tau_k)$, i.e. the calibrations themselves. The only application of the calibrations is to determine the mean value C_o for the computation of $x(t)$ after (24).

Evidently, this kind of equations are to be solved by the Method of the least squares.

6. Some results.

This technique was applied on the gravity observations by a LCR gravimeter in Lanzarote. An interesting moment in these data is that there are several artificial changes of the sensitivity. There were slow inclination of the gravimeter which produced slow linear variations of the calibration coefficient.

When there was a new adjustment of the position of the gravimeter, it provoked a jump in the sensitivity. Evidently, before and after these jumps there were made corresponding calibrations.

The jumps are clearly seen on Fig. 1.a on which is plotted the empirically obtained calibration curve. There are indicated all determinations of the calibration coefficients.

On Fig. 1.b is plotted the quantity (24), $x(t_i) = C_o/\delta_N(t_i)$, where $\tilde{\delta}_N$ is obtained through the processing of the calibrated data. The applied calibration coefficients are those on Fig. 1.a. In the ideal case of a perfect calibration $x(t_i)$ should be a constant. One can see that there are some systematic deviations of $x(t_i)$ from a constant.

On Fig. 1.c again $x(t_i) = C_o/\delta_N(t_i)$ is plotted but now $\delta_N(t_i)$ is obtained from the raw data $y(t)$, i.e. the data before the calibration. are used. There is plotted the quantity (24) which, according to our consideration above, should describe the variation of the sensitivity. There is possible a systematic shift due to the more or less arbitrary choice of C_0 in (24). The variations of this curve should be related with the real variations of the sensitivity. One can see indeed that there is a close relation with the curve on Figure 1.a.

The data from Fig. 1.c were adjusted as it was suggested in paragraph 5. The adjustment allows jumps at the points where are made changes in the sensitivity. The curve obtained is plotted on Fig. 1.d. It is close to Fig. 1.a but not identical. In particular, there are some differences in the estimated jumps and the experimental jumps.

Through the last adjusted curve the data were again calibrated. On the last Fig. 1.e the quantity $x(t_i)$ is again plotted. Now the normalized δ_N used is taken from the newly calibrated data. Compared to Fig. 1.b, here we are somewhat closer to the ideal case $x(t) = \text{const}$.

Acknowledgments

This work has been done in the Institute of Astronomy and Geodesy in Madrid. One of the authors (A.P. Venedikov, Institute of Geophysics, Sofia) has been supported by the Sabbatical Program of the University Complutense of Madrid.

The idea for the "normalized parameters" was first developed in collaboration with Prof. J. Zschau in the Institute of Geophysics in Kiel with the support of the Deutsche Forschungsgemeinschaft.

Fig. 1.a

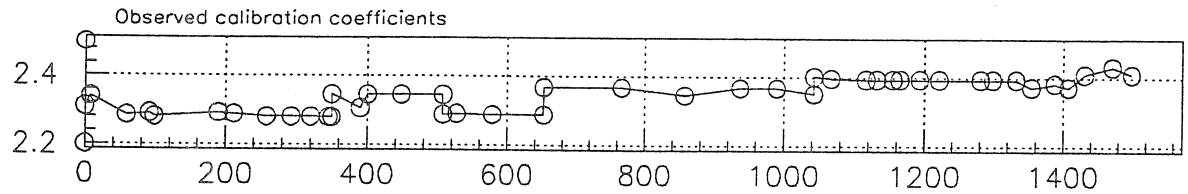

Fig. 1.b

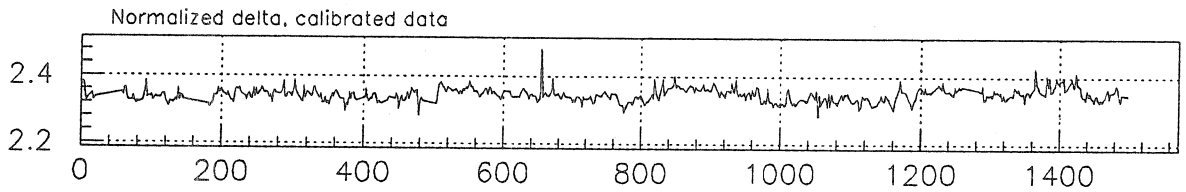

Fig. 1.c

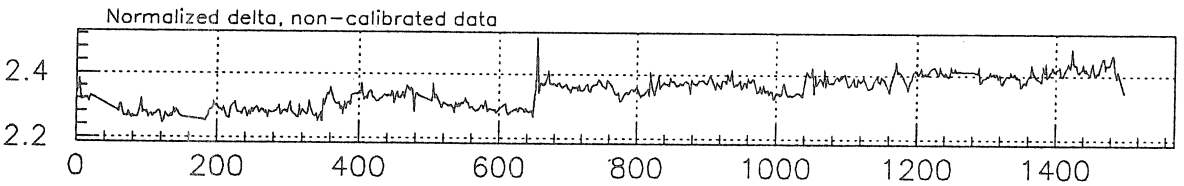

Fig. 1.d

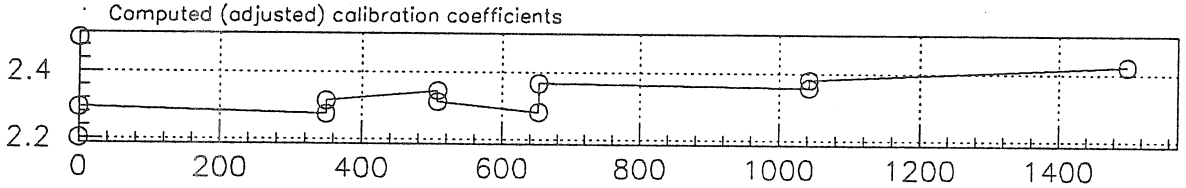

Fig. 1.e

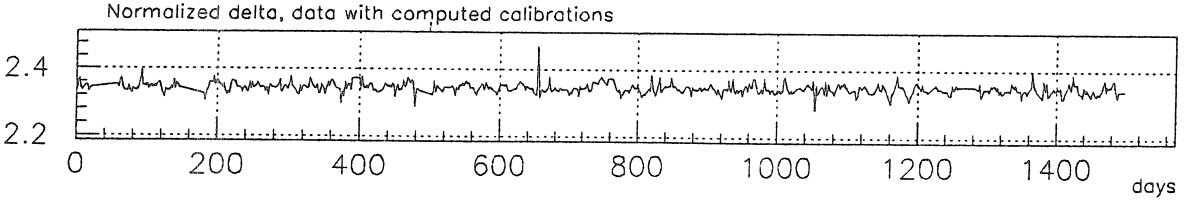

Cueva de los Verdes, gravity data, 1987-1991

A New Method for Earth Tide Data Analysis.

C. De Toro, A.P. Venedikov, R. Vieira
Instituto de Astronomia y Geodesia
Madrid
Spain

1. Introduction.

Let Y is an Earth tide observation, i.e. an ordinate of a record like those on Fig. 1. The general model for Y is

$$Y = G + D + \varepsilon \tag{1}$$

where G is the pure tidal component of the record, D is the drift and ε is the error of the observation. If the popular slang of the communication technique is used, G is the useful signal of the record, ε is the noise and D - somewhat between signal and noise.

The task of the tidal analysis is to estimate the parameters upon which depends G, or, which is the same, to get the estimate $\tilde{G}$ of G. Form this point of view D is a function of the time which describes the zero-line of the record.

The same data Y can be used for non-tidal problems like recent crustal movements, superficial deformations, volcano and earthquake precursors etc. These problems need the determination of the second component of (1), i.e. the estimate $\tilde{D}$ of D. For example as precursors can be considered some accelerations and jumps of $\tilde{D}$ (by the way, we can look for precursors in G as well).

In order to get $\tilde{G}$ we need to separate it from D. This can be done only if we obtain, in one or another way, the estimate $\tilde{D}$. Thus we see that the tidal analysis of Y has to satisfy both tidal and non-tidal problems.

Evidently, we shall have good estimates $\tilde{G}$ and $\tilde{D}$ if we can reduce the effect of the noise ε on both of them. It is out of question to estimate ε directly. We can only define the residuals,

$$r = Y - \tilde{G} - \tilde{D}, \tag{2}$$

and set up a reasonable condition about them. When ε is a white noise most reasonable is the condition of the Method of the Least Squares (here and further MLS),

$$\sum r^2 = \text{Min.} \tag{3}$$

For the use of (3) we need analytical models of G and D. There are no problems with the model of G but we have not a good theory about D. That is why a crucial moment of the analysis is how it deals with the drift.

In a classical effort to apply the MLS Horn (1959) suggested to approximate the drift by a polynomial over the whole interval of the observations. The method of Horn could not accept gaps and data like those on Fig. 1.b.

In another application of the MLS (Venedikov, 1966, Melchior and Venedikov, 1968, see also Melchior, 1978), which will be called here M67, a more flexible model of the drift was accepted. The record to be processed is subdivided into intervals, we shall call them Δ, of length n = 48 hours as it is shown on the following scheme

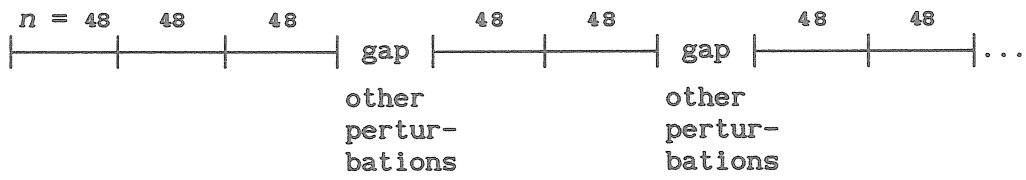

Intervals Δ in the method of analysis M67.

The drift is approximated independently in every Δ by a polynomial of low fixed order (Figure 2). This kind of approximation admits any changes in the drift as well as any gaps between the Δ.

In M67 the hourly ordinates Y are replaced as observations by a pair of filtered numbers for every Δ and every one of the main tidal bands D (diurnal), SD (semidiurnal) and TD (terdiurnal). This is made in order to avoid the correlation of ε and get a severe estimate of the precision, different for the D, SD and TD tides.

Afterwards several methods were proposed, e.g. (Chojnicki, 1973,

Schüller, 1977, Jentzsch, 1977) as well as a more flexible variant of M67 (Venedikov, 1984). However, none of these methods could show significant advantages with respect to M67.

A most interesting modern approach to the problem was made by the method used in Mizusawa (Ishiguro, Akaike, Ooe & Nakai, 1983, Tamura, Sato, Ooe & Ishiguro, 1991). In this method the gaps define natural intervals of the record. In each interval we get a separately estimated drift. The drift model is related with a condition for every sequence of three ordinates.

Here we shall propose a method (here and further M92) which is partly a generalization of M67, partly its alternative. The motives for its creation are the following.

First, there are modern observations of high quality with very stable drift. For them the model used by M67, which is good for an irregular drift, may be not necessary. We can hope that the drift can be approximated in intervals Δ much longer than 48 hours.

Second, for such observations the correlation of the noise may be not so important. We can try to avoid the use of the filtered numbers and return to the hourly ordinates.

Finally, now we have powerful computers which allow the development of very sophisticated methods. We can make very complicated experiments and we are, in a way, obliged to exploit these possibilities.

However, a more sophisticated method does not yet means a better method and we do not suggest necessarily to replace M67 by M92. What seems quite sure, it could be useful to apply in parallel both methods.

2. The tidal model.

If G_t is the value of G at time t, we have the theoretical model

$$G_t = \sum_k \delta H_k \cos (\Phi_k + \omega_k t + \kappa) \tag{4}$$

where each term represents a tidal wave with an index k.

The quantities ω_k (angular velocity), H_k (theoretical amplitude) and Φ_k (initial theoretical phase) are well known. The parameters δ

(amplitude factor) and κ (phase shift) are the unknown parameters of G whose estimates are the object of the analysis. They can be considered as functions of the angular velocity ω,

$$\delta = \delta(\omega_k) \quad \text{and} \quad \kappa = \kappa(\omega_k). \tag{5}$$

A problem is the great number of the tides in (4) - in the modern tidal potential developments of Tamura (1987) and Xi Quinwen (1985) there are more than 1000 tidal waves.

This is easy to overcome this problem by using that (5) are slowly varying functions. We can shape groups of tides, say g groups, with close ω_k and accept that δ and κ are constants within a group. If $k = k_j$ are the indices of the tides in the j-th group, we can set up

$$\delta(\omega_k) = \delta_j = \text{const.} \text{ and } \kappa(\omega_k) = \kappa_j = \text{const.} \quad \text{for } k = k_j,\ j = 1,2,\ldots g \tag{6}$$

and introduce the unknowns (Venedikov, 1961, 1966)

$$\xi_j = \delta_j \cos \kappa_j \quad \text{and} \quad \eta_j = -\delta_j \sin \kappa_j \tag{7}$$

With them the expression (4) becomes,

$$G_t = \sum_{j=1}^{g} (\xi_j\, c_j(t) + \eta_j\, s_j(t)) \quad \text{where} \tag{8}$$

$$c_j(t) = \sum_{k=k_j} H_k \cos(\Phi_k + \omega_k t) \text{ and } s_j(t) = \sum_{k=k_j} H_k \sin(\Phi_k + \omega_k t)$$

The grouping or the separation of the tides should be made in dependence on the total length of the record. It should guarantee a linear independence (close to orthogonality) of the functions $c_j(t)$ as well as $s_j(t)$.

For a more convenient manipulation with (8) we can replace it by

$$(9) \qquad G_t = \sum_{j=1}^{m} a_{tj} x_j,$$

where x_j and a_{tj}, $j = 1,2,\ldots m = 2g$, replace the unknowns (7) and the functions (8) respectively.

3. Model of the drift.

The model of D in M92 is related with the scheme

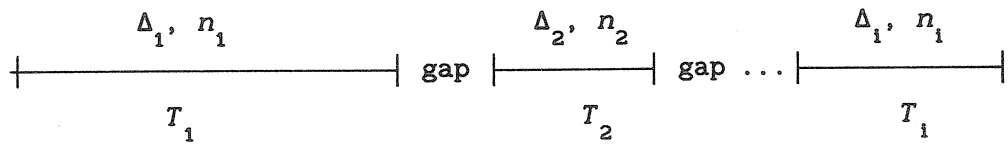

Intervals Δ_i in the method of analysis M92.

The record is subdivided into N intervals denoted by Δ_i, with a central epoch T_i and, generally, a variable length n_i hours. Within any interval Δ_i are no gaps so that n_i is also the number of the hourly ordinates in Δ_i.

In the following the letter i ($i = 1,2,\ldots N$) will used exclusively as an index of an interval Δ_i.

In every Δ_i we have separate approximation of the drift through

$$(10) \qquad D_t = \sum_{k=0}^{v_i} z_{ki} p_{tk} \quad \text{for a given } \Delta_i.$$

At the moment we shall accept that

$$(11) \qquad p_{tk} = (t-T_i)^k \quad \text{for } \Delta_i$$

so that (10) is a polynomial of power v_i. The coefficients z_{ki} of the polynomial are unknowns specific for Δ_i. The power v_i is also specific for every Δ_i. The selection of v_i will be discussed a little bit later.

In the practical application of M92, Δ_i are defined by:

(i) in any case by the gaps, like in the method of Mizusawa, and, optionally,

(ii) by the epochs of the calibrations,

(iii) by epochs given as input data, related with places where we suspect changes in the drift's behaviour,

(iv) in dependence on two integers n_{min} and n_{max} which $n_{min} \leq n_i \leq n_{max}$ or

(v) by choosing a length n and $n_i = n$ = const. In this case we have the scheme of M67 with $n = 48$ replaced by the chosen value of n.

Let us return to the powers v_i in (10).

We must be able to work with v_i depending on i, i.e. with polynomials (10) of different order for every Δ_i. When n_i is variable, we can expect higher v_i for longer Δ_i and lower v_i for shorter Δ_i. We may need different v_i corresponding to the changes in the drift properties and behaviour, independently of whether the length n_i is variable or $n_i = n$ = const.

Evidently, we are not able to choose, before the processing, a set of fixed values v_i, $i = 1,2,\ldots N$. That is why M92 presumes a variation of v_i separately for every Δ_i and selection of optimum values. This will be discussed in paragraphs 5 and 6. Now, in the next paragraph, we shall consider the use of the models (9) and (10) for getting the estimates of the unknowns only for a given fixed set of powers $v_1, v_2, \ldots v_N$.

4. Observational equations and their solution after the MLS.

If we joint (9) and (10) into (1) we get the observational equations

$$(12) \qquad Y_t = \sum_{j=1}^{m} a_{tj} x_j + \sum_{k=0}^{v_i} p_{tk} z_{ki} \quad \text{for } \Delta_i,\ i = 1,2,\ldots N$$

where Y_t is an ordinate at time t. Here the error ε is ignored but we keep it in mind.

According to (11) p_{tk} is related with T_i and Δ_i and it would be more correct to write p_{itk}. In order to avoid too many indices we shall

drop away the index i.

In a given Δ_i we have n_i hourly ordinates Y_t. For them the argument time t takes the values

(13) $$t = T_i - \nu_i,\ T_i - \nu_i + 1, \ldots\ T_i + \nu_i, \quad \text{where} \quad \nu_i = (n_i - 1)/2.$$

We shall deal first with the equations (12) for a given Δ_i and we shall introduce the following matrices related with the values (13) of t:

(14) $(n_i \times 1)$ dimensional column vector

$$\mathbf{Y}_i = \|Y_t\|, \qquad t = T_i - \nu_i,\ T_i - \nu_i + 1, \ldots T_i + \nu_i,$$

(15) $(n_i \times m)$ dimensional matrix

$$\mathbf{A}_i = \|a_{tj}\|, \quad j = 1, 2, \ldots m,$$
$$t = T_i - \nu_i,\ T_i - \nu_i + 1, \ldots T_i + \nu_i \text{ and}$$

(16) $(n_i \times \nu_i + 1)$ dimensional matrix

$$\mathbf{P}_i = \|p_{tk}\|, \quad k = 0, 1, \ldots \nu_i$$
$$t = T_i - \nu_i,\ T_i - \nu_i + 1, \ldots T_i + \nu_i.$$

Further we shall arrange the unknowns in the column vectors:

(17) $$\mathbf{z}_i = \|z_{ki}\|, \ k = 0, 1, \ldots \nu_i, \text{ dimension } (\nu_i + 1 \times 1),$$

$$\mathbf{x} = \|x_j\|, \quad j = 1, 2, \ldots m, \quad \text{dimension } (m \times 1),$$

where $\mathbf{x}$ represents the tidal unknowns (ξ and η) which are common for all Δ_i while $\mathbf{z}_i$ represents the drift unknowns, which are related with Δ_i, i.e. which depend on i. The number of the elements of $\mathbf{z}_i$, $\nu_i + 1$, is also depending on i.

By using these matrices we can rewrite (12) in the matrix form

(18) $$\mathbf{Y}_i = \mathbf{A}_i\mathbf{x} + \mathbf{P}_i\mathbf{z}_i \quad \text{for} \quad \Delta_i, \ i = 1, \ldots N.$$

In principle, (18) can be directly solved by the MLS. However, this is difficult even for a powerful computer because the number of the drift unknowns in all z_i can be very high. For example, if we use fixed length intervals with $n_i = 48$ and polynomials of fixed power $v_i = 2$, a record of length one year will provide 546 drift unknowns.

This inconvenience can be avoided if we separate the unknowns z_i from x. Namely, we can orthogonalize P_i, then A_i towards P_i, in the following classical way.

We replace P_i by a matrix

$$(19) \qquad Q_i = P_i S_i, \quad \text{with} \quad S_i S_i^* = (P_i^* P_i)^{-1}$$

where S_i is an upper triangular matrix of dimensions $(v_i+1 \times v_i+1)$, Q_i has the same dimensions as P_i and * means the transpose of a matrix.

We replace also A_i by the matrix

$$(20) \qquad B_i = A_i - Q_i(Q_i^* A_i)$$

which has the dimensions of A_i.

It is easy to see that Q_i is orthonormal and B_i is orthogonal to both Q_i and P_i, i.e.

$$(21) \qquad Q_i^* Q_i = I \quad \text{and} \quad B_i^* Q_i = B_i^* P_i = 0$$

where I is a unit matrix and 0 is a zero matrix. The properties (21) are observed separately for every Δ_i.

Now with Q_i and B_i we transform the equations (18) into

$$(22) \qquad Y_i = A_i x + P_i z_i = B_i X + Q_i Z_i, \quad i = 1,2,\ldots,N,$$

where Z_i and X are new unknowns which replace z_i and x. From here and the expressions (19) and (20) about Q_i and B_i we get

$$(23) \qquad X = x \quad \text{and} \quad Z_i = S_i^{-1}(z_i + (Q_i^* A_i)X)$$

i.e. the tidal unknowns $\mathbf{x}$ are not changed, but the drift unknowns $\mathbf{z}_i$ are transformed into $\mathbf{Z}_i$.

Now we can apply the MLS by taking into account (21). Then we get the following systems of normal equations for the estimates $\tilde{\mathbf{Z}}_i$ of $\mathbf{Z}_i$ and $\tilde{\mathbf{X}}$ of $\mathbf{X}$:

First N matrix equations for the drift unknowns

$$(24) \qquad (\mathbf{Q}_i^*\mathbf{Q}_i)\tilde{\mathbf{Z}}_i = \mathbf{Q}_i^*\mathbf{Y}_i, \quad i = 1,2,\ldots N,$$

then a matrix equation for the tidal unknowns

$$(25) \qquad (\mathbf{B}^*\mathbf{B})\tilde{\mathbf{X}} = \mathbf{B}^*\mathbf{Y}, \qquad \mathbf{B} = \|\mathbf{B}_i\|, \ \mathbf{Y} = \|\mathbf{Y}_i\|, \quad i = 1,\ldots N$$

Here $\mathbf{B}$ is obtained through the arrangement of $\mathbf{B}_i$ $(i = 1,\ldots N)$ into a single matrix and $\mathbf{Y}$ - through the arrangement of $\mathbf{Y}_i$ into a single column vector. If $\tilde{n}$ is the sum of n_i, i.e. the total number of the data, $\mathbf{B}$ has the dimensions $(\tilde{n} \times m)$ and $\mathbf{Y}$ - $(\tilde{n} \times 1)$.

From the solution of (24) and (25) we can get the estimates

$$(26) \qquad \tilde{\mathbf{Z}}_i = (\mathbf{Q}_i^*\mathbf{Q}_i)^{-1}(\mathbf{Q}_i^*\mathbf{Y}) = \mathbf{Q}_i^*\mathbf{Y}$$

$$(27) \qquad \tilde{\mathbf{X}} = (\mathbf{B}^*\mathbf{B})^{-1}(\mathbf{B}^*\mathbf{Y}),$$

Thus $\mathbf{Z}_i$ are obtained in a most simple way. However, if we want to get the original drift unknowns, i.e. the coefficients z_{ki} of the polynomials (10), we have to go back from $\mathbf{Z}_i$ to $\mathbf{z}_i$ through the computation of

$$(28) \qquad \tilde{\mathbf{z}}_i = \mathbf{S}_i(\tilde{\mathbf{Z}}_i - (\mathbf{Q}_i^*\mathbf{A}_i)\tilde{\mathbf{X}})$$

For the computations it is important that we can get directly $\mathbf{B}^*\mathbf{B}$ and $\mathbf{B}^*\mathbf{Y}$ through $\mathbf{A}_i$ and $\mathbf{Q}_i$ after

$$(29) \qquad B*B = \sum_{i=1}^{N} B_i*B_i = \sum_{i=1}^{N} \left(A_i*A_i - (Q_i*A_i)*(Q_i*A_i) \right)$$

$$B*Y = \sum_{i=1}^{N} B_i*Y_i = \sum_{i=1}^{N} \left(A_i*Y_i - (Q_i*A_i)*(Q_i*Y_i) \right).$$

5. Variation of the drift model.

Practically this is done by choosing two parameters v_{min} and v_{max}. Then v_i, for every Δ_i, is let taking all values

$$(30) \qquad v_{min} \le v_i \le v_{max} .$$

A most natural value of v_{min} seems to be $v_{min} = 1$. This is a default value of M92 but it can be changed optionally.

The concrete variation of v_i, for $v_{min} = 1$ and $v_{max} = 4$, is demonstrated through the following scheme, where v'_i means an optimum value of v_i for Δ_i:

$v_{min} = 1$, $v_{max} = 4$, v'_i means an optimum value.

variation of v_1 in Δ_1

v_1	v_2	...	v_N
1	1	...	1
2	1	...	1
3	1	...	1
4	1	...	1
v'_1			

variation of v_2 in Δ_2

v_1	v_2	...	v_N
v'_1	1	...	1
v'_1	2	...	1
v'_1	3	...	1
v'_1	4	...	1
	v'_2		

...

variation of v_N in Δ_N

v_1	v_2	...	v_N
v'_1	v'_2	...	1
v'_1	v'_2	...	2
v'_1	v'_2	...	3
v'_1	v'_2	...	4
			v'_N

- We make the analysis of all data, i.e. all Δ_i, by choosing
  $v_1 = 1, 2, \ldots v_{max}$, while $v_2 = v_3 = \ldots = v_N = 1$
- Through statistical criteria we choose

the optimum value v_1' of v_1

- We make the analysis of all data, i.e. all Δ_i, by choosing

$v_1 = v_1'$, $v_2 = 1, 2, \ldots v_{max}$, $v_3 = \ldots = v_N = 1$

- Through statistical criteria we choose

the optimum value v_2' of v_2

and so on till we choose

the optimum value v_N' of v_N.

The whole procedure can be repeated by getting as initial values, instead of $v_i = v_{min} = 1$, the selected optimum values v_i' and look for new optimum values.

The analysis, i.e. the creation and the solution of the normal equations (24) and (25), is made for all indicated values of v_i. Thus, when the initial value is $v_{min} = 1$, we have to process a number of Nv_{max} analyses.

Such a quantity of computations is too big and needs as many as possible facilitations. A most important facilitation is the following. It consists in using the matrices created for a given variant of v_i for the next variant.

Let us suppose that we have made the computation for a given set of values of $v_1, v_2, \ldots v_N$, in particular for $v_i = v$ for a given interval Δ_i. Then the matrices $\mathbf{P}_i$ and $\mathbf{Q}_i$ related with Δ_i have $v + 1$ columns, i.e. they can be represented as

$$(31) \qquad \mathbf{P}_i = \|\mathbf{p}_o\ \mathbf{p}_1 \ \ldots\ \mathbf{p}_v\|,\ \mathbf{Q}_i = \|\mathbf{q}_o\ \mathbf{q}_1 \ \ldots\ \mathbf{q}_v\|,$$

where $\mathbf{p}_k$ and $\mathbf{q}_k$ are columns of dimension $(n_i \times 1)$. Here, as far as $\mathbf{S}_i$ is triangular, $\mathbf{q}_k$ depends on $\mathbf{p}_o, \ldots \mathbf{p}_k$ only and it does not depend on $\mathbf{p}_{k+1}, \ldots \mathbf{p}_v$ $(k < v)$.

Let us now increase $v_i = v$ to $v_i = v + 1$. Then $\mathbf{P}_i$ and $\mathbf{Q}_i$ are to be replaced by

$$(32) \qquad \mathbf{P}_i' = \|\mathbf{p}_o\ \mathbf{p}_1 \ \ldots\ \mathbf{p}_v\ \mathbf{p}_{v+1}\|,\ \mathbf{Q}_i = \|\mathbf{q}_o\ \mathbf{q}_1 \ \ldots\ \mathbf{q}_v\ \mathbf{q}_{v+1}\|.$$

Due to the above considerations, the first v+1 columns of $\mathbf{Q}_i$ remain the

same and we need only to compute the additional q_{v+1}.

For the new value $v_i = v + 1$ the estimates of the drift unknowns $\tilde{Z}_i$ are to be replaced by

$$\tilde{Z}'_i = Q'_i * Y_i \tag{33}$$

where $\tilde{Z}'_i$ has $v + 2$ elements, while $\tilde{Z}_i$ has $v + 1$ elements. The first $v + 1$ elements of $\tilde{Z}'_i$ remain the same as in $\tilde{Z}_i$, while the new element of $\tilde{Z}'_i$ is

$$\tilde{Z}_{iv+1} = q_{v+1} * Y_i . \tag{34}$$

We shall have a new matrix B'_i instead of B_i, a new matrix B' instead of B and, instead of (25), new normal equations

$$(B' * B')\tilde{X}' = B' * Y, \tag{35}$$

for new estimates $\tilde{X}'$ of the same tidal unknowns.

For the practical application it is important that

$$B' * B' = B * B - (q_{v+1} * A_i) * (q_{v+1} * A_i) \tag{36}$$

$$B' * Y = B * Y - (q_{v+1} * A_i)(q_{v+1} * Y_i) .$$

For a given variant with normal equations (24) and (25) the sum of squares of the residuals can be obtained, according to the theory of the MLS, after

$$S_o^2 = Y * Y - \sum_{i=1}^{N} \tilde{Z}_i * \tilde{Z}_i - \tilde{X} * (B * Y), \quad \text{d.f. } f = \sum_{i=1}^{N} (n_i - v_i - 1) - m \tag{37}$$

where d.f. means degrees of freedom.

When $v_i = v$ is increased to $v_i = v + 1$, as above, the corresponding sum of squares becomes

$$(38) \qquad S_1^2 = Y^*Y - \sum_{i=1}^{N} \tilde{Z}_i^*\tilde{Z}_i - \tilde{Z}^2_{iv+1} - \tilde{X}'^*(B'^*Y), \quad \text{d.f. } f_1 = f - 1$$

where $\tilde{X}'$ are the new tidal estimates, related with $v_i = v + 1$.

The estimates of the variances of the observations are respectively

$$(39) \qquad \sigma_o^2 = S_o^2/f \quad \text{and} \quad \sigma_1^2 = S_1^2/f_1$$

where σ_o and σ_1 are the corresponding standard deviations or mean square errors. The estimation of the precision of $\tilde{X}$ and $\tilde{X}'$ can be obtained, according to the MLS, through σ_o and $(B^*B)^{-1}$ and σ_1 and $(B'^*B')^{-1}$ respectively.

6. Selection of an optimum variant.

We shall denote by V_o the variant with $v_i = v$ and by V_1 the variant with $v_i = v+1$ for a fixed Δ_i. The difference in V_o and V_1 is in the models of the drift for Δ_i which are

$$(40) \qquad V_o: \quad D_t = z_o p_{to} + z_1 p_{t1} + \ldots + z_v p_{tv}$$

$$V_1: \quad D_t = z_o p_{to} + z_1 p_{t1} + \ldots + z_v p_{tv} + z_{v+1} p_{tv+1} \quad \text{for } \Delta_i$$

where the index i at z_{ki} is dropped away for convenience.

We see that V_o can be obtained from V_1 under the "zero hypothesis"

$$(41) \qquad H_o: \quad z_{v+1} = 0$$

Then the problem to select a better variant among V_o and V_1 is equivalent to the testing of H_o. If H_o is rejected then V_1 is to be chosen and, vice versa, if H_o cannot be rejected than V_o can be preferred.

This can be done by the method of analysis of variances. We have to compute the famous ratio F of Fisher, in this case

$$(42) \qquad F = (S_o^2 - S_1^2)/\sigma_o^2.$$

When H_o is true and V_o is to be chosen F should be a small number. When H_o is not true and V_1 is to be chosen, F should be a big number. We can decide what is a big or a small number according to the following.

Considered as a random variable, F has the F-distribution of Snedecor with d.f. $1:f$ (practically $1:\infty$). For a given confidential probability P or level of significance $\alpha = 1-P$, like $P = 95\%$ or $\alpha = 5\%$, we can find a critical value F_{crit}. Then we can accept that the computed F is big or small if

$$F \geq F_{crit} \quad or \quad F < F_{crit} \tag{43}$$

respectively.

A practical inconvenience is that through F we can easily compare only two variants. When we have to use many variations in the model function it becomes rather complicated the comparison of all variants, two by two.

Much more comfortable way to choose the optimum variant is the Akaike's Information Criterion (AIC) (Sakamoto, Ishiguro & Kitagawa, 1986) which has also a serious theoretical background. It can be computed after

$$AIC = \tilde{n} \log 2\pi + \tilde{n} \log \sigma^2 + \tilde{n} + 2(\tilde{m} + 2) \tag{44}$$

where $\tilde{n}$ is the total number of the data, $\tilde{m}$ is the total number of all unknowns (including the drift ones) and $\sigma^2$is the estimate of the variance. As an optimum variant can be accepted the case with the lowest computed (observed) AIC.

In the practical application of M92 the program search automatically the minimum of AIC for every Δ_i. If the minimum is found for the variant $v_i = v'$, then the quantity F is computed for the variants

$$F_1 \text{ for } (v'-1, v') \quad \text{and} \quad F_2 \text{ for } (v', v'+1). \tag{45}$$

We have a confirmation of the solution taken on the basis of AIC if F_1 is a big number and F_2 - a small number, in the sense discussed above.

7. Separation of the main tidal groups.

In M67, as well as in the earlier methods of Lecolazet, Doodson-Lennon and Pertsev, there is a separation of the D and SD tides at the same stage as the elimination of the drift. More concretely, in M67 this means that in every interval of 48 hours the filters for the SD tides eliminate the D tides and the filters for the D tides eliminate the SD tides.

This is reasonable as far as there are variable meteorological waves, S_1 with period 24^h and S_2 with period 12^h.

In M92 a similar option is included in the following way for the separation of the SD tides from the S_1 D tide in every Δ_i.

Optionally, we can set up

$$(46) \qquad p_{t1} = c_{S_1}(t) \quad \text{and} \quad p_{t2} = s_{S_1}(t)$$

where c and s are the functions (8) computed for the S_1 tidal group. Then p_{to} is kept as before, after (11), but the other polynomial terms are shifted as

$$(47) \qquad p_{3k} = (t-T_i)^1, \; p_{4k} = (t-T_i)^2, \; \ldots$$

Then, following just the same algorithm, together with the drift elimination, we get an elimination of the S_1 tide when SD tides are determined. Just in the same way, by replacing S_1 by S_2 in (46), we can get an elimination of S_2 when the D tides are determined.

Thus, in addition to the variants with different power for the drift, we get the variants with and without elimination of the S_1 or S_2 tide.

8. Practical application and some results.

M92 and the corresponding computer program has been applied on two series of data:

LAN - gravity observations by an LCR gravimeter installed in the volcanic geodynamic station Cueva de los Verdes in Lanzarote and

BRU - gravity observations with a superconducting gravimeter in Brussels (Observatoire Royal de Belgique).

It has to be immediately declared that the "first" hypothesis, made in paragraph 1 has not been justified. It appeared practically impossible, i.e. absolutely inefficient, the approximation of the drift in very large time intervals. Generally, when the drift was approximated in longer intervals we used to get higher variances (mean square errors).

This is a conclusion made through the analyses of the whole series. For a graphic demonstration we have used two pieces of monthly series without gaps:

LANM: 1000 hourly ordinates of LAN, Figures 3.a, 4.a and 5.a

BRUM: 770 hourly ordinates of BRU, Figures 3.b, 4.b and 5.b.

The units used on the plots are : abscissa - time in hours, ordinate - gravity in 0.1 μgal.

On Fig. 3 the drift D is approximated through a single polynomial of a fixed power $v = 4$, without the variation discussed in Paragraph 6. We see important residuals r which are evidently auto-correlated. There is, possibly, a deterministic signal in the r.

On Fig. 4 we see the approximation of D in LANM and BRUM again by a single polynomial but this time the power v is allowed to vary. The optimum power v' is selected automatically through the AIC criterion. The resulted v' is: for LANM $v' = 17$ and for BRUM $v' = 8$.

Here is a more complicated estimated $\tilde{D}$ which is charged by a part of the residuals from the case $v = 4$ on Fig.3. The residuals have a lower level but still important correlation, better seen for BRUM.

The comparison between Fig. 3 and 4 shows the importance of the variation of the power v as well as that the statistical criterion runs well, at least not too badly.

At the last Fig. 5, we have an approximation of D in intervals of 48 hours, in a way like in M67, with a variation of the power v for every interval. An interesting numerical result is that for the whole series LAN and BRU we have got the following mean values of the optimum powers

LAN: mean $v' = 1.71$, BRU: mean $v' = 2.44$.

Thus, somewhat unexpectedly, D in BRU has a more complicated behaviour than in LAN. This can be seen from the plotted curves of the estimated $\tilde{D}$.

Now we have a much lower level of the r with a much less evident correlation, for both LANM and BRUM.

Nevertheless, from the study of r for the whole series LAN and BRU, we have stated that the auto-correlation does not disappear totally.

On Fig. 6 we have the estimated auto-correlation of R for BRU when the intervals of the approximation are of length $n = 36 = \text{const}$. The picture is quite similar for $n = 48$ and much less favorable for higher values of n.

Here we see that we have an improvement of the auto correlation if the S_1 tide is removed (when SD are determined). This is an indication that the auto correlated noise has really a meteorological origin. Nevertheless, with or without the elimination of S_1, we have a non-negligible auto-correlation. This may affect considerably the estimates of the precision. Namely, we can expect lower estimated variances (mean square errors σ) than the actual ones.

Generally, one way to avoid a correlated noise of meteorological origin, is to incorporate meteorological data in the analysis. This problem needs deeper consideration and we shall not discuss it here.

Tables 1 and 2 represent the results for LAN and BRU respectively from the application of M67 and M92.

In all cases we have lower σ for M92 compared to M67. The ratio between σ for the two methods, grossly estimated, is

$$\begin{aligned} \sigma(\text{M67})/\sigma(\text{M92}) \cong 3{:}2 \text{ for } & \text{LAN, SD tides} \\ & \text{LAN, D tides} \\ & \text{BRU, SD tides} \\ \cong 4{:}1 \text{ for } & \text{BRU, D tides} \end{aligned}$$

even higher than 4:1 in the last case.

The ratio 3:2 is not too big and, with some optimism, we can believe that we have a real raise of the precision due to a new powerful technique of the analysis. However, 4:1 is a too big ratio, too beautiful, to be true.

When these results are interpreted it is necessary to take into account that in M92 we have not a separate estimation of the precision as in M67. For the computation of σ and its interpretation a very important condition is the independence of the errors ε, i.e. the assumption that ε is a white noise. If actually this condition is not observed, it is possible M92 to provide lower σ, in particular for the D tides.

One should think carefully what is better - to have lower or higher estimates of the precision. When the computed σ are lower than the actual errors we can be mislead to make interpretations and conclusions going too far. When the computed σ are higher we are prevented from this but some details in the results can escape from our attention.

Anyway, our final conclusion is that M92 can be a good numerical and mathematical tool for the analysis of the Earth tide data. However, it should be used carefully, in parallel with other methods, e.g. M67. What seems quite certain, M92 can procure a rather good and detailed description of the drift function. The latter can be useful for studying problems of the non-tidal Earth deformations.

Acknowledgments

This work has been done in the Institute of Astronomy and Geodesy in Madrid. One of the authors (A.P.Venedikov, Institute of Geophysics, Sofia) has been supported by the Sabbatical Program of the University Complutense of Madrid.

The data from the suppercondictive gravimeter has been kindly offered by Prof. P.Melchior and Dr. B.Ducarme from the Belgian Royal Observatory.

REFERENCES:

Chojnicki, T., 1973. Ein verfahren zur Erdgezeitenanalyse in Amlehnung an das Prinzip der kleinsten Quadrate, *Mitt. Inst. Theoretische Geodäsie Univ. Bonn,* Nr 15.

Horn, W., 1959. The harmonic analysis, according to the least square rule, of tide observations upon which an unknown drift is superposed, *Third Int. Symp. Earth Tides, Trieste,* p. 218.

Ishiguro, M., Akaike, H.,Ooe, M., & Nakai, S., 1983. A Bayesian approach to the analysis of Earth tides, *Proc. 9th Int. Symp. Earth Tides,* New York 1981, Schweizerbart'sche Verlangsbuchhandlung, Stutgart, pp. 283-292.

Jentzsch, G., 1977. The analysis of tidal constituencies by selective filtering, *8th Int. Symp. Earth Tides, Bonn.*

Melchior, P., 1978. The tides of the planet Earth, *Pergamon Press,* Chapter 7, pp. 161-191.

Melchior, P., Venedikov, A.P., 1968. Derivation of the wave M3 (8^h279) from the periodic tidal deformation of the Earth, *Physics Earth Plan. Interiors,* vol 1, pp. 363-372.

Sakamoto, Y., Ishiguro, M., Kitagawa, G., 1986. Akaike Information Criterion statistics, D. Reidel Publ. Company, KTK Scientific Publishers/Tokyo, Chapter 8, p. 172.

Schüller, K., 1977, Tidal analysis by the Hybrid Least Squares frequency domain convolution method, *8th Int. Symp. Earth Tides, Bonn.*

Tamura, Y., 1987. A harmonic development of the tide-generating potential, *Bull. d'Inform. Marées Terrestres,* Nr 99, pp. 6813-6855.

Tamura, Y., Sato, T., Ooe, M., & Ishiguro, M., 1991. A procedure for tidal analysis with a Bayesian information criterion, *Geophys. J. Int.,* 104, pp. 507-516.

Venedikov, A.P., 1961. Application à l'analyse harmonique des observations des marées terrestres de la Méthode des moindres carrées, *C.R. Acad. Bulg. Sci., v. 14, No 7,* pp. 671-674.

Venedikov, A.P., 1966. Une méthode pour l'analyse des marées terrestres, à partir d'enregistrements de longueurs arbitraires, *Acad. Roy. Belg., Bull. Cl. Sci., LII,* pp. 437-459.

Venedikov, A.P., 1984. Analyse des enregistrement des marées terrestres, *Bull. d'Inform. Marées Terrestres,* Nr 92, pp. 6078-6120.

Xi Quinwen, 1985. The algebraic deduction of harmonic development for the tide-generating potential with the IBM-PC, *Proc. 10th Int. Symp. Earth Tides, pp. 481-490.*

06/10/92 15.12

Fig. 1.a

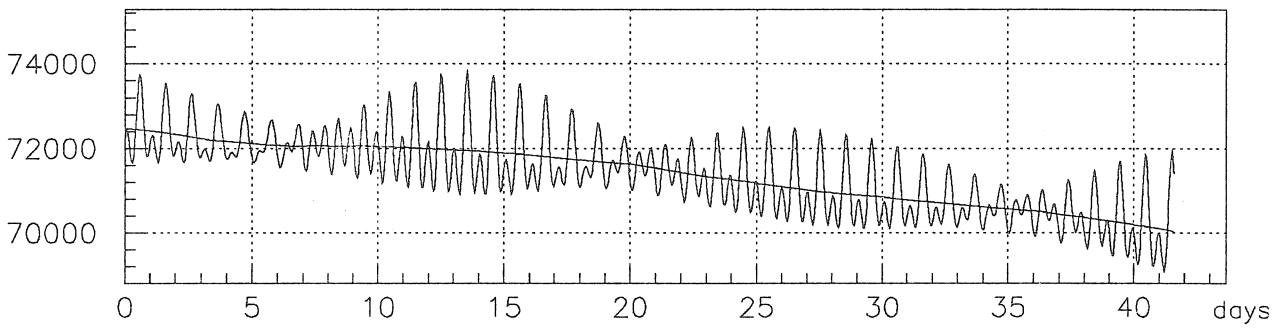

Observed tidal variations of the gravity with a drift

Fig. 1.b

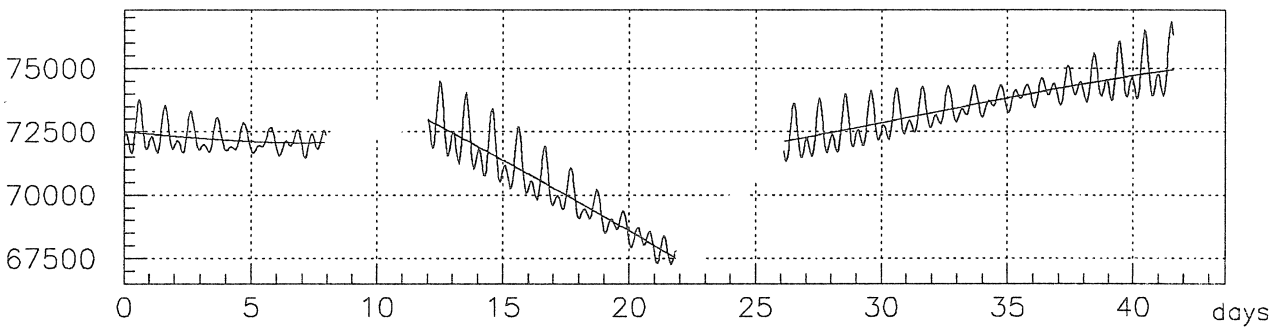

Observed tidal variations of the gravity with gaps and irregular drift
unit = 0.1 microgal

Figure 1

Fig. 2.

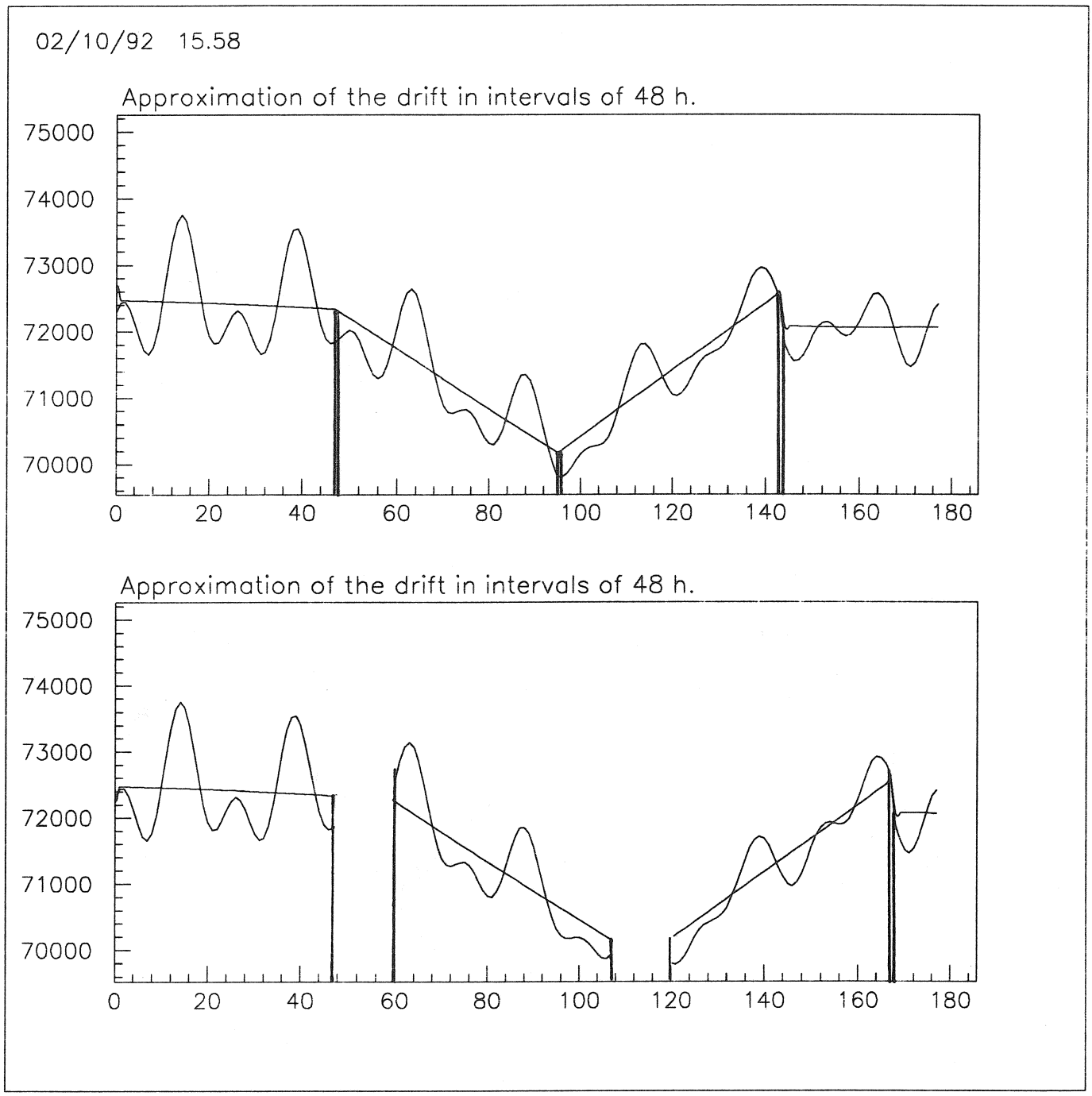
02/10/92 15.58
Approximation of the drift in intervals of 48 h.
75000
74000
73000
72000
71000
70000
0
20
40
60
80
100
120
140
160
180
Approximation of the drift in intervals of 48 h.
75000
74000
73000
72000
71000
70000
0
20
40
60
80
100
120
140
160
180

Fig. 3.a

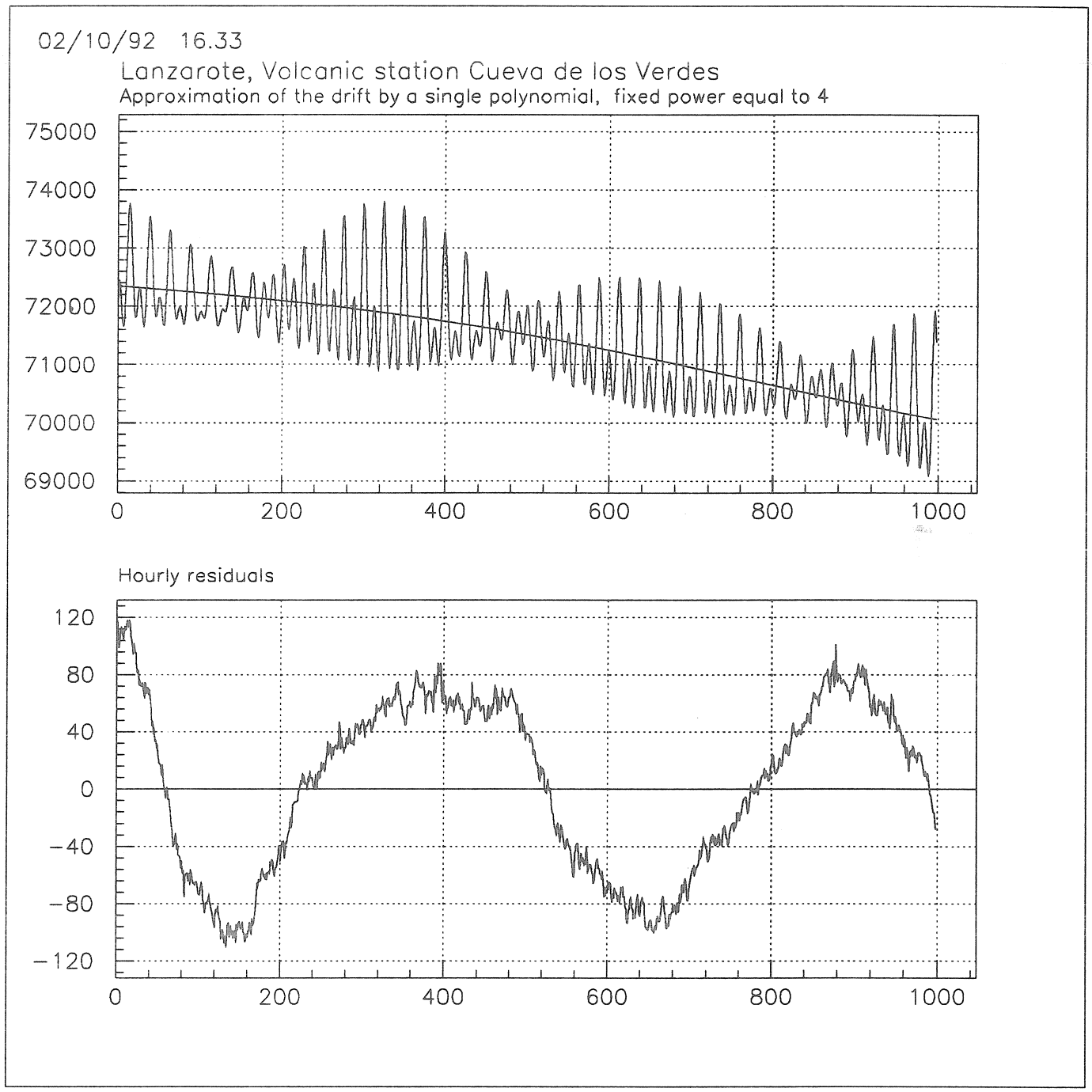
02/10/92 16.33
Lanzarote, Volcanic station Cueva de los Verdes
Approximation of the drift by a single polynomial, fixed power equal to 4
75000
74000
73000
72000
71000
70000
69000
0
200
400
600
800
1000
Hourly residuals
120
80
40
0
-40
-80
-120
0
200
400
600
800
1000

Fig. 3.b

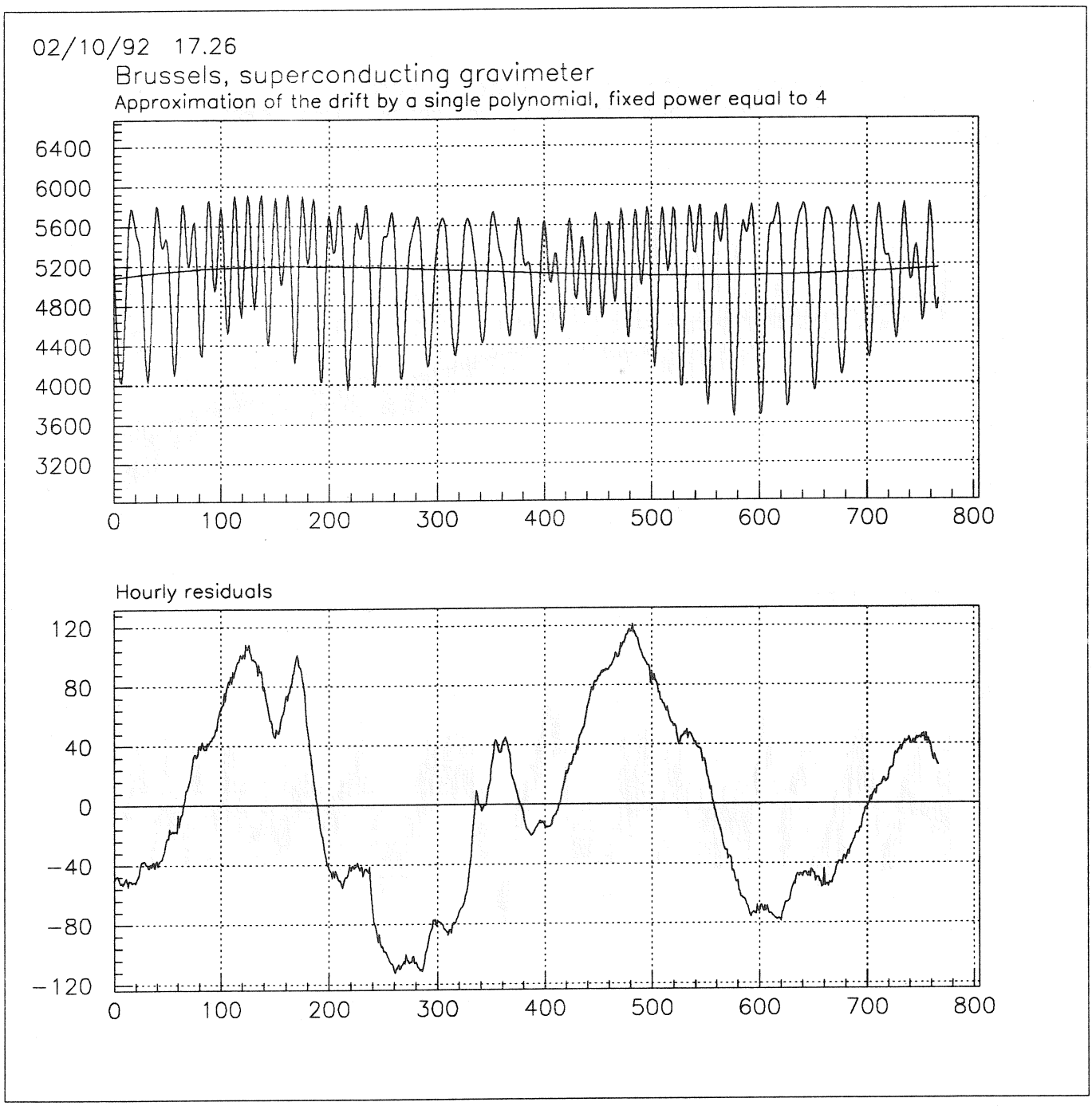
02/10/92 17.26
Brussels, superconducting gravimeter
Approximation of the drift by a single polynomial, fixed power equal to 4
6400
6000
5600
5200
4800
4400
4000
3600
3200
0
100
200
300
400
500
600
700
800
Hourly residuals
120
80
40
0
−40
−80
−120
0
100
200
300
400
500
600
700
800

Fig. 4.a

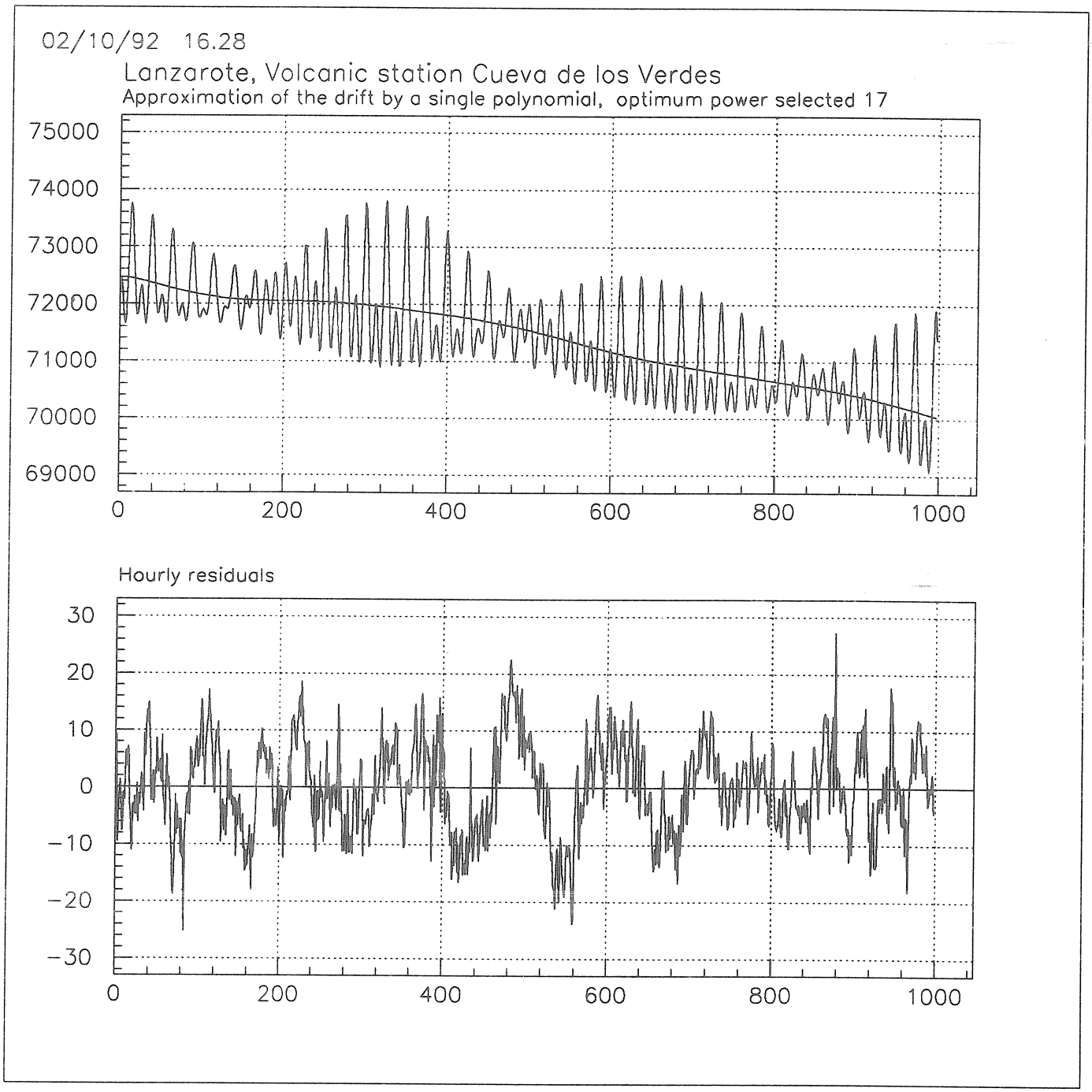
02/10/92 16.28
Lanzarote, Volcanic station Cueva de los Verdes
Approximation of the drift by a single polynomial, optimum power selected 17
75000
74000
73000
72000
71000
70000
69000
0
200
400
600
800
1000
Hourly residuals
30
20
10
0
-10
-20
-30
0
200
400
600
800
1000

Fig. 4.b

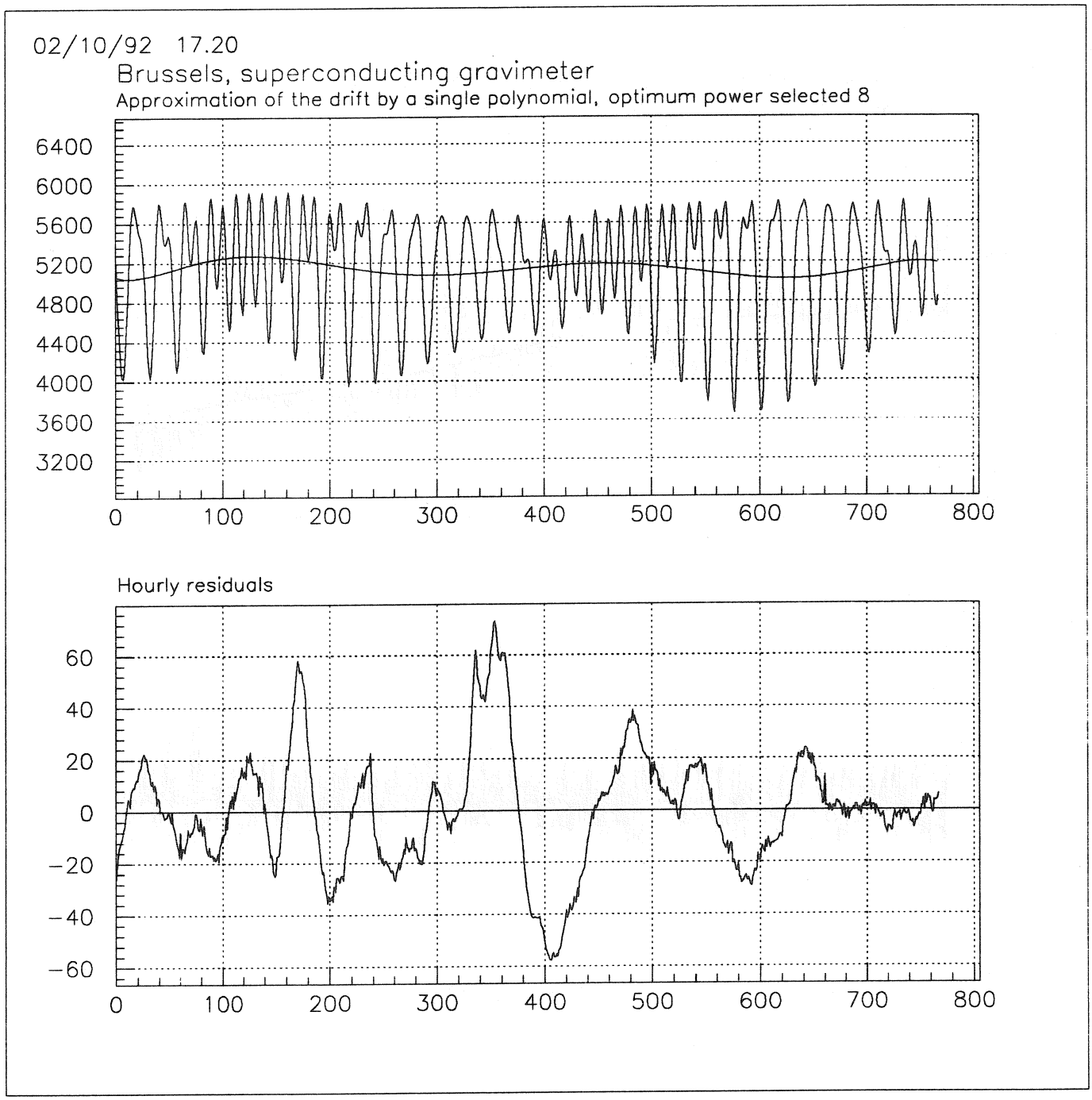
02/10/92 17.20
Brussels, superconducting gravimeter
Approximation of the drift by a single polynomial, optimum power selected 8
6400
6000
5600
5200
4800
4400
4000
3600
3200
0
100
200
300
400
500
600
700
800
Hourly residuals
60
40
20
0
−20
−40
−60
0
100
200
300
400
500
600
700
800

Fig. 5.a

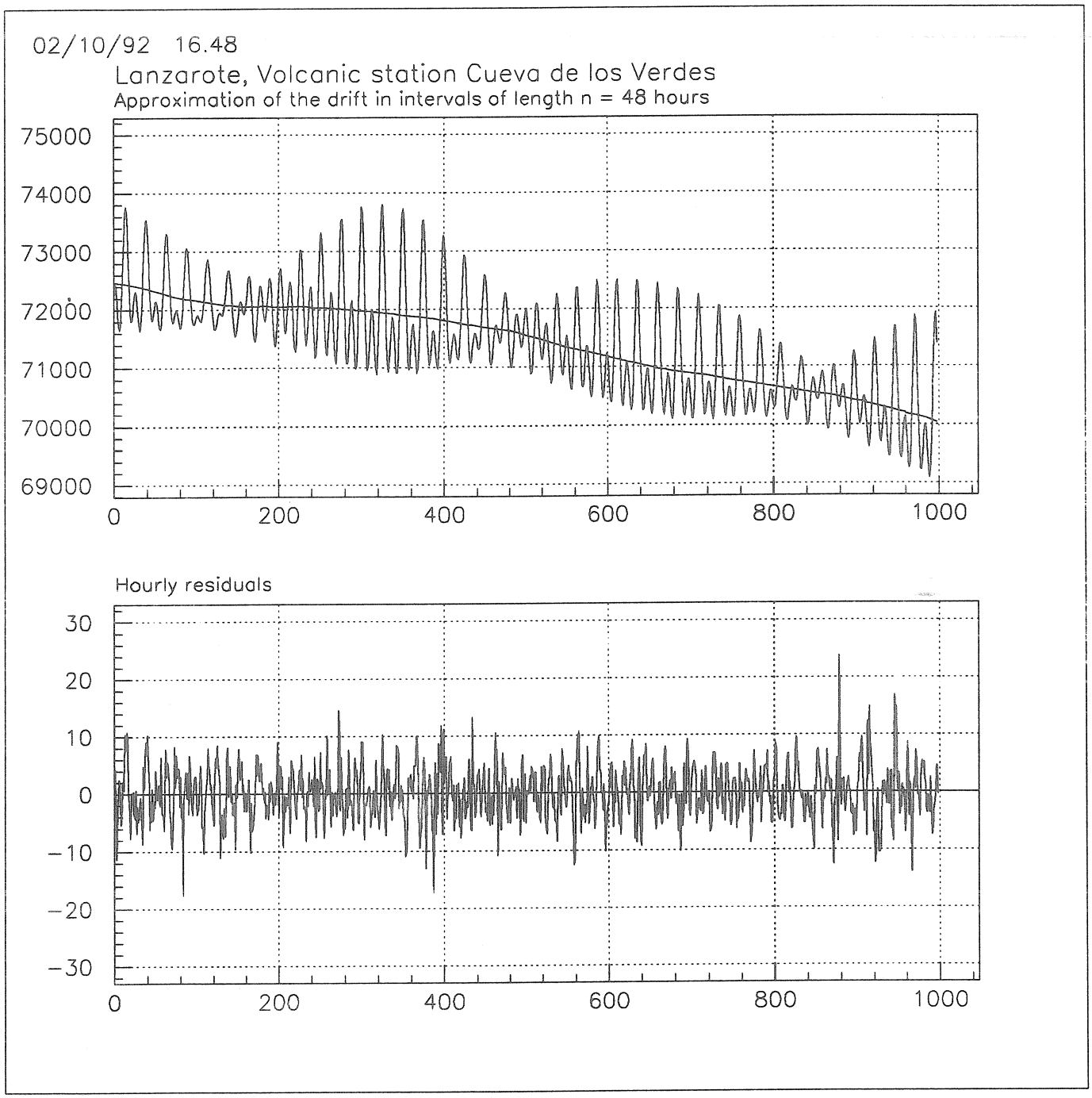
02/10/92 16.48
Lanzarote, Volcanic station Cueva de los Verdes
Approximation of the drift in intervals of length n = 48 hours
75000
74000
73000
72000
71000
70000
69000
0
200
400
600
800
1000
Hourly residuals
30
20
10
0
−10
−20
−30
0
200
400
600
800
1000

Fig. 5.b

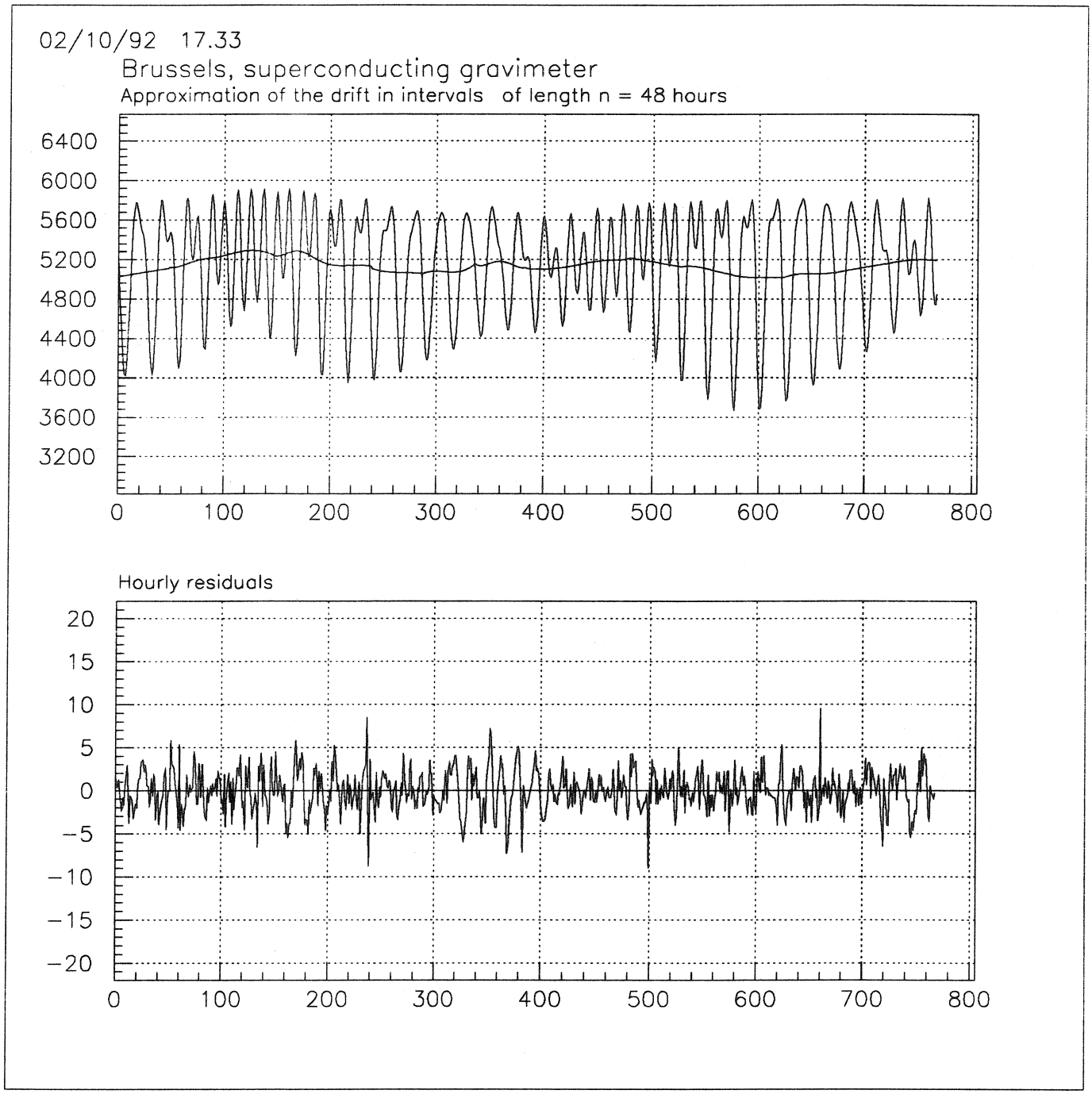
02/10/92 17.33
Brussels, superconducting gravimeter
Approximation of the drift in intervals of length n = 48 hours
6400
6000
5600
5200
4800
4400
4000
3600
3200
0
100
200
300
400
500
600
700
800
Hourly residuals
20
15
10
5
0
−5
−10
−15
−20
0
100
200
300
400
500
600
700
800

Fig. 6.

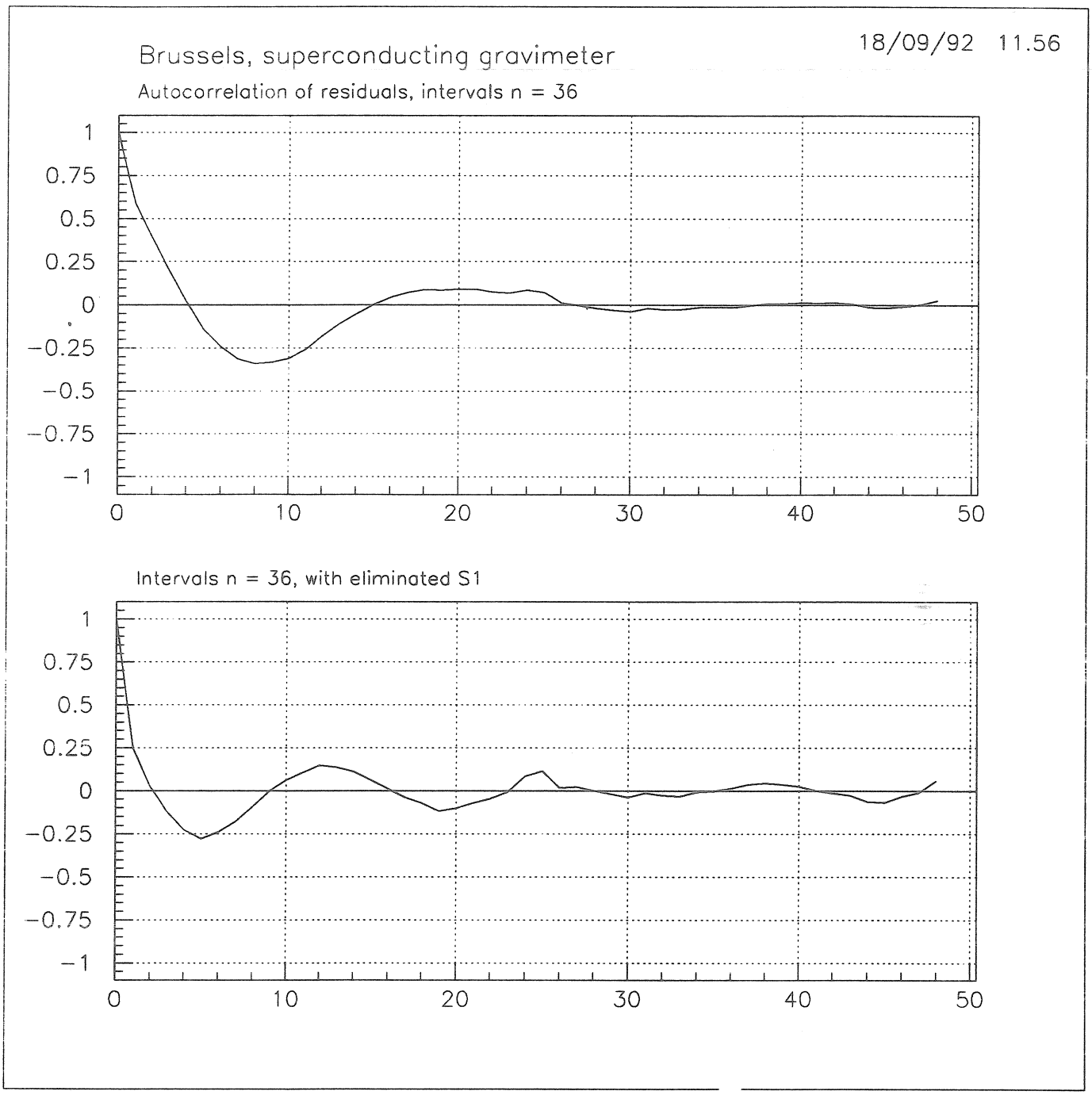
Brussels, superconducting gravimeter
18/09/92 11.56
Autocorrelation of residuals, intervals n = 36
1
0.75
0.5
0.25
0
−0.25
−0.5
−0.75
−1
0
10
20
30
40
50
Intervals n = 36, with eliminated S1
1
0.75
0.5
0.25
0
−0.25
−0.5
−0.75
−1
0
10
20
30
40
50

TABLE 1

Lanzarote, volcanic station Cueva de los Verdes, gravimeter LCR

Time interval: 87.05.14./91.06.12.
Comparison between the methods of analysis M67 and M92.
University Complutense of Madrid, computer VAX 9000
Length of the intervals for the approximation of the drift n = 48h

D tides	amplit. factor δ		phase shift κ	
	M92	M67	M92	M67
σQ_1	1.2059 ± 413	1.3036 ± 772	6°.283 ±1.954	0°.552 ±3.389
$2Q_1$	1.2528 132	1.2637 237	-1.410 605	-1.660 1.074
σ_1	1.2097 110	1.2433 195	1.090 519	0.602 898
Q_1	1.1823 18	1.1831 30	-2.136 84	-2.202 146
ρ_1	1.1527 93	1.1600 158	-2.709 460	-1.021 781
O_1	1.1500 3	1.1500 6	-1.684 16	-1.661 38
τ_1	1.2057 345	1.0330 574	-6.299 1.643	-1.009 3.184
NO_1	1.1535 40	1.1488 66	-0.699 198	-0.355 327
χ_1	1.1585 220	1.0993 360	1.648 1.088	0.577 1.873
π_1	1.1519 143	1.0995 231	2.809 709	0.834 1.205
P_1	1.1321 8	1.1320 14	0.215 42	0.191 69
S_1	0.7495 509	0.9180 843	24.29 4.087	11.00 5.259
K_1	1.1172 3	1.1166 4	0.205 12	0.201 21
ψ_1	0.9763 340	1.0261 552	-18.11 1.998	-9.869 3.081
φ_1	1.1162 200	1.0877 325	5.329 1.023	5.413 1.711
ϑ_1	1.2279 222	1.1430 363	-3.738 1.038	0.190 1.818
J_1	1.1486 42	1.1494 69	1.251 212	0.467 346
SO_1	1.2429 245	1.1122 405	0.800 1.131	-0.626 2.084
OO_1	1.1681 53	1.1507 88	0.367 261	0.786 440
ν_1	1.1686 265	1.1166 451	2.550 1.303	0.655 2.317

SD tides	amplit. factor δ		phase shift κ	
	M92	M67	M92	M67
ε_2	1.0529 ± 210	1.0792 ± 390	-8°.862 ±1.142	-6°.847 ±2.069
$2N_2$	0.9630 67	0.9888 118	-2.000 397	-2.022 684
μ_2	0.9958 57	0.9836 100	-4.360 327	-3.782 582
N_2	0.9960 9	0.9970 15	0.780 51	0.855 88
ν_2	0.9963 48	1.0008 81	1.472 276	1.251 462
M_2	1.0179 18	1.0173 3	2.167 9	2.160 16
λ_2	1.0571 239	1.0765 381	3.832 1.295	1.997 2.029
L_2	1.0666 61	1.0677 96	3.368 325	4.114 518
T_2	1.0368 63	1.0424 98	5.838 346	4.863 541
S_2	1.0689 4	1.0677 6	4.001 19	3.991 31
K_2	1.0594 11	1.0583 17	3.795 58	3.862 91
η_2	1.0947 167	1.0712 261	5.606 871	4.800 1.393
$2K_2$	1.1023 413	1.0810 651	0.499 2.147	2.447 3.451
M_3	1.1018 103	1.0958 76	1.697 537	1.757 396

TABLE 2

Brussels, superconducting gravimeter, P.Melchior, B.Ducarme.

82.04.21/82.05.24 82.06.02/86.10.14 86.11.15/87.11.25
Comparison between the methods of analysis M67 and M92.
Un versity Complutense of Madrid, computer VAX 9000
Length of the intervals for the approximation of the drift n = 48h

D tides	amplit.factor δ		phase shift κ	
	M92	M67	M92	M67
σQ_1	1.2745 ± 105	1.2575 ± 487	-0.°262 ± 470	-0.°332 ±2.219
$2Q_1$	1.1611 33	1.1642 150	-1.749 162	-1.885 737
σ_1	1.1540 27	1.1524 122	-1.181 134	-1.152 608
Q_1	1.1605 4	1.1603 19	-0.469 20	-0.473 093
ρ_1	1.1644 22	1.1769 98	-0.647 108	-0.780 477
O_1	1.1630 08	1.1634 3	-0.088 3	-0.086 17
τ_1	1.1415 73	1.1026 319	-1.948 366	-5.174 1.660
NO_1	1.1668 10	1.1682 42	0.844 47	0.717 208
χ_1	1.1779 51	1.1710 225	0.481 250	-0.292 1.102
π_1	1.1830 32	1.1856 138	0.503 151	0.169 668
P_1	1.1643 19	1.1648 8	0.150 9	0.152 40
S_1	1.3160 112	1.3218 494	-4.203 498	-5.406 2.141
K_1	1.1505 06	1.1505 3	0.147 2	0.142 12
ψ_1	1.2509 76	1.2740 332	0.596 345	-0.125 1.491
φ_1	1.1928 44	1.1848 193	0.675 210	0.494 933
ϑ_1	1.1470 51	1.1540 226	-1.133 254	-0.988 1.124
J_1	1.1671 10	1.1651 44	0.557 47	0.504 214
SO_1	1.1220 57	1.1309 257	0.974 290	0.917 1.304
OO_1	1.1748 13	1.1805 60	-0.033 65	0.133 294
ν_1	1.1666 66	1.1755 311	0.314 326	0.253 1.515

SD tides	amplit.factor δ		phase shift κ	
	M92	M67	M92	M67
ε_2	1.1307 ± 98	1.1463 ± 180	3.°420 ± 494	3.°341 ± 900
$2N_2$	1.1473 32	1.1494 55	2.324 157	2.444 276
μ_2	1.1946 26	1.1981 46	4.365 126	4.150 219
N_2	1.1767 4	1.1770 7	2.807 20	2.821 34
ν_2	1.1776 22	1.1760 37	2.672 107	2.807 180
M_2	1.1950 08	1.1949 1	2.482 3	2.481 6
λ_2	1.1492 109	1.1432 174	3.062 544	3.571 870
L_2	1.1952 22	1.1946 34	1.565 104	1.592 165
T_2	1.2081 29	1.2091 45	1.224 138	1.134 215
S_2	1.2141 17	1.2143 3	1.123 8	1.133 12
K_2	1.2118 5	1.2112 8	1.216 25	1.208 39
η_2	1.1868 89	1.1806 139	0.424 430	0.967 672
$2K_2$	1.2348 224	1.2420 350	-2.993 1036	-2.165 1.614
M_3	1.0751 64	1.0781 59	0.620 342	0.824 312

FRAMET, a Data Preparatory Program for ETERNA 2.0 Version.

GY. Katona
Geodetic and Geophysical Research Institute
Hungarian Academy of Sciences
H-9401 Sopron
POB 5
Hungary

The main goal of the **FRAMET** program is to give a good tool to the users of **ETERNA** 2.0 (Wenzel, 1991) for data-preparation. This interactive, menu guided, user-friend, graphical program is suitable for checking, scanning and modifying of your observed tidal data and its parameters in ETERNA-format.

Advantages of the **FRAMET** program

1. Input of **ETERNA**-format (international) data file by blocks

The **FRAMET** program gives a list of the data files (in **ETERNA** 2.0 version defined format with blocks in international format) and reads the chosen block from the chosen data file.

2. Plotting the whole dataset and any part of it on the EGA screen

The **FRAMET** program plots the whole dataset in the upper section of the screen and a part being in the moving window in the lower section.

3. Scanning the dataset part by part, point by point, date by date

The user can change the length and the step of the window and move it on the dataset. The chosen part of the dataset is plotted by using two kinds of enlargement. With cross-hairs the user can scan and if necessary modify the dataset point by point.

4. Search of raw errors and jumps in the dataset

The **FRAMET** program searches the raw errors and jumps (above a limit defined by user) by algorithms of Lecolazet (1959, 1961) and plots the wrong part of the dataset in lower section of the screen.

5. Cutting the wrong part from the dataset with graphical help

The begining and ending part of the dataset can be cut by the user with a moving line in the upper part of the screen.

6. Modification and elimination of raw errors and jumps with graphical help

In the error searching case the error curve of the section is also shown and the FRAMET program offers a possibility for the modification. In the case of searching step-funtion the FRAMET program eliminates the jump automatically unless the user forbids it.

7. Computing and eliminating the drift by Pertsev-filter

The FRAMET program computes the drift by algorithm of Pertsev (1957) and plots it on the screen together with the original dataset. It is possible to subtract the drift from the dataset.

8. Drift scanning and modifying

The user can scan and modify the drift similarly to the dataset process.

9. Computing power spectrum

The FRAMET program computes the power spectrum of the dataset or the drift by Fourier Transform.

10. Plotting and scanning the power spectrum

The computed power spectrum is plotted on the screen. The user can change the view-window of the spectrum.

11. Checking the dates

There is an option for checking the dates of the chosen dataset based on the first date. If there are some wrong dates the FRAMET program will correct them.

12. Modification of the ETERNA 2.0 version input parameters

There are many input parameters of the ETERNA 2.0 version: kinds of filter, printing parameters, wave-group limits etc. These parameters can be changed in a table by an option of the program .

13. Calling the ETERNA 2.0 version

The user can run the ETERNA 2.0 program from the FRAMET program.

14. Saving the modified dataset, drift and spectrum

The user can save the modified dataset and drift in many way: by overwriting the original file block, by saving into a new file or into TAPE5 (ETERNA input file), by saving the drift into a new file or overwriting the original one. The peaks of the chosen part of the power spectrum can be saved in the option of power spectrum plotting.

15. Possibility of return to FRAMET

After the running of ETERNA 2.0 program the user may return to FRAMET from DOS with EXIT command.

Using of the program is very simple, controlled by ENTER, ESC, F1, PgUp, PgDn, End, Home, +, -, and curzor moving keys.
These features ensure that your dataset-file being full of jumps, raw data and typing errors can be modified and corrected in a comfortable way by FRAMET program.
If you are interested in the FRAMET program, please send a letter to the above mentioned adress and we will send you a detailed user's guide and the FRAMET program floppy.

References

Lecolazet,R.: Sur l'estimation des erreurs internes affectant les résultats d'une analyse harmonique mensuelle, BIM No 17.,269-278.,1959.

Lecolazet,R.:Sur la reconstitution des observations par l'interpolation, IV.me Symp. Int. Marrées Terr. Comm. Obs. Royal Belgique No 188, Sér. Géoph. No 58., 267-272., 1961.

Pertsev,B.P.:On the Calculation of the Drift Curve in Observations of Bodily Tides. BIM No 5., 71-72., 1957.

Wenzel, H.:Earth Tide Analysis Program System ETERNA, "Readme.1st" of the distributed floppy, 1991.

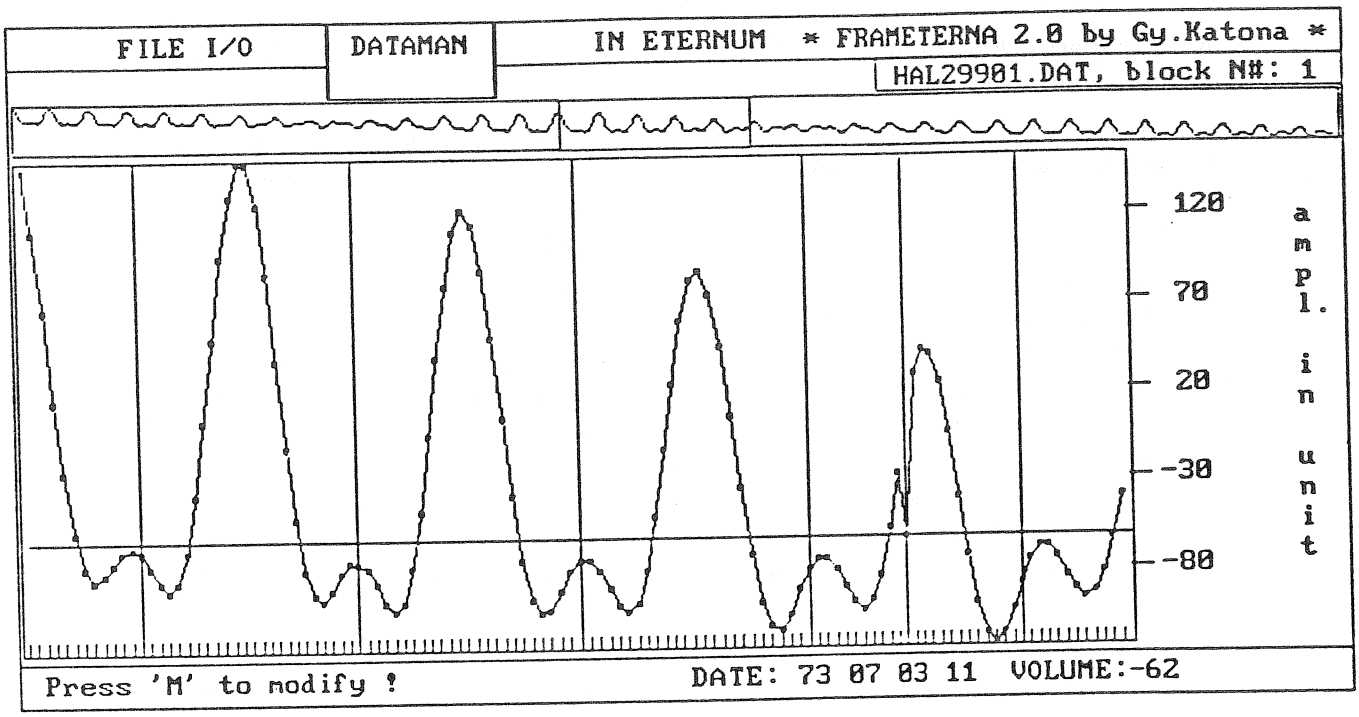

A screen copy of data scanning option of the FRAMET program

Analysis of the Superconducting Gravimeter Data Outside the Tidal Frequency Band: Around the 50 Day and the 14hr Periods.

Defraigne P., Billiau A., Collin F., Ducarme B., Dehant V.
Royal Observatory of Belgium
Avenue Circulaire, 3
B-1180 Brussels
Belgium

Abstract

In this paper, we perform spectral analyses on the gravity variation measurements obtained with the superconducting gravimeter installed at the Royal Observatory of Belgium since 1982. Using a new spectral analysis method, the Wavelet Transform, which is compared with the classical Fast Fourier Transform, we look separately at the time evolution of the spectrum around the 50 day and the 13.9hr periods.

On the one hand, we show that the 50 day fluctuation which is well known in Earth's rotation and solar activity can also be detected in the superconducting gravimeter data of Brussels. From the comparison with other geophysical spectra, it is demonstrated that the time evolution of this fluctuation in the gravity data is related to the one found in the other data sets and particularly in the local atmospheric pressure, as it is shown in Defraigne et al. (1992). This suggests, as we mentioned, that the origin of this fluctuation can be found in the atmospheric loading, ignoring or not the ocean response.

On the other hand, we confirm the existence of the 13.9hr period identified by Melchior and Ducarme (1986) in the power spectrum of the superconducting gravimeter data of Brussels, and which they interpreted as a normal mode of the Earth's core, excited by strong and deep earthquakes. In Dehant et al. (1992), we show that the epochs when the peak appears do not correspond with the occurrences of earthquakes so that its origin, as proposed by Melchior and Ducarme, is probably not correct. Billiau (1992) reconfirms this by using the wavelet transform analysis. For this reason, we looked for other origins of the excitation of the gravity spectrum between the semi-diurnal and diurnal tidal bands. The comparison between the spectrum of the superconducting gravimeter data with pressure and oceanic spectra shows a good correlation between the time of occurrence of the episodic perturbations of the spectrum. This has been shown using moving window spectral analysis (Dehant et al., 1992) as well as using wavelet transform analysis (Billiau, 1992).

1 Introduction

The 50 day period is a well known geophysical period. Since several years, it has retained the attention of many authors: Feissel et al. (1980) identified it in the Earth's rotation (ΔUT1), Langley et al. (1981) found a similar fluctuation in the polar component of the atmospheric angular momentum (AAM), and several authors confirmed the existence of this fluctuation. Djurovic and Pâquet (1988 and 1991) analysed solar activity and geophysical observation series which all exhibited the same spectral behaviour around the 50 day period. They attributed the origin of this fluctuation in Earth's rotation to the solar activity: the role of the interplanetary magnetic field in the transmission of the fluctuation to the Earth's rotation could be very important, but the mechanism remains uncertain.

The second subject on which we focus concerns the 13.9 hour peak, identified by Melchior and Ducarme (1986) in the super conducting gravimeter data after some deep earthquakes. The peaks found by Melchior and Ducarme (1986) were interpreted, at that time, as normal modes of the Earth's core. Indeed, core undertones for a rotating, homogeneous, stratified fluid in a spherical container exhibit periods in that frequency band (see Aldridge and Lumb, 1987 or Melchior et al. 1989). The most general theoretical solutions for a spheroid of arbitrary ellipticity filled completely with fluid, was obtained by Kudlick (1966, see also Guo, 1991). Another important fact is that the 13.9 hr peak observed at Brussels after the Hindu Kush earthquake was not detected by the superconductiong gravimeter of Bad Homburg in Germany at 320 kilometers from Brussels (Zürn et al., 1987). This could be explained by trapping of core normal mode waves in some regions of the core, and thus, the energy measured at the surface would be higher or lower over regions where they are respectively trapped or not. But Bad Homburg is so close to Brussels that this explanation would be not plausible.

In a previous paper (Dehant et al., 1992), we reanalyse the Brussels data in order to verify the existence of those particular peaks and search for other possible explanations of their presence. We have shown in this paper that whatever spectral analysis method is used, the existence of the 13.9 hr peak in the Brussels superconducting gravimeter data is confirmed and is not an artefact. Concerning its origin, we have shown that the peak can appear before an earthquake or in a period during which no strong and deep or very strong earthquake occurs; in other cases no peak at all appears although a strong and deep earthquake occurred. Hence it appears that there is no direct relation between earthquake occurrences and energy in the spectrum between the semi-diurnal and diurnal frequencies. Rather we think that the origin of such harmonic energy in the superconducting gravimeter data could be related to a regional effect, not yet taken into account in the computation of the tidal residues; the moving window spectral analysis also indicates that in Brussels the spectra of the gravity, atmospheric pressure and Ostend sea level data are correlated and for example, simultaneously perturbed in November each year. In the present paper, we will reconfirm all these results and we will show that this correlation ocean-pressure-gravity is not only in the frequency band between diurnal and semi-diurnal tides.

In order to study the two ranges of periods in the superconducting gravimeter data of Brussels, we use a new spectral analysis method : the wavelet transform (WT). The WT is a time and frequency analysis which allows us to trace the temporal evolution of the periods detected in a signal. We also compare the results with those obtained on the

one hand by the classical fast Fourier transform (FFT) which gives only a global spectral contents of the analysed data set. On the other hand, we will apply moving window Fourier transforms and compare the results with those obtained by WT.

In Section 2, we present the theoretical background of the wavelet transform. In Section 3, we describe the data and the data reduction. In Section 4, we analyse the superconducting gravimeter data with both WT and FFT. We present, in Section 5, a comparison between the spectra of the superconducting gravimeter data and other geophysical observation series. For the 50 day period, we also compare the gravity spectrum with spectra of data related to solar activity. Finally, in Section 6, we discuss the results and present conclusions.

2 The Wavelet Transform

2.1 Definition

The WT is a new spectral analysis method which gives the time evolution of the frequencies contained in the signal. The wavelet transform of a signal $s(t) \in L^2(R, dt)$ is given by:

$$S(a,b) = \int_{-\infty}^{+\infty} s(t)\, \overline{g_{ab}(t)}\, dt \qquad \text{with} \qquad g_{ab}(t) = C\ g\left(\frac{t-b}{a}\right) \tag{1}$$

where:

- C is a normalization factor which must be chosen equal to a^{-1}, $a^{-\frac{1}{2}}$ or 1. Usually, one takes a^{-1}, respectively 1, to better detect the high, respectively low, frequencies. In this work we use, as a compromise, $C = a^{-\frac{1}{2}}$.
- $g(t)$ is the analysing wavelet. It satisfies the following conditions:
  - $\star$ $g \in L^1 \bigcap L^2(R, dt)$;
  - $\star$ g must be localized in time. Therefore, its Fourier transform, $\hat{g}$, is localized in the frequency domain;
  - $\star$ $\hat{g}(\omega)$ must be real and must satisfy the inequality $\int \frac{|\hat{g}(\omega)|^2}{|\omega|} d\omega < \infty$. The latter condition implies that $\hat{g}(0) = 0$, so g has a zero mean;
  - $\star$ $\hat{g}(\omega) = 0 \ \ \forall \omega \leq 0$, i.e. g is a progressive wavelet.
- $a > 0$ is the scale parameter.
- $b \in R$ represents the time.

One can easily show that expression (1) is similar to :

$$S(a,b) = \int_{-\infty}^{+\infty} \sqrt{a}\ \overline{\hat{g}(a\omega)}\ \ \hat{s}(\omega)\ \ e^{i\omega b}\, d\omega \tag{2}$$

which relates the wavelet transform to the Fourier transform.

2.2 Intuitive Approach

The wavelet transform (WT) of a signal corresponds to its projection on a wavelet family $(g_{ab})_{a>0,b\in R}$. Because the mean of the analysing wavelet is zero, the WT can be considered as a time and scale filter; this is explained in the following example.

At times b and b', we superpose the wavelet dilated by a scale factor a on the signal $s(t)$ (Fig. 1). We then compute the scalar product between the signal and the wavelet to obtain the WT (Fig. 2). At time b, the product $s(t)\ g_{ab}(t)$ is positive everywhere, the integral (1) gives therefore a large $S(a,b)$. At time b', the coefficient $S(a,b')$ can be expressed by:

$$S(a,b') \simeq M \int g_{ab'}(t)dt$$

where M is a constant factor, so that $S(a,b')$ is nearly zero.

Consequently, when the signal is almost constant with respect to the wavelet, the WT is negligible. When the signal vibrates at the same frequency as the wavelet, the WT is significantly more important.

2.3 Analysing Wavelet

To perform this analysis, we will use Morlet's wavelet which can be expressed as:

$$g(t) = e^{i\omega_0 t}\ e^{-t^2/(2\sigma_0^2)} - \sqrt{2}\ e^{-(\omega_0\sigma_0)^2/4}\ e^{i\omega_0 t}\ e^{-t^2/\sigma_0^2} \qquad (3)$$

The real part of Morlet's wavelet is illustrated on Figure 3. The second term in the right-hand side of (3) is a corrective term added in order to have a wavelet mean equal to zero; this term is negligible when $(\omega_0\,\sigma_0) > 5$. Morlet's wavelet is therefore a gaussian function, of width at half maximum proportional to σ_0, modulated at the frequency ω_0 and to which a corrective term is added. Usually ω_0 is taken equal to 5.336 and σ_0 to 1, so that the corrective term becomes negligible. The width of the wavelet is determined by the parameter σ_0: the closer the frequencies we want to distinguish are, the larger σ_0 must be. This is illustrated on Figures 4 and 5. More details on wavelets can be found in Antoine (1992), Billiau (1992), Combes et al. (1990), Daubechies (1990) and Meyer (1991).

3 Data and Data Reduction

We use gravity measurements obtained with the superconducting gravimeter installed at the Royal Observatory of Belgium (in Brussels). The instrument has been continuously operating since 1982 except during one month, from 15.10.86 to 15.11.86, for which we interpolate in order to get a longer series. The data we analyse are either hourly data (for the 13.9hr period) or daily means (for the 50 day period) obtained from the recordings as follows: the hourly data are corrected for the local atmospheric pressure by the impulse response relation (Ducarme et al., 1987):

$$a(t) = -0.2628\ p(t)\ -\ 0.0779\ p(t-1)\ -\ 0.0167\ p(t-2)$$

where $a(t)$ is the correction at the instant t for the local atmospheric pressure p measured at times t, $t-1$, $t-2$. The units are chosen so that if the pressure is in *mbar*

($1mbar = 100Pa$), the correction is expressed in μgal ($1\mu gal = 10nms^{-2}$). This formula was obtained by adjusting simultaneously tidal and pressure input signals to gravity data (De Meyer and Ducarme, 1987). The data corrected for the local atmospheric pressure in the time domain are then corrected for the tides using an extended tidal potential of 1200 terms (Tamura, 1987). The resulting residues are expressed in $0.01\mu gal$. Daily means (if necessary) are computed after the application of a Pertzev filter (Pertzev, 1957) in order to avoid aliasing. The effects of polar motion and instrumental drift (De Meyer and Ducarme, 1991) are subtracted from the data, but they do not provide any significant change in the spectrum around the 50 day period or in the sub-daily period range. Outside these frequency bands there exists an annual term clearly dominating in the resulting signal. Fluctuations of this peak could provide harmonics in the vicinity of the 50 day period. We present in Figure 6 the different steps of the latter data reduction and the corresponding spectra obtained by a classical FFT.

4 Analysis of the Superconducting Gravimeter Data

4.1 Around the 50 day period

In this section, we apply the wavelet analysis described in the second paragraph to the daily means of the superconducting gravimeter data and we compare our results to those obtained with a classical FFT. We perform the analysis on the data set of the epoch from 15.10.83 to 10.06.88 in order to avoid artefacts due to the discontinuities at the beginning and at the end of the observed signal (boundary effects). Because we only want to obtain the spectrum around the 50 day period, we look at the frequency band between 30 and 100 days. For other frequency bands, see for example Antoine et al. (1992). We use Morlet's wavelet with $\omega_0 = 5.336$ *cycle/day* and $\sigma_0 = 4.5$ *days*. This value of σ_0 allows us to separate a 50 day period from a 45 day period.

Several periods can be pointed out in the modulus of the WT (Figure 7). First, two periods are observed: a 62 and a 45 day period. They are probably harmonic terms of the annual fluctuation. Furthermore, they are not constant with time and do not always appear at the same frequency. Besides these peaks, the 50 day period can be identified with the following characteristics: the peak is visible at the beginning of the analysed series and it decreases after some months until it disappears. From the graph, the evolution of the peak with time might also be interpreted in another way: the peak, after its obvious presence in the beginning of the analysis, may drift in frequency. We use an iterative frequency estimation algorithm based on the fixed point theorem (Seip, 1989 and Guillemain et al., 1989) in order to get a good determination of the periods detected by the WT. We then obtain the frequencies and periods presented in Table 1.

The periods of 68 and 37 days found in the gravity spectrum have already been selected in solar activity and Earth's rotation spectra (Djurovic and Pâquet, 1988) but the 37 day period can also be related to the 10th harmonic term of the annual fluctuation.

One hypothesis for the origin of the 50 day period is that it could be the 7th harmonic term of the annual fluctuation. Nevertheless, in any spectral analysis, the harmonics of a given fluctuation always appear with decreasing amplitudes for increasing order (for even and odd components separately) so that the absence of a 73 day period in the spectrum

(corresponding to the 5th harmonic of the annual fluctuation) pushes us to forsake this hypothesis. We then seek for another origin for the 50 day period.

As we can see in Figure 8, the power spectrum of the superconducting gravimeter data obtained by a classical FFT gives the same periods as the WT, but without any time localization. Such a global analysis gives for the peak an amplitude of 86 ngals. Furthermore, a moving window spectral analysis similary as in Defraigne (1991) can be performed by FFT (Fig. 9); it produces the same characteristics as the WT for the different peaks identified in the spectrum. Nevertheless, the moving window FFT analysis produces a spectrum less precise than the WT. Indeed, the resolution of the FFT in the frequency domain depends on the length of the windows. Then, in order to get the same resolution as for the WT, we need very large windows and thus the time evolution begins later and ends earlier. Consequently one gets much less information on the spectrum evolution than with the WT. In Figures 7 and 9, the number of computed frequencies is respectively 50 for WT and 30 for FFT, and moreover the FFT plot begins 150 days after the one of the WT and ends 150 days earlier, so that the time evolution is 300 days shorter.

4.2 Around the 13.9 hour period

By reanalysing the data, with the WT, in the frequency range between the diurnal and semi-diurnal periods, one can observe (Figure 10) that the peaks behave in the same way as presented in the introduction. The presence of the 13.9hr peak is clear, as already shown in Dehant et al. (1992), but the frequency drift mentionned in this latter paper is not confirmed. In fact, the precise temporal evolution given by the WT let us see that the amplitude of the peak presents a succession of maxima and minima, rather than a frequency drift.

5 Comparison with Other Spectra

5.1 Around the 50 day period

The 50 day period already identified in the Earth's rotation (ΔUT1), in the atmospheric angular momentum, in the interplanetary magnetic field and in other solar activity observation series, is probably transmitted to the Earth's gravity by atmospheric loading. The superconducting gravimeter data have been corrected for local atmospheric pressure effects, but local pressure corrections do not represent the whole atmospheric effect: regional or global effects are not sufficiently accounted for. Consequently, the residues contain remaining atmospheric effects, so that some spectral peaks may have an atmospheric origin. In order to verify this idea we perform a spectral analysis of atmospheric pressure recordings. We find the same 50 day period as in the superconducting gravimeter data (Figures 11 and 12). Moreover, the maximum amplitudes of this peak appear at the same epochs. However, the peak seems to decrease more rapidly in the atmospheric pressure than in the gravity. Furthermore, we have performed another analysis which favours the relation between gravity and global or regional pressure effects at the 50 day period. We performed FFT and WT analyses on the superconducting gravimeter data without local atmospheric pressure correction (Figures 13 and 14). From these figures,

one sees that the amplitude of the peak decreases when local atmospheric pressure corrections are performed. This indicates that the corrections already account for a part of the spectral power at 50 days. Nevertheless the relative amplitudes of the 50 day period with respect to its neighbouring peaks become larger in the case of local atmospheric pressure corrections than in the case of the uncorrected data. This shows that local atmospheric pressure is not as suitable for explaining the 50 day peak as it is for the others. On one hand, the fact that local atmospheric pressure already explains a part of the 50 day peak favours the atmospheric origin for the remaining part. On the other hand, the fact that local atmospheric pressure does not explain the entire amplitude pushes us to think that the remaining part is related to global or regional atmospheric pressure variations.

We then compare the superconducting gravimeter spectrum with other spectra in which the 50 day period has already been identified. So, we perform the analysis of the following data sets :

- Wolf number from 02.06.82 to 31.12.90. It gives the product between the number of sunspots and the number of groups of sunsposts multiplied by ten (dimensionless number) (Koeckelenbergh, 1982 – 1992).

- Corona index of solar activity from 02.06.82 to 31.12.87. It is a numerical expression of the total radiation energy of the corona emission line $530.3nm$ (dimensionless number) (Rybanský, 1988).

- AAM (pressure and wind) from 01.05.83 to 31.12.90. It is the axial component of the atmospheric angular momentum which is involved in the changes of the length of day. This component is partitioned into contributions of pressure and contributions of wind. It is expressed in $10^{26} kgm^2 s^{-1}$ (IERS annual report, 1991).

- Earth's rotation (ΔUT1) from 01.01.67 to 31.12.90. It represents the fluctuation of the Earth's rotation with respect to the International Atomic Time. It is expressed in 10^{-4} seconds (Djurovic et al., 1991).

Comparing all the spectra (Fig. 15 and Fig. 16), we can conclude that the presence and the absence of the 50 day peak coincide. Indeed, the 50 day period appears at the same epoch in every observation series (except for the corona index for which it appears just after it has disappeared in the others). This implies that the 50 day period in the superconducting gravimeter data is most probably related to the same phenomenon as the one involved in the other data sets. These results were deduced from the comparison of the amplitudes of the peaks. We now make a comparison of the values of the period itself in the FFT spectra. Although the 50 day period appears in each plot, its exact period fluctuates between 48 and 53 days. This has already been mentioned by Djurovic and Pâquet (1988) for all the data sets except for the superconducting gravimeter data. The wavelet analysis allows us to show that the peak is indeed not constant in frequency and that it drifts in every spectrum but not exactly in the same way.

5.2 Around the 13.9 hr peak.

The comparison between the WT of gravity, local pressure in Brussels and ocean tide in Ostend (about 100 km far from Brussels), leads to the same conclusions as the comparison

of the same spectra, but computed by using Fourier transforms. There are epochs where local pressure and/or ocean are well correlated with gravity, and other epochs where they are not. As examples, we show firstly, in Figure 17, WT over about one month of pressure data and superconducting gravimeter data, and secondly, in Figure 18, we show WT over about three months of ocean data and superconducting gravimeter data. Both Figures show a good correlation. This reinforces our idea that gravity data corrected for local pressure still contain atmospheric effects which are more global or regional, ignoring or accounting for the oceans.

6 Conclusions

In this paper, firstly the 50 day period which is well known in solar activity and Earth's rotation has also been identified in the superconducting gravimeter data of Brussels. Using a new spectral analysis, the wavelet transform, we get the temporal evolution of this fluctuation in the gravity data and also in the other data sets. The same characteristics can be observed in all the spectra: the epochs of the presence of the 50 day peak and those of its absence coincide. That pushes us to conclude that the 50 day period in the superconducting gravimeter data is most probably related to the same phenomenon as the one involved in the other geophysical data sets. Furthermore, because the 50 day fluctuation is also visible in the local atmospheric pressure and in the atmospheric angular momentum, we attribute its presence in the gravity data to the atmospheric loading (directly (ignoring the ocean), or with the ocean acting as an inverted barometer). Indeed, on one hand, the local atmospheric pressure corrections performed on the superconducting gravimeter recordings do not completely account for regional or global atmospheric effects, and on the other hand, the data are unperfectly corrected for the ocean loading outside the tidal band. This correlation between pressure-ocean and gravity can be extended, as we have secondly shown, in another spectral band. The 13.9 hr peak identified by Melchior and Ducarme in 1986 is no more related to possible core normal modes induced by an earthquake as proposed by these authors, but more probably related to uncorrected regional or global atmospheric effects. These results suggest, firstly to perform a comparison with other superconducting gravimeter data in order to confirm this correlation, and secondly to improve the procedures to correct for regional pressure.

Acknowledgements

Jean-Pierre Antoine by his lectures on wavelets has initiated the idea of using the wavelet transform on geophysical data. He is gratefully acknowledged for the scientific discussions on the mathematics behind the method.

Three of us (P. Defraigne, V. Dehant and B. Ducarme) are supported by the National Fund for Scientific Research (Belgium).

References

- Aldridge, K., and Lumb, I., 1987. Inertial waves identified in the Earth's fluid outer core. Nature, 325: 421-423.

- Antoine, J.-P., 1992. Wavelet analysis in image processing. In: Proc. EUSPICO-92, Brussels, Belgium.

- Antoine, J.-P., Billiau, A. and Collin, F., 1992. Wavelet analysis of geophysical signals. In: Proc. of the Int. Conference on 'Wavelets and Applications', Toulouse, France.

- Billiau, A., 1992. Analyses en ondelettes de données gravimétriques. Mémoire de Licence de l'Université Catholique de Louvain, in French, 91pp.

- Combes, J.-M., Grossmann, A. and Tchamitchian, Ph., 1990. Wavelets, time-frequency methods and phase space. Springer-Verlag, 2d ed., Berlin.

- Daubechies, I., 1990. The wavelet transform, time-frequency localization and signal analysis. IEEE Trans. Inform. Theory, 36: 961 – 1005.

- Defraigne, P., 1991. Analyses spectrales de données du gravimètre à supraconductivité. Mémoire de Licence de l'Université Catholique de Louvain, in French, 117pp.

- Defraigne P., Billiau A., Collin F., Ducarme B., Dehant V., 1992, "50 Day Oscillation in the Superconducting Gravimeter Data of Brussels", submitted to Phys. Earth planet. Inter.

- Dehant V., Ducarme B., Defraigne P., 1992, "New Analysis of the Superconducting Gravimeter data of Brussels", in: Proc. of the Symp. U6 of the 20th General Assembly of the IUGG, Vienna, Austria, 1991, Geophys. Monogr., IUGG/AGU Publ., ed. J.-L. Le Mouël, accepted for publication.

- De Meyer, F. and Ducarme, B., 1987. Input-output of the observations of the superconducting gravimeter. In: R. Vieira and Consejo Superior de Investigationes Cientificas (editors), Proc. of the 10th Int. Symp. on 'Earth tides', Madrid, Spain, 1985: 531 – 554.

- De Meyer, F. and Ducarme, B., 1991. Nontidal gravity changes observed with a superconducting gravimeter. In: J. Kakkuri and E. Schweizerbart'sche Verlagsbuchhandlung (Nägele u. Obermiller) (editors), Proc. of the 11th Int. Symp. on 'Earth tides', Helsinki, Finland, 1989: 167 – 184.

- Djurovic, D. and Pâquet, P., 1988. The solar origin of the 50 day fluctuation of the Earth's rotation and atmospheric circulation. Astron. Astrophys., 204: 306 – 312.

- Djurovic, D. and Pâquet, P., 1991. Variations common to the interplanetary magnetic field, the zonal atmospheric circulation and the Earth's rotation. Q. J. R. Meteor. Soc., 117: 571 – 586.

- Ducarme, B., Van Ruymbeke, M. and Poitevin, C., 1987. Three years of registration with a superconducting gravimeter at the Royal Observatory of Belgium. In: R. Vieira and Consejo Superior de Investigationes Cientificas (editors), Proc. of the 10th Int. Symp. on 'Earth tides', Madrid, Spain, 1985: 113 – 130.

- Feissel, M. and Gambis, D., 1980. La mise en évidence de variations rapides de la durée du jour. C. R. Acad. Sci., Paris, B 291: 271 – 273.

- Guillemain, P., Kronland-Martinet, R. and Martens, B., 1989. Estimation of spectral lines with the help of the wavelet transform; applications in NMR spectroscopy. In: Springer-Verlag, Berlin (editor), Wavelet and Applications: 38 – 60.

- Guo, J., 1991. Les développements analytiques de Kudlik sont applicables au noyau liquide de la Terre. Annex Ph. D. thesis, Université Catholique de Louvain, Louvain-la-Neuve, Belgium, in French, 47 pp.

- Koeckelenbergh., A. and Cugnon, P., 1982–1992. Provisional sunspot number. Sunspot index data center, sunspot bulletin, epoch from 1982 to 1992.

- Kudlik, M.D., 1966. On transient motions in a contained rotating fluid. Ph. D. thesis, M.I.T.

- Langley, R.B., King, R.V., Shapiro, I.I., Rosen, R.D. and Salstein, D.A., 1981. Atmospheric angular momentum and the length of day: a common fluctuation with a period near 50 days. Nature, 294: 730 – 732.

- Melchior, P., and Ducarme, B., 1986. Detection of inertial gravity oscillations in the Earth's core with a superconducting gravimeter at Brussels. Phys. Earth planet. Inter., 42: 129-134.

- Melchior, P., Crossley, D.J., Dehant, V., and Ducarme, B., 1989. Have inertial waves been identified from the Earth's core? Geophys. Monograph, 46 (1), IUGG/AGU Publ., eds. D.E. Smylie and R. Hide: 1-12.

- Meyer, Y., 1991. Wavelets and their applications. Springer- Verlag, Berlin and Masson, Paris.

- Pertzev B.P., 1957. On the calculation of the drift curve in observations of bodily tides. Bull. inf. Marées Terrestres, 5: 71 – 72.

- Rybanský, M., Rušin, V. and Dzifčáková, E., 1988. Coronal index of solar activity, V. Years 1977 – 1986. Bull. astron. inst. Czechosl., 39: 106 – 119.

- Seip, K., 1989. Some remarks on a method for detection of spectral lines in signals. Centre de Physique Théorique de Marseille. Private communication.

- Tamura, Y., 1987. A harmonic development of the tide generating potential. Bull. inf. Marées Terrestres, 99: 6813 – 6855.

- Zürn, W., Richter, B., Rydelek, P.A., and Neuberg, J., 1987. Comments on 'Detection of inertial gravity oscillations in the Earth's core with a superconducting gravimeter at Brussels' by P. Melchior and B. Ducarme. Phys. Earth planet. Inter., 49, (1-2): 176-178.

0.01205 cycle/day	82.9* days
0.01460	68.4*
0.01600	62.4*+
0.01780	56.1
0.01924	51.9*
0.02214	45.1+
0.02375	42.0
0.02693	37.1*+

* found in other series (Figures 15 and 16)
+ even harmonics of the annual period.

Table 1: Frequency and period estimations of the peaks detected in the WT of the superconducting gravimeter data.

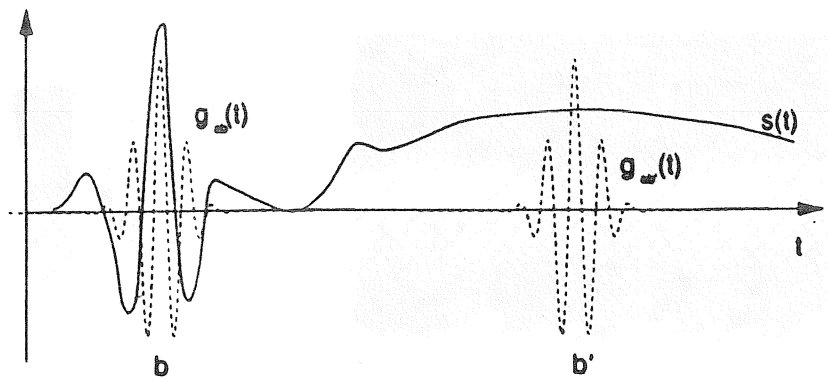

Figure 1: Superposition of the wavelet on the signal at times b and b'.

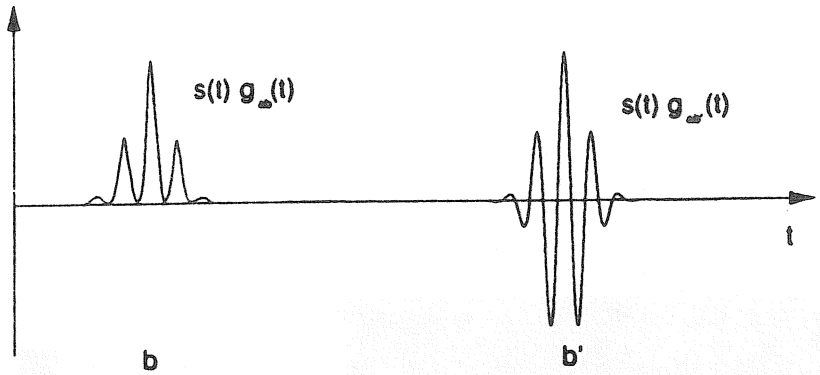

Figure 2: Scalar product between the wavelet and the signal at times b and b'.

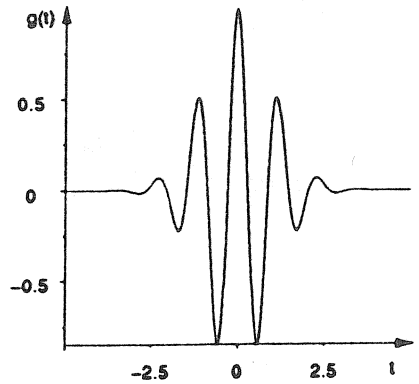

Figure 3: Real part of Morlet's wavelet.

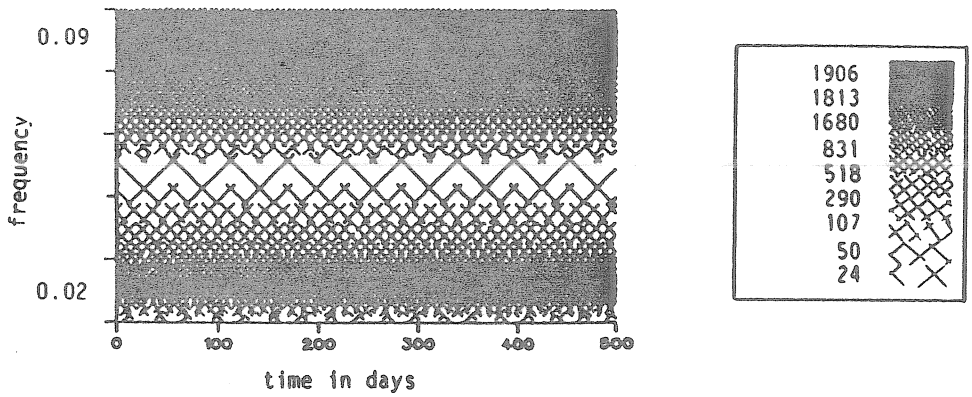

Figure 4: Modulus of the wavelet transform of a bi-harmonic signal. The two frequencies are really different: $\omega_1 = 0.02$ and $\omega_2 = 0.09$. The analysis parameters are $\omega_0 = 5.336$ and $\sigma_0 = 1.0$.

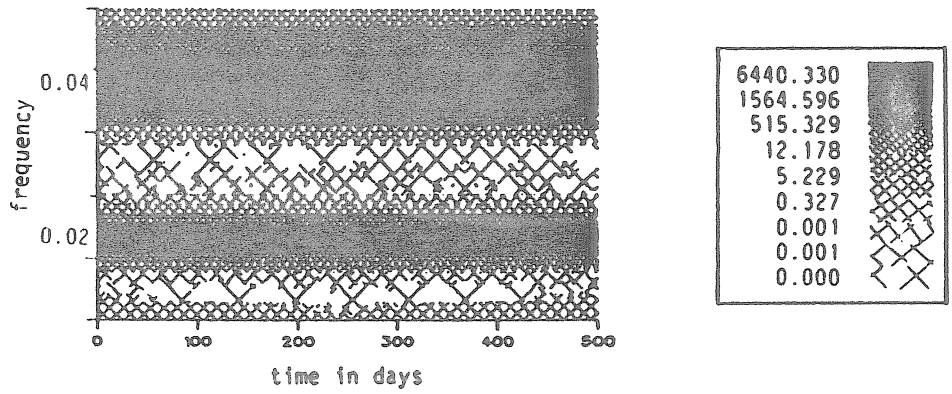

Figure 5: Modulus of the wavelet transform of a bi-harmonic signal. The two frequencies are really close: $\omega_1 = 0.02$ and $\omega_2 = 0.04$. The analysis parameters are $\omega_0 = 5.336$ and $\sigma_0 = 4.5$.

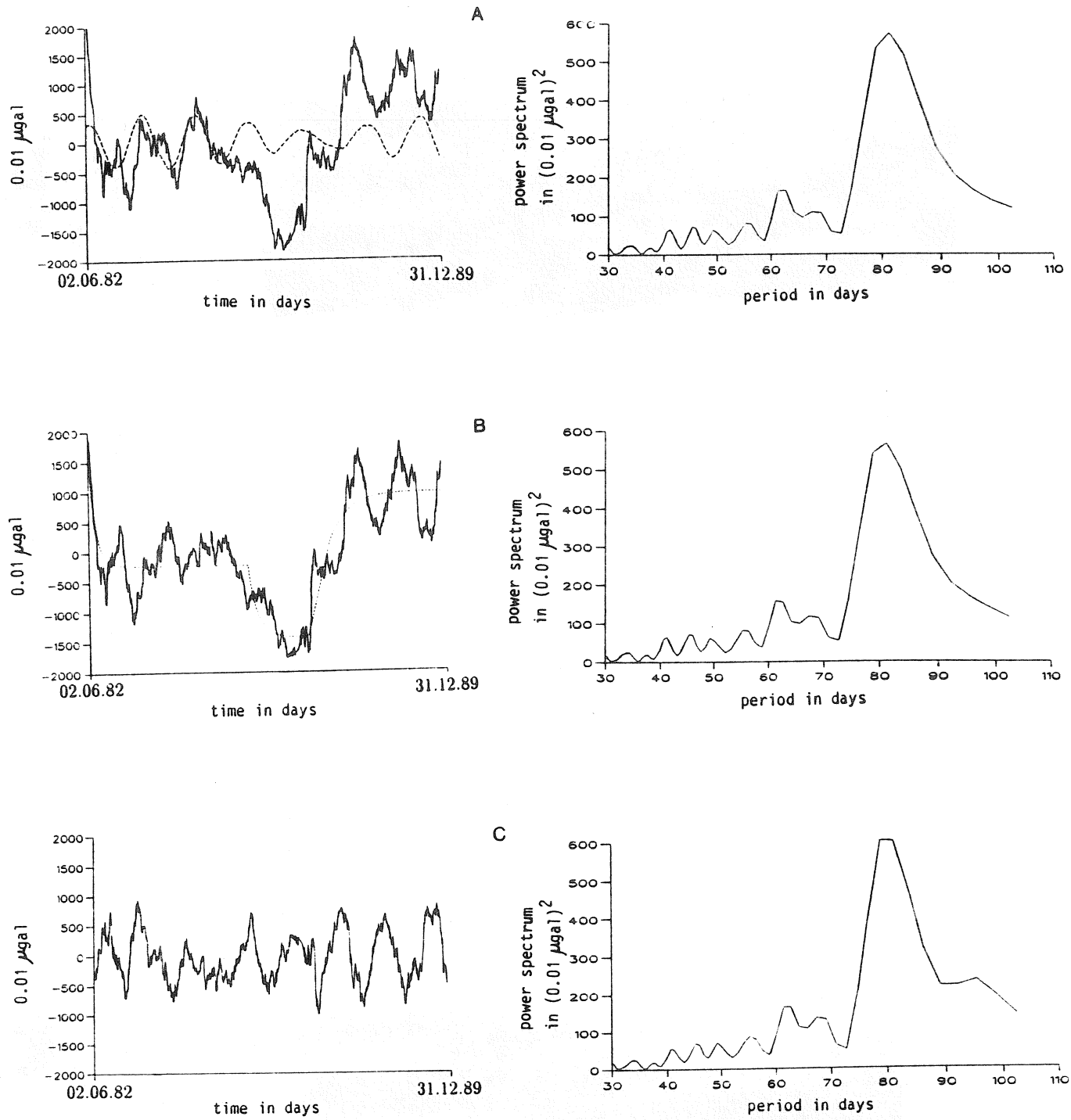

Figure 6: Different steps of the data reduction with the corresponding power spectra. A) —— is the superconducting gravimeter data set only corrected for the local atmospheric effect; - - - is the polar motion. B) —— is the gravity data set corrected also for the polar motion; - - - is the instrumental drift. C) —— is the superconducting gravimeter data set corrected for polar motion and instrumental drift.

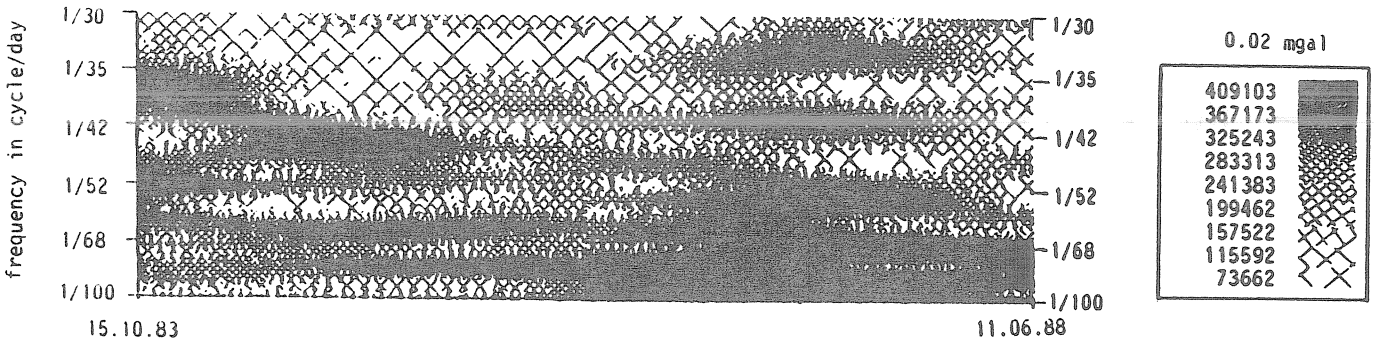

Figure 7: Modulus of the wavelet transform of the superconducting gravimeter data.

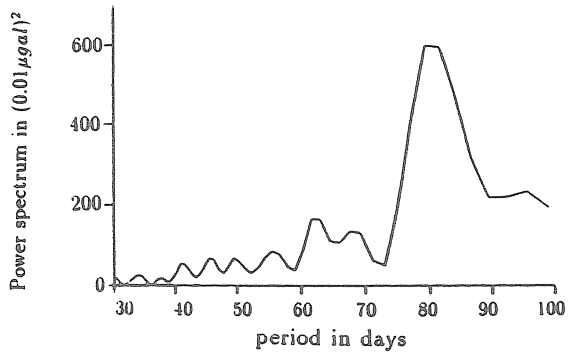

Figure 8: Power spectrum of the superconducting gravimeter data obtained by FFT.

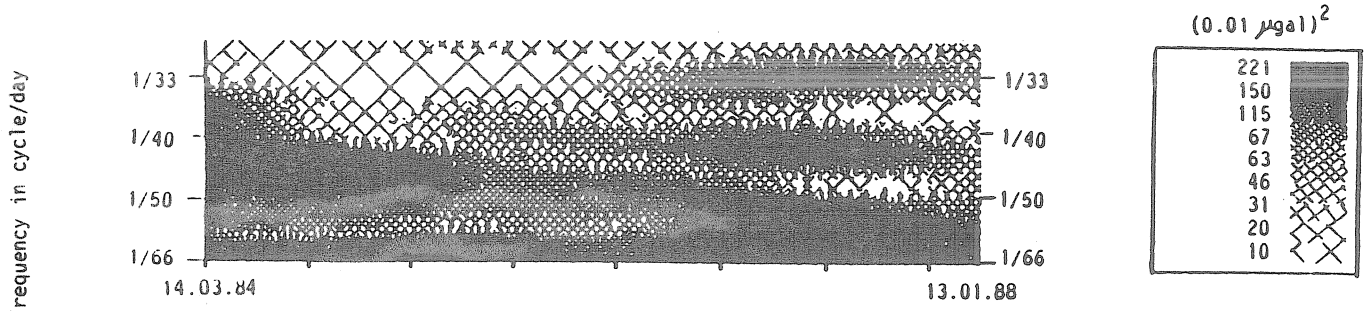

Figure 9: Moving window spectral analysis (FFT) of the superconducting gravimeter data.

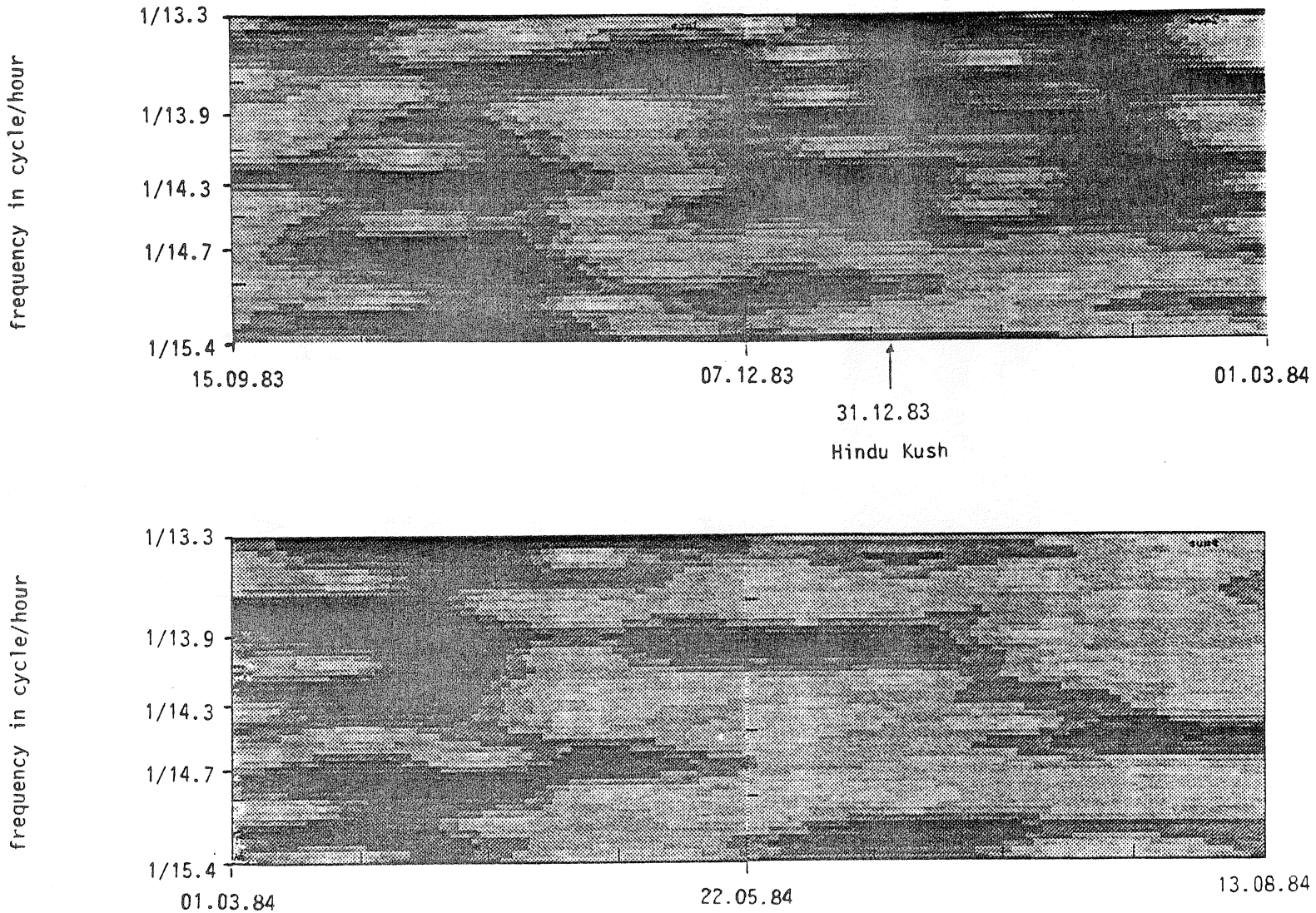

Figure 10: : Modulus of the WT of the superconducting gravimeter data between the diurnal and semi-diurnal frequency bands.

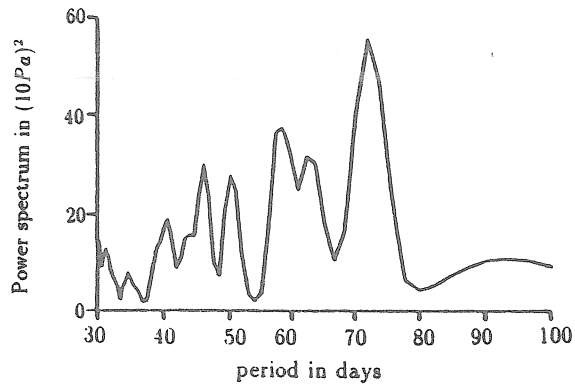

Figure 11: Power spectrum of the local atmospheric pressure in Brussels obtained by FFT.

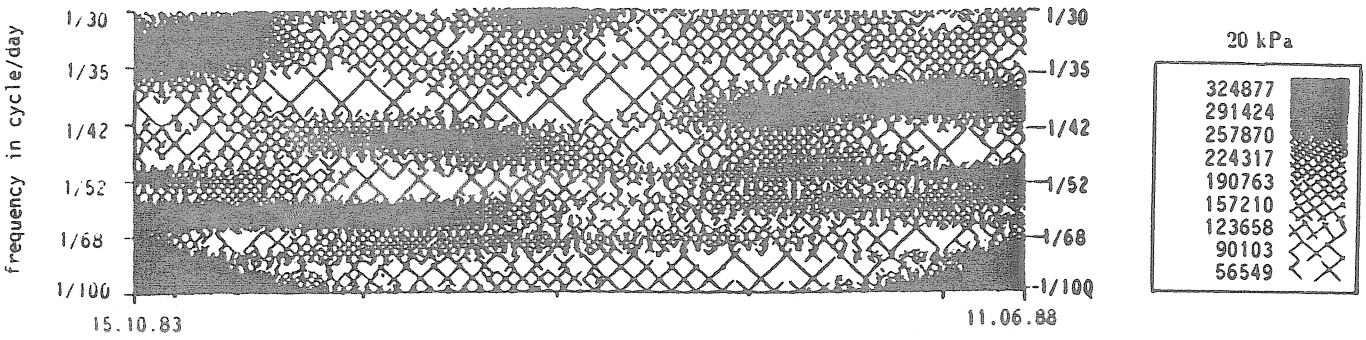

Figure 12: Modulus of the WT of the local atmospheric pressure in Brussels.

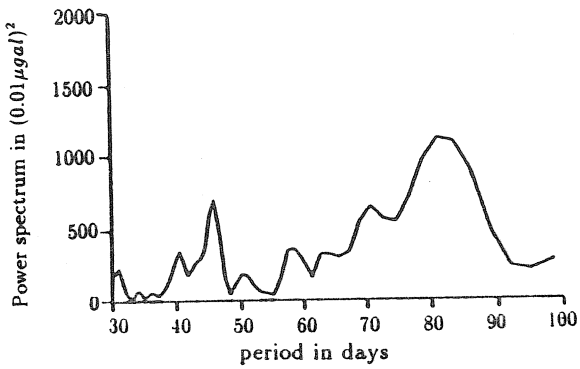

Figure 13: Power spectrum of the gravity data without local atmospheric pressure correction obtained by FFT.

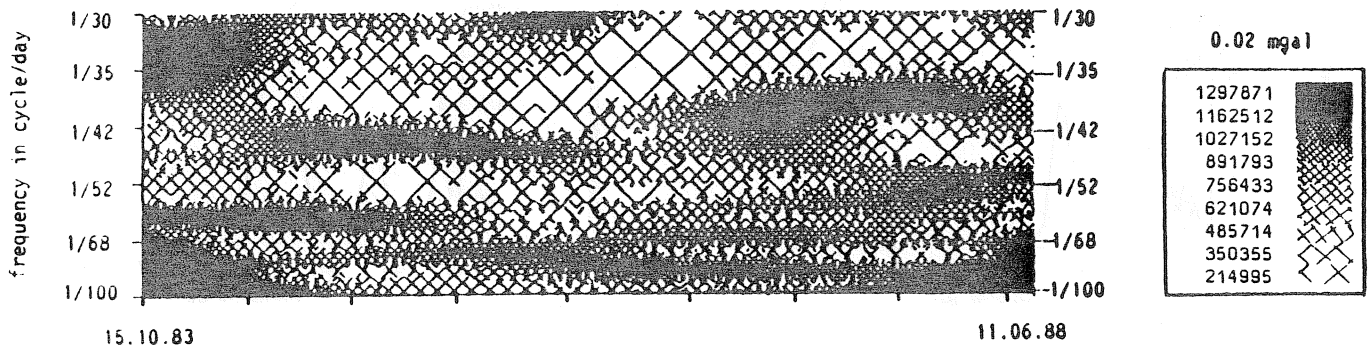

Figure 14: Modulus of the WT of the gravity data without local atmospheric pressure correction.

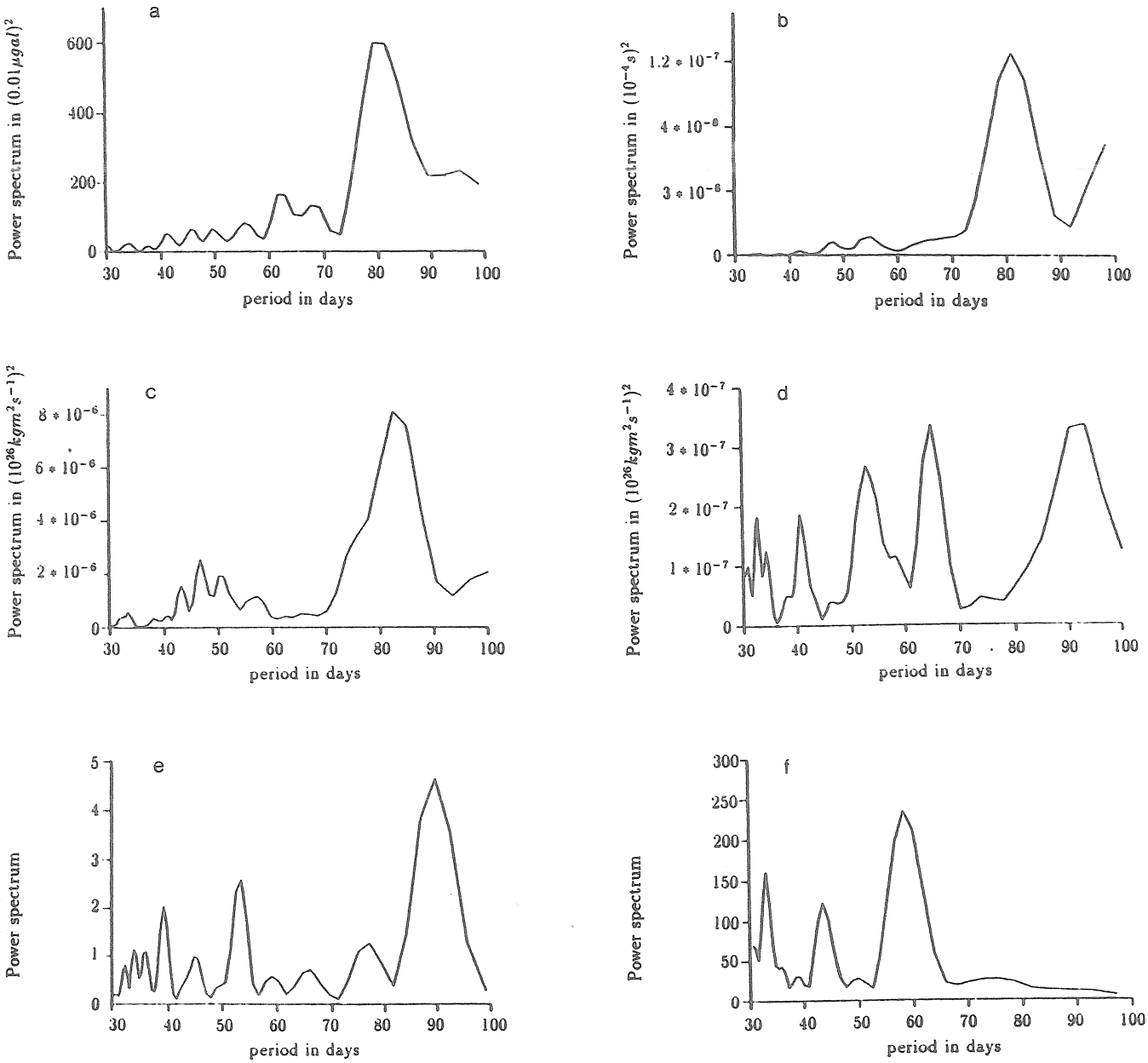

Figure 15: Power spectrum obtained by a classical FFT of a) the superconducting gravimeter data, b) the Earth's rotation (ΔUT1), c) the AAM wind component, d) the AAM pressure component, e) the Wolf number, f) the corona index of the solar activity.

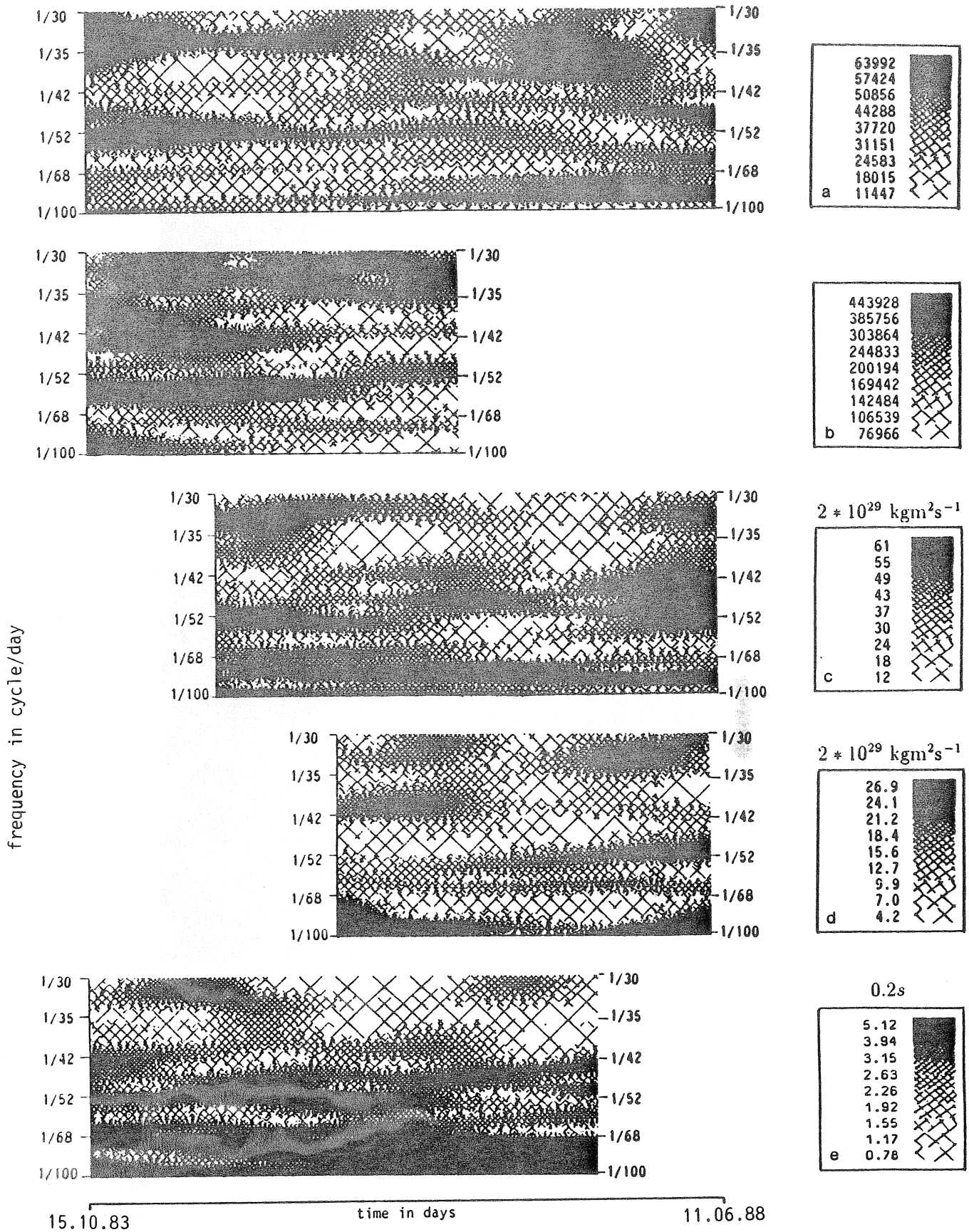

Figure 16: Modulus of the WT of a) the Wolf number, b) the corona index of the solar activity c) the AAM wind component, d) the AAM pressure component, e) the Earth's rotation (ΔUT1).

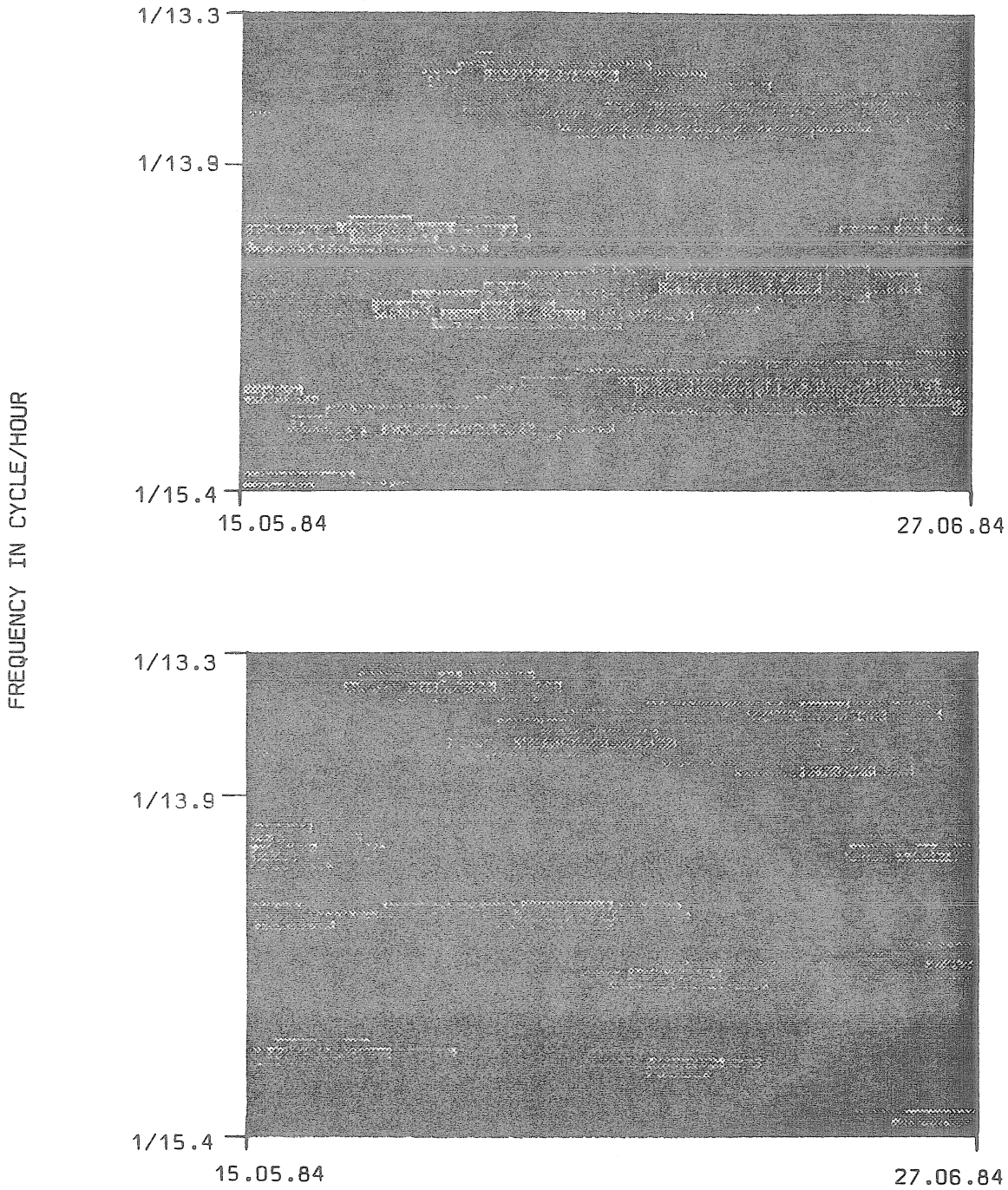

Figure 17: Modulus of the WT, between the diurnal and semi-diurnal frequency bands, of (a) the superconducting gravimeter data, and (b) the local atmospheric pressure in Brussels.

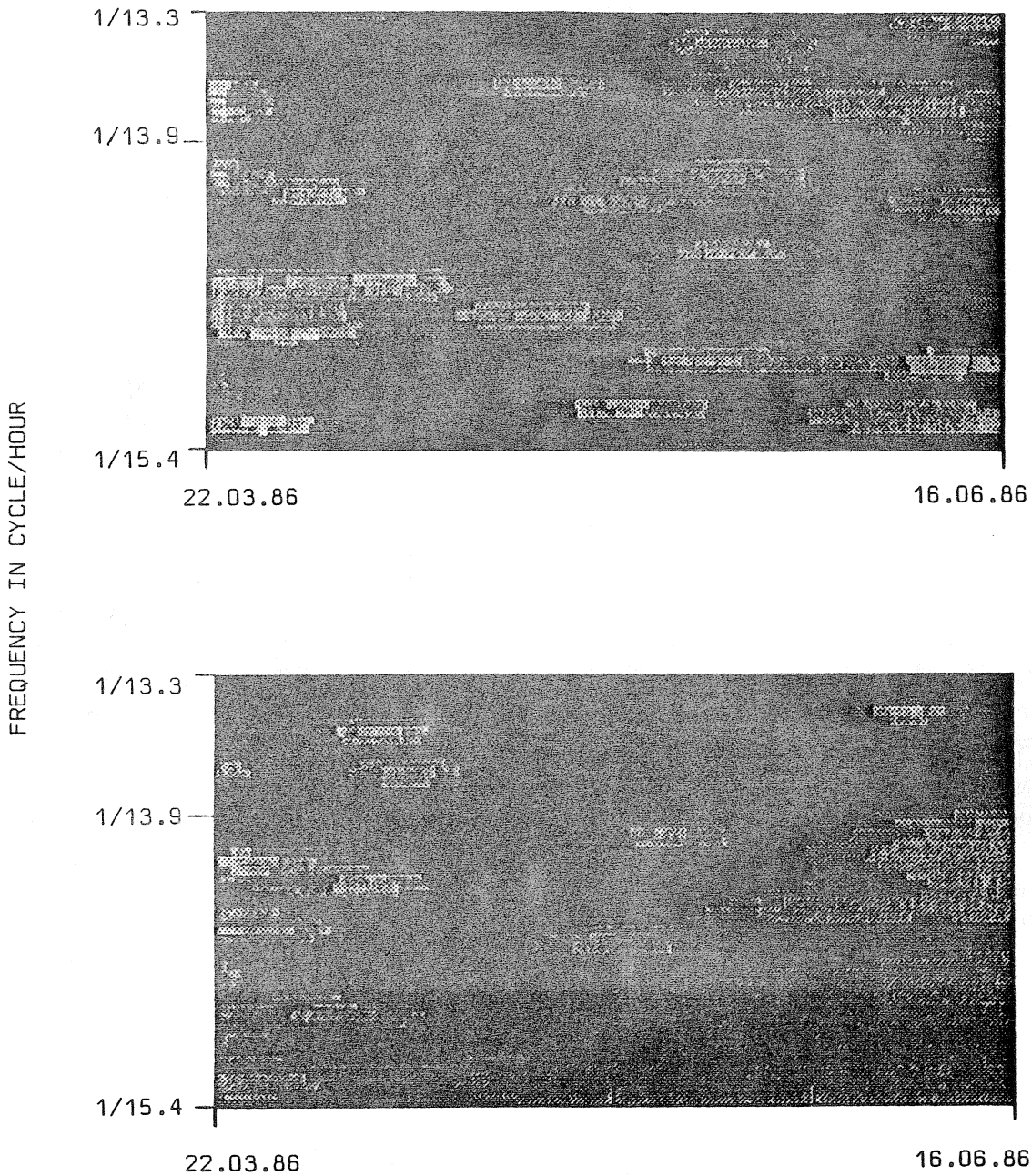

Figure 18: Modulus of the WT, between the diurnal and semi-diurnal frequency bands, of (a) the superconducting gravimeter data, and (b) the ocean tide in Ostend.

Gravity Noise Levels from a 2 Year Comparison of Two Superconducting Gravimeter Data.

J. Hinderer
Institut de Physique du Globe
rue Descartes, 5
67084 Strasbourg
France

D. Crossley, Xu Hui
Department of Earth and Planetary Sciences
McGill University
3450 University Street
Montreal H3A2A7
Canada

Abstract.

We show here a comparison of gravity records provided by two geographically well separated superconducting gravimeters over a common 2 year observing period. The data sets are processed for the first time following exactly the same numerical steps. We first perform a classical least squares fit of unfiltered data to tides taking into account a single coefficient for the effect of the local barometric pressure fluctuations and a second order polynomial approximation for the instrumental drift. The results show a totally different drift behaviour between the two instruments. The time evolution of the resulting residual gravity signals, as well as the corresponding power spectral density, are given. In another step, we first remove low-frequency contributions from the observed gravity and pressure signals by a high-pass filtering procedure. An automatic method to detect and remove obvious spikes is used and a new least squares fit then provides new residual gravity signals. The corresponding power spectral density is shown to be reduced in all frequency bands, especially in the subtidal band. We finally provide cross spectral estimates of these two gravity residual data sets.

Introduction

Because of the high sensitivity of superconducting gravimeters (SCG) of about one *nanogal* (one part in 10^{12} of the mean Earth's surface gravity), there were several studies investigating the content of SCG records for the search of small geophysical signals originating in the Earth's core (e.g. Melchior and Ducarme 1986; Zürn et al. 1987; Mansinha et al. 1990; Florsch et al. 1991; Smylie et al. 1992). However, the clear identification of some detected peaks is still very controversial for a number of reasons (e.g. local effects, influence of data processing, agreement with theory). These studies were conducted either on individual stations or on different European stations (stacking method). Additionally, the raw gravity signals were often processed in significantly different ways. In this study, we compare the records of two geographically well-separated stations which are identically processed. Our primary aim is to compare the residual gravity noise levels according to different processing methods. The gravity records are provided by the French and Canadian superconducting gravimeters over a common observing period of 2 years (14 December 1989 - 13 December 1991). The two meters are located at comparable latitudes (48.62 ° N and 45.58 ° N for the French station (J9) near Strasbourg and the Canadian station (CSGI) at Cantley, Quebec, respectively), although the difference in longitude reaches more than 80 degrees (7.68 ° E

and 75.80 ° W respectively). Moreover, to make the comparison even more meaningful, we process the two data sets by following exactly the same numerical steps starting from the original 2 *sec* sampling rate of the digitized gravity signal. Different data analysis procedures are investigated and the resulting gravity residual noise levels shown.

Pre-processing of raw gravity data

The original digitizing rate of the gravity feedback voltage (which keeps the superconducting levitating sphere in the same position) is 1 value every 2 *sec* for the Strasbourg instrument and 1 value every *sec* for the Cantley meter. The signal is first decimated to 1 point every 5 *min* by applying to the 2 *sec* data a numerical low-pass symmetric filter running over 20 *min* designed in Strasbourg by R. Lecolazet. We pre-process the 5 *min* gravity signal in order to remove the major disturbances of instrumental origin (helium transfer, instrumental maintenance), due to data acquisition problems or caused by earthquakes. In a very traditional way, we have edited our 5 *min* raw gravity samples by locating by eye these disturbances and filling the related gaps with a local synthetic tide using a set of known (from a previous tidal fit at each station) gravimetric amplitude and phase factors for the major tidal groups. A new decimation with a second low-pass filter running over 24 *h* and having a cut-off period of 3 *h* is then performed which provides hourly samples of gravity and local pressure. Both gravimeters have been calibrated against absolute gravity meters and the expected calibration accuracy is of the order of 1 % (Hinderer et al. 1991; Bower et al. 1991).

The time evolution of the raw gravity is shown in Fig. 1 (the reference levels are arbitrary). The tidal gravity changes reach about 200 μgal and show the multiple long-period (e.g. fortnightly and semi-annual) modulation of the major semi-diurnal and diurnal tides; an intrumental drift, fairly large for the Canadian station, superimposes onto the tides. We have also computed the power spectral densities (PSD) (in μgal^2 per cycle/hour (*cph*)) of the gravity signals; they are shown on a logarithmic scale in Fig. 2. The PSD are smoothed periodograms. We applied a cosine bell data taper (with a length ratio of 1/10 with respect to the total length of the data, meaning that 90 per cent of the data are undisturbed) to the signals which are then padded and Fourier transformed. In order to reduce the scatter and hence achieve an acceptable level of statistical stability, the spectra are also further smoothed by a simple running average of 11 frequency samples (the same amount of smoothing will be used in all the spectra shown hereafter). Basically, to retrieve the total power of the signal, one has simply to integrate the PSD over the entire frequency band (from 0 to 0.5 *cph*) and multiply by a factor 2 (because of the symmetric PSD for negative frequencies). However, there is slight attenuation because of the taper windowing effect and, from calibrating synthetic data, we found that the power estimates have to be multiplied by a correcting factor of 1.066. We clearly see tidal harmonic lines (long-period, diurnal, semi-diurnal and terdiurnal) emerging from a power law decrease in the gravity signal as a function of the frequency f; of course, the rapid attenuation starting at 0.3 *cph* is caused by the decimation filter. The non-tidal signal might be seen as a combination of instrumental drift and disturbances, atmospheric loading, and other physical signals such as

hydrogeological changes, which are predominantly low-frequency.

Least squares fit of unfiltered data

We have performed for each station a traditional tidal fitting procedure of the raw gravity signal with respect to a theoretical tidal potential, introducing a low-order polynomial for the drift behaviour and taking into account the local pressure as an additional channel. We used a standard tidal package called HYCON (hybrid least squares frequency domain convolution) (Schüller 1986) based on the CTE tidal development (Cartwright and Tayler 1971; Cartwright and Edden 1973) with 505 waves and introduced a parabolic function for the drift, as well as a single coefficient for the atmospheric pressure admittance. In this comparative study where we concentrate on gravity residuals outside the tidal bands, we accept the limitations of the CTE potential and do not further investigate the use of more precise tidal potentials (e.g. Tamura 1987; Xi Qinwen 1987). The gravity residual signal is the result of subtracting from the raw gravity the HYCON fit of tides, drift and local pressure correction. Assuming linearity, the effect of a better tidal potential on the residuals should have a minimal effect outside the tidal bands, but will improve the determination of the gravimetric amplitude and phase factors of tidal wave groups (Wenzel and Zürn 1990).

As expected, the CSGI drift term is well represented by a large linear drift towards negative gravity values; on the other hand, the drift component in J9 is much smaller and leads to increase gravity with time. There is hence a completely different instrumental drift behaviour, the peculiar characteristics of the superconducting components used in the Canadian meter being probably the main cause. The time evolution of the gravity residuals is plotted in Fig. 3. It is worth noting that, because an annual tidal wave of gravitational origin (S_a) was included in the tidal potential used in HYCON, any geophysical signal of annual period has been removed by the fitting procedure. The gravity residuals have zero mean and a range of a few μgal. The CSGI residual gravity standard deviation (SD) is approximately 0.6 the J9 SD. This result demonstrates that the removal of a well-defined instrumental drift is not a major obstacle in reaching low amplitude gravity residuals.

The PSD of the gravity residuals (same smoothing as before) are shown in Fig. 4 and 5, for Strasbourg and Cantley respectively; frequencies higher than 0.3 *cph*, which are attenuated by the decimation filter, are omitted. The 95% confidence intervals, which are parallel transportable on a logarithmic scale, are given. Each PSD estimate is χ^2_n distributed, where n is the equivalent degree of freedom. The smoothing method provides 2979 independent PSD estimates from 17520 real-valued time samples and leads to 5.9 equivalent degrees of freedom for each spectral estimate. The appropriate percentiles of the corresponding cumulative distribution were found from synthetic data calibration and lead to the values 0.20M and 2.36M for the 95% confidence interval, where M is the mean PSD. Most of the tidal energy has now disappeared and there is still a decrease of the residual signal with frequency (power law type) in both stations, the low-frequency power dominating the rest. As a reference for further comparison, we have quoted on both figures the mean PSD level in the subtidal band ranging from 0.17 to 0.3 *cph* (roughly 6 to 3 hours in period) where geophysical signals originating from the core might be present (e.g. Crossley et al. 1992;

Smylie 1992).

Least squares fit of high-passed and despiked data

We investigate now the content of the gravity signal for periods shorter than one day by first removing the low frequencies in the hourly data. Such an approach was previously used by Florsch et al. (1991) to investigate non-tidal periodicities in the Strasbourg SCG record. The high-pass filter used is more than 2 weeks long and has a cut-off period of 3 days. One of the motivations to first high-pass (HP) the 1 hour gravity (and pressure) before the fitting procedure is to reduce the effect of various low-frequency contributions which cannot be well accounted for like the global atmospheric loading (Merriam 1992). Besides, the long-term drift will also be strongly attenuated by the HP filter.

The remaining spikes in the HP gravity residuals, either man-made (instrumental maintenance, helium transfer) or caused by earthquakes, are removed by an automatic despiking procedure that has a threshold level of 3 times the SD of the residuals (respectively 0.5 μgal for CSGI and 0.7 μgal for J9), as given by the histograms of the HP residuals. The correcting (despiking) function is shown in Fig. (6a) and (6c) for J9 and CSGI respectively. This signal is then subtracted from the HP hourly gravity signal prior to a new HYCON fit. Fig. (6b) and (6d) show the HP gravity residuals for J9 and CSGI respectively obtained from this new fit.

Our final pair of PSD is shown in Fig. 7. The HP filter clearly reduces long-period power and, as previously, we omit the high frequencies ($\geq$ 0.3 *cph*) because of the decimation filter. Again the gravity noise level is slightly lower for the Canadian station compared to the French one. The mean PSD levels in the subtidal band (0.17 - 0.30 *cph*) are smaller than for unfiltered gravity signals (cf. Fig. 4 and 5).

We have finally performed a cross spectral analysis of these two residual records and computed the resulting cross PSD estimates (defined as the magnitude of the product of the 2 complex Fourier transforms relative to each individual record). As expected from a stacking procedure, we found that the noise level of the unsmoothed cross PSD (not shown) is somewhere in-between the individual levels for each station shown on Fig. 7. We used the same smoothing procedure as before (11 point running average applied to the complex cross spectrum) to obtain the smoothed cross PSD shown on Fig. 8. Residual tidal lines, which are expected to be present in both records, are re-inforced by the method and emerge clearly from the ambient noise which tends to decrease because of the smoothing effect on incoherent random signals. The mean level of the smoothed PSD is then further decreased and reaches a value of about 0.98 10^{-3} μgal^2 per *cph* in the subtidal band (0.17 - 0.30 *cph*). This level appears to be substantially lower than the one derived from the product spectrum of 4 European SCG records (Smylie et al. 1992) (which we estimate to be a factor 3 higher in PSD than here). However, one has to keep in mind that these European data sets and the ones discussed here are for different time intervals and, even more importantly, were processed in different ways (disturbance corrections, spectral analysis). From synthetic data calibration, we found that a pure harmonic signal of 1 *nanogal* amplitude injected at the

same frequency in each of our records would appear at a level of 1.11 10^{-3} μgal^2 per *cph* in the cross spectrum and therefore would be marginally above the mean noise level and virtually undetectable in the subtidal band of the cross spectrum shown in Fig. 8. Remembering that the detectability limit of surface gravity effects related to core dynamics (Crossley et al. 1991; Hinderer and Crossley 1992) is indeed one *nanogal*, we see that a clear identification of such effects is a very difficult task even with good quality SCG data.

Let us finally mention that a new promising method based on slew corrections (threshold applied to residual gravity derivative rather than to gravity itself) (Jensen et al. 1992; Crossley et al. 1993) is able to further reduce the residual noise level by a significant amount (Hinderer et al. 1992).

Conclusion

We have presented for the first time a comparison of data from two well-separated superconducting gravimeters over a common observing period of 2 years. These data have been treated following exactly the same numerical procedure (decimation, filtering, least squares fit) for each station. The comparison of the raw gravity data (low frequencies included) shows that the drift behaviour of the two instruments is totally different, the Canadian station exhibiting a large almost linear drift towards negative gravity while the French station drift is much smaller towards positive gravity. The power levels found in the gravity residual signal are comparable, though the Cantley station shows a lower level in almost every frequency band compared to Strasbourg. After a high-pass filtering procedure was applied to the raw pressure and gravity signals, the power level in the residual gravity signal was found to be reduced in all bands (tidal and non-tidal) with respect to the unfiltered residual signal. To remove obvious spikes in the high-passed residuals, we applied an automatic detection procedure with a threshold equal to 3 times the standard deviation of the uncorrected gravity residual signal. We finally performed a cross spectral analysis of these two residual data sets. The smoothed cross spectrum showed a further reduction in the noise level which however appears to be still too high to allow detection of *nanogal* harmonic signals in the 2-year data sets. We finally would like to emphasize the need in the future to extend this stack to more world-wide distributed SCG stations in order to further enhance the residual gravity signal to noise ratio.

Acknowledgments. J. Hinderer would like to thank NSERC for providing an International Research Fellowship during his sabbatical at McGill University. This research has been supported by Operating and Infrastructure grants from NSERC and EMR (Canada).

References

Bower, D. R., J. Liard, D. Crossley and Bastien, R., Preliminary calibration and drift assessment of the superconducting gravimeter GWR12 through comparison with absolute

gravimeter JILA2, Proc. ECGS Workshop on 'Non-tidal gravity changes: intercomparison between absolute and superconducting gravimeters', Cahiers du Centre Européen de Géodynamique et de Séismologie, Walferdange, Luxemburg, 3, 129-142, 1991.

Cartwright, D. E. and R. J. Tayler, New computations of the tide-generating potential, *Geophys. J. R. Astr. Soc.*, *23*, 45-74, 1971.

Cartwright, D. E. and A. C. Edden, Corrected tables of tidal harmonics, *Geophys. J. R. Astr. Soc.*, *33*, 253-264, 1973.

Crossley, D. J., J. Hinderer and H. Legros, On the excitation, detection and damping of core modes, *Phys. Earth Planet. Int.*, *68*, 97-116, 1991.

Crossley, D. J., M. Rochester and Z. Peng, Slichter modes and Love numbers, *Geophys. Res. Lett.*, *19*, 1679-1682, 1992.

Crossley, D. J., Hinderer, J., Jensen, O., and Xu, H., A slewrate detection criterion applied to superconducting gravimeter data processing, *Bull. Inf. Marées Terrestres*, this issue, 1993.

Florsch, N., J. Hinderer, D. Crossley, H. Legros and B. Valette, Preliminary spectral analysis of the residual signal of a superconducting gravimeter for periods shorter than one day, *Phys. Earth Planet. Int.*, *68*, 85-96, 1991.

Hinderer, J. and D. Crossley, Core Dynamics and surface gravity changes, in Dynamics of the Earth's Deep Interior and Earth Rotation, Geophys. Monograph Ser., AGU, 1992, in press.

Hinderer, J. Florsch, N., Mäkinen, J., Legros, H. and Faller, J.E., On the calibration of a superconducting gravimeter using absolute gravity measurements, *Geophys. J. Int.*, *106*, 491-497, 1991.

Hinderer, J., Crossley, D. and Xu, H., Gravity noise levels and periodic signals inferred from a common 2 year analysis of the French and Canadian superconducting gravimeters, *Eos, 73*, no. 43, 60, 1992 (abstract).

Jensen, O., Crossley, D. and Hinderer, J., Simple data decomposition reveals a surprisingly rich harmonic spectrum in superconducting gravimeter data, *Eos, 73*, no. 43, 60, 1992 (abstract).

Mansinha, L., D. Smylie and B. Sutherland, Earthquakes and the spectrum of the Brussels superconducting gravimeter data for 1982-1986, *Phys. Earth Planet. Int.*, *61*, 141-148, 1990.

Melchior, P. and B. Ducarme, Detection of inertial gravity oscillations in the Earth's core with a superconducting gravimeter at Brussels, *Phys. Earth Planet. Int.*, *42*, 129-134, 1986.

Merriam, J. B., Atmospheric pressure and gravity, *Geophys. J. Int.*, *109*, 488-500, 1992.

Schüller, K., Simultaneous tidal and multi-channel input analysis as implemented in the HYCON-method, in *Proc. 10th Int. Symp. on Earth Tides*, edited by Vierra, R., 515-520, Cons. Sup. Inv. Cient., Madrid, 1986.

Smylie, D. E., The inner core translational triplet and the density near Earth's center, *Science*, *255*, 1678-1682, 1992.

Smylie, D. E., J. Hinderer, B. Richter, B. Ducarme and L. Mansinha, A comparative analysis of superconducting gravimeter data, in Dynamics of the Earth's Deep Interior and Earth Rotation, Geophys. Monograph Ser., AGU, 1992, in press.

Tamura, Y., An harmonic development of the tide generating potential, *Bull. Inf . Marées Terrestres*, *99*, 6813-6855, 1987.

Wenzel, H. G. and W. Zürn, Errors of the Cartwright-Tayler-Edden 1973 tidal potential displayed by gravimetric Earth tide observations at BFO Schiltach, *Bull. Inf. Marées Terrestres*, *107*, 755-7574, 1990.

Xi Qinwen, A new complete development of the tide generating potential for the epoch J 2000.0, *Bull. Inf. Marées Terrestres, , 99*, 6786-6812, 1987.

Zürn, W., B. Richter, P. Rydelek and J. Neuberg, Comments on Detection of inertial gravity oscillations in the Earth's core with a superconducting gravimeter at Brussels, *Phys. Earth Planet. Int.*, *49*, 176-178, 1987.

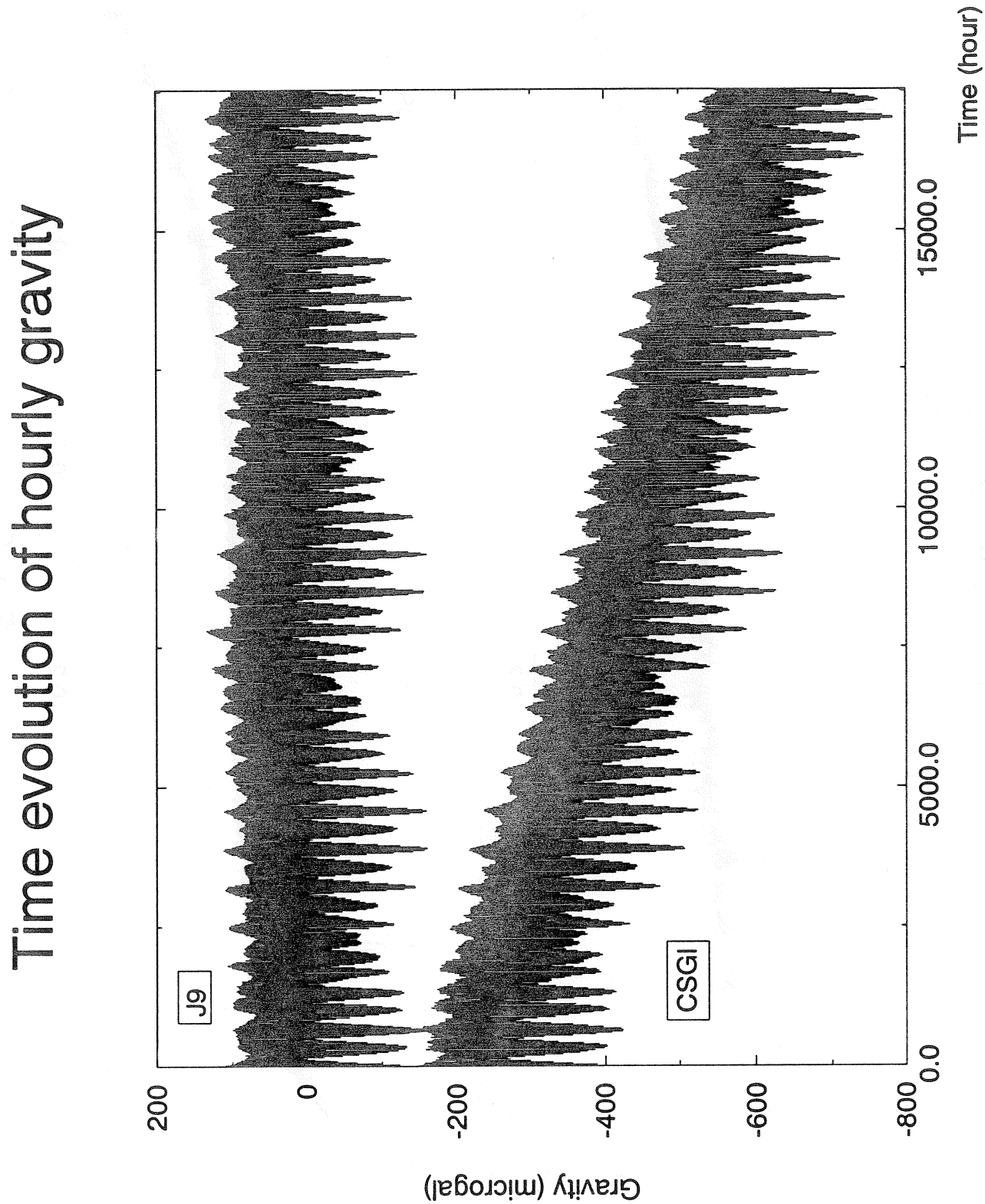
Time evolution of hourly gravity
J9
CSGI
200
0
-200
-400
-600
-800
0.0
5000.0
10000.0
15000.0
Gravity (microgal)
Time (hour)

Fig. 1

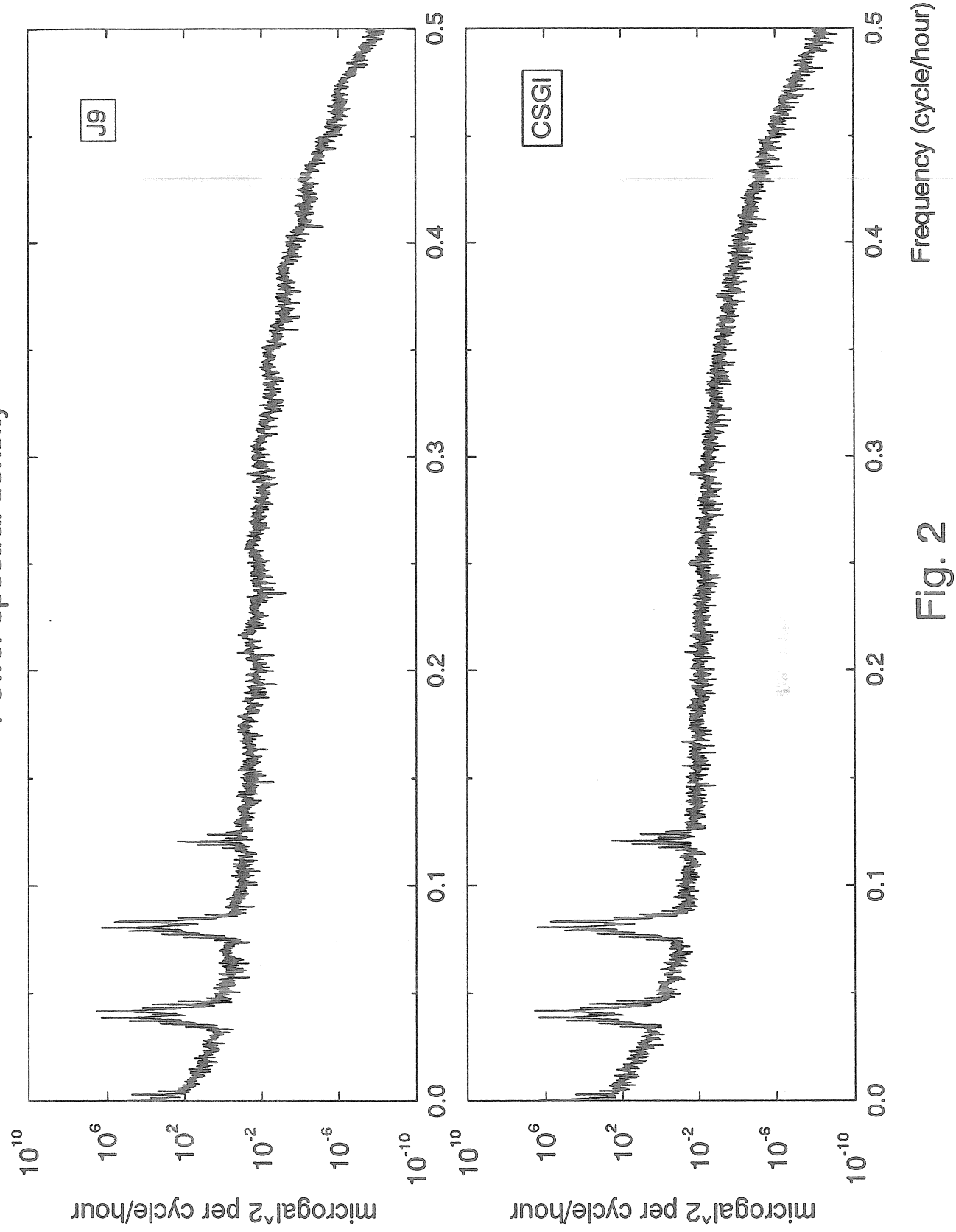
Hourly gravity
Power spectral density
J9
CSGI
microgal^2 per cycle/hour
microgal^2 per cycle/hour
Frequency (cycle/hour)
10^10
10^6
10^2
10^-2
10^-6
10^-10
0.0
0.1
0.2
0.3
0.4
0.5

Fig. 2

Time evolution of unfiltered gravity residuals

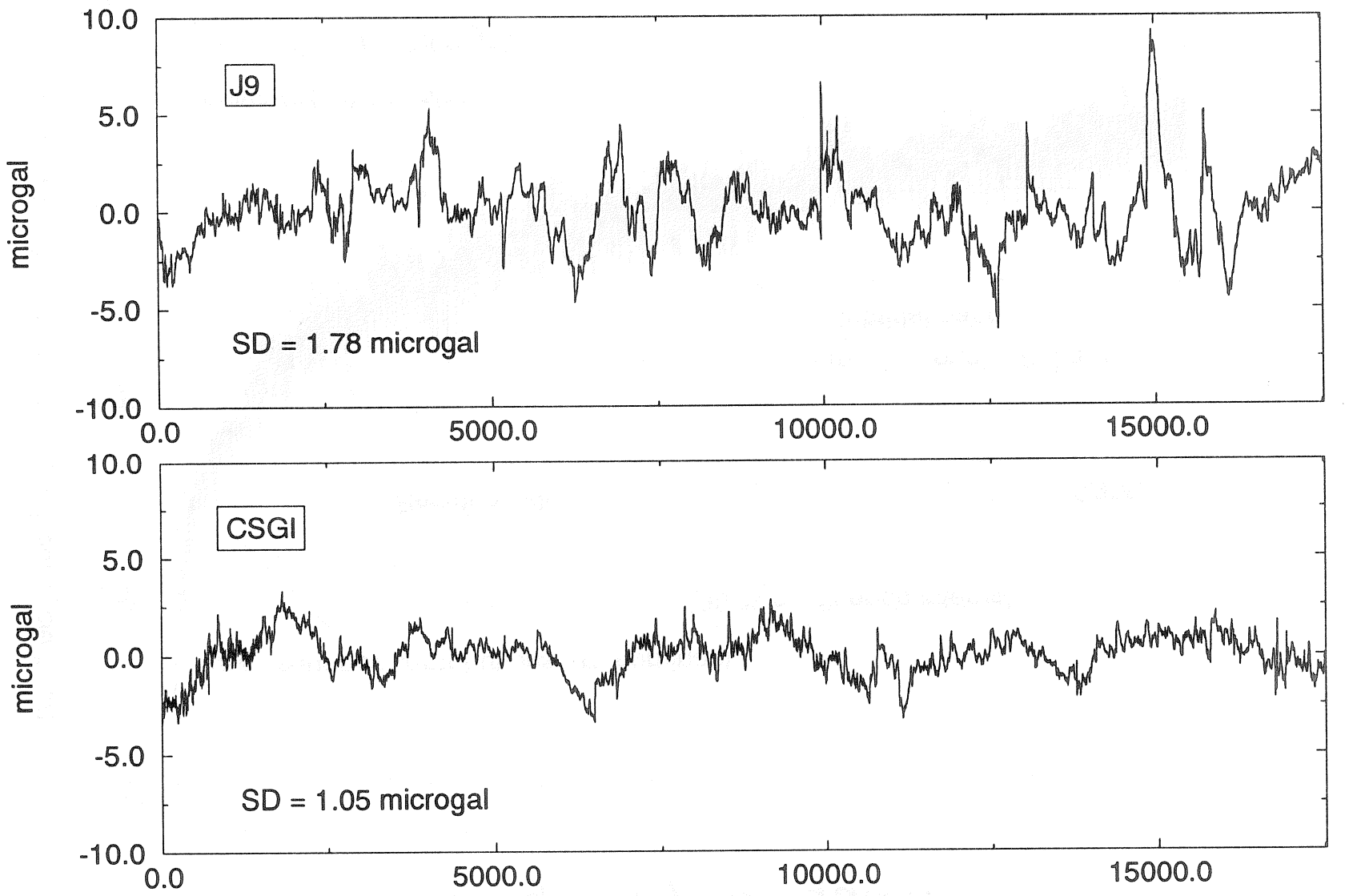

Fig. 3

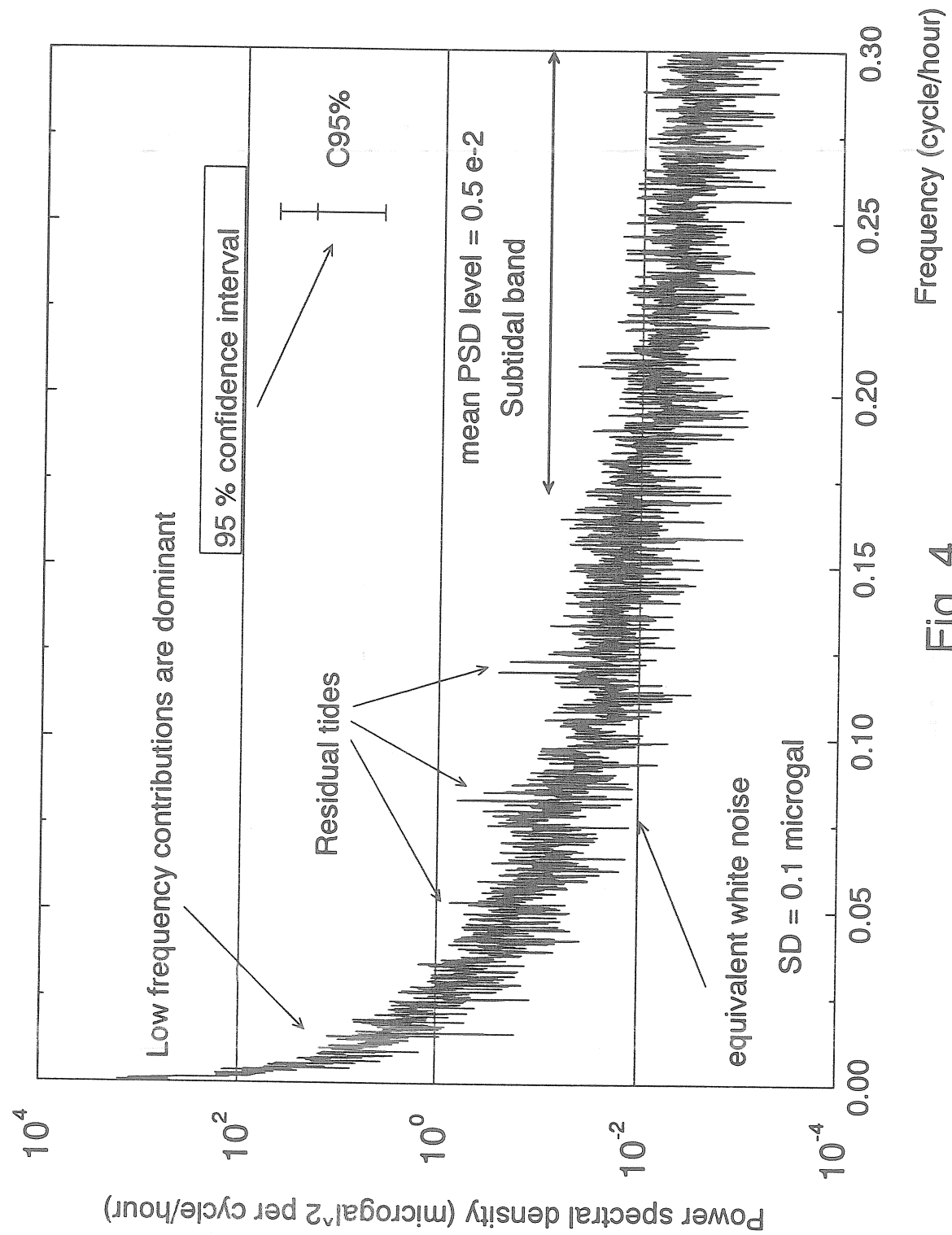
J9 gravity residuals
Low frequency contributions are dominant
95 % confidence interval
C95%
Residual tides
mean PSD level = 0.5 e-2
Subtidal band
equivalent white noise
SD = 0.1 microgal
Power spectral density (microgal^2 per cycle/hour)
Frequency (cycle/hour)
10^4
10^2
10^0
10^-2
10^-4
0.00
0.05
0.10
0.15
0.20
0.25
0.30

Fig. 4

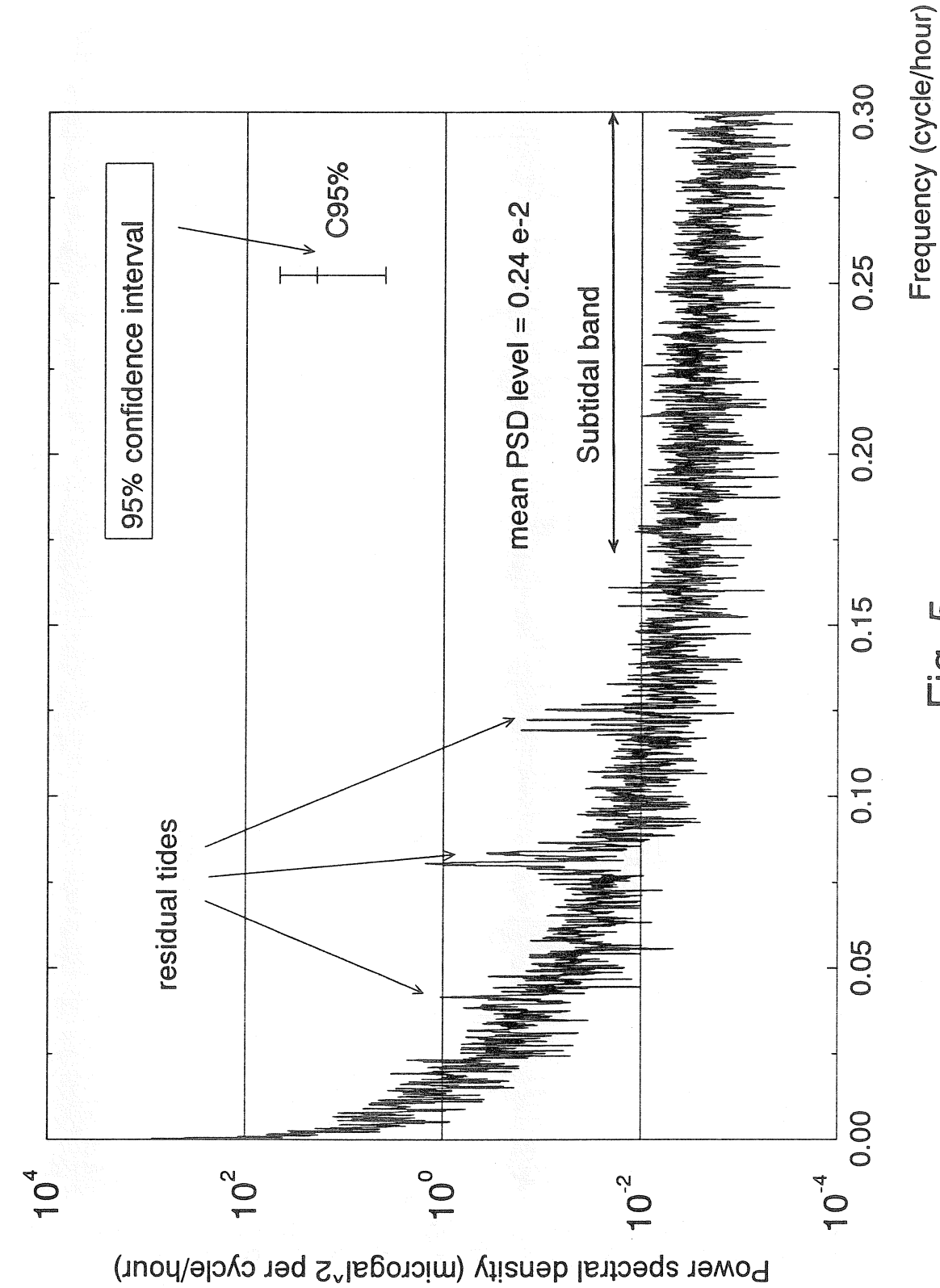
CSGI gravity residuals
95% confidence interval
C95%
residual tides
mean PSD level = 0.24 e-2
Subtidal band
Power spectral density (microgal^2 per cycle/hour)
Frequency (cycle/hour)
10^4
10^2
10^0
10^-2
10^-4
0.00
0.05
0.10
0.15
0.20
0.25
0.30

Fig. 5

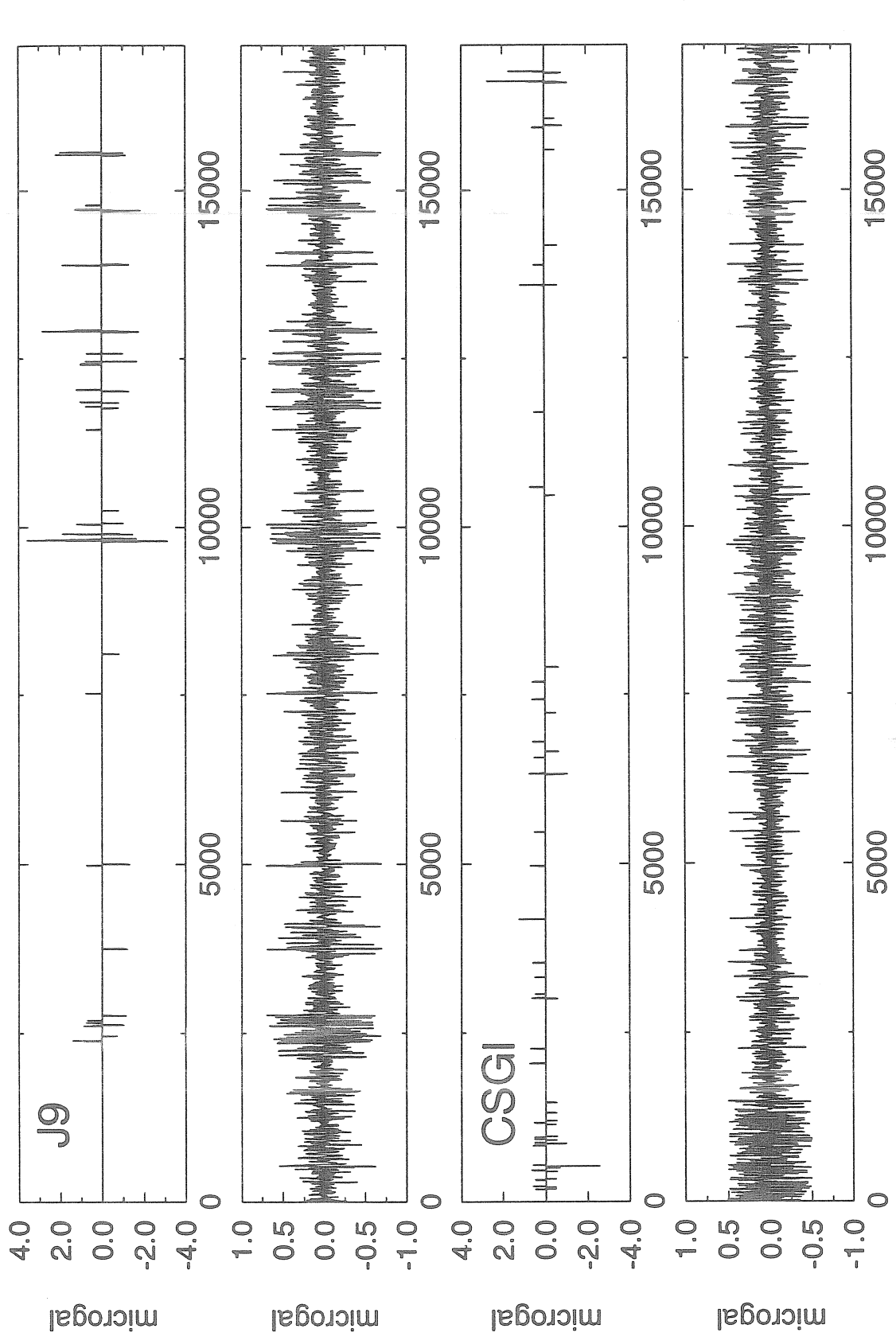
Despiking high-passed gravity residuals
a
b
c
d
J9
CSGI
microgal
4.0
2.0
0.0
-2.0
-4.0
1.0
0.5
-0.5
-1.0
0
5000
10000
15000
Time (hour)

Fig. 6

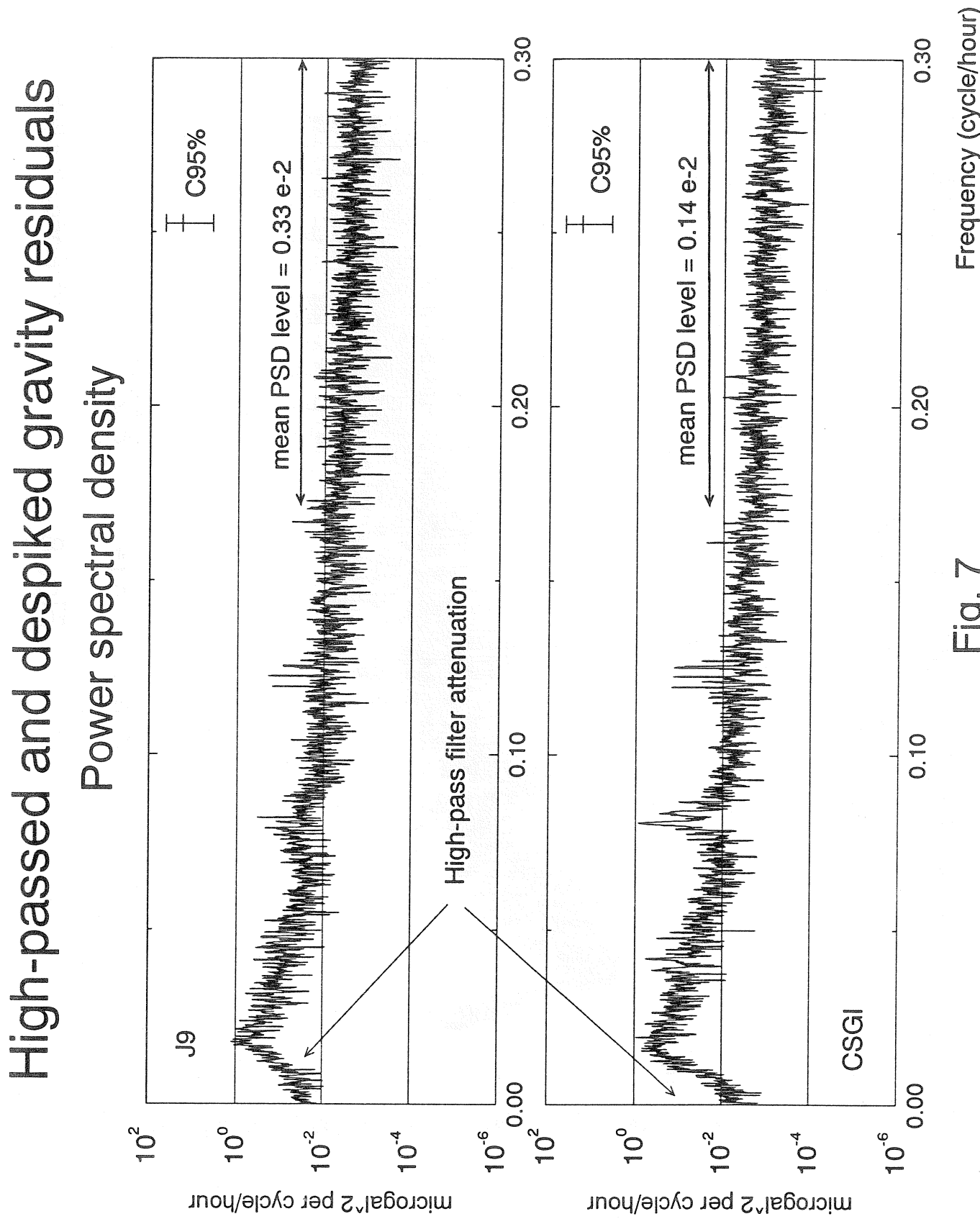
High-passed and despiked gravity residuals
Power spectral density
J9
C95%
mean PSD level = 0.33 e-2
High-pass filter attenuation
CSGI
C95%
mean PSD level = 0.14 e-2
microgal^2 per cycle/hour
microgal^2 per cycle/hour
Frequency (cycle/hour)
0.00
0.10
0.20
0.30

Fig. 7

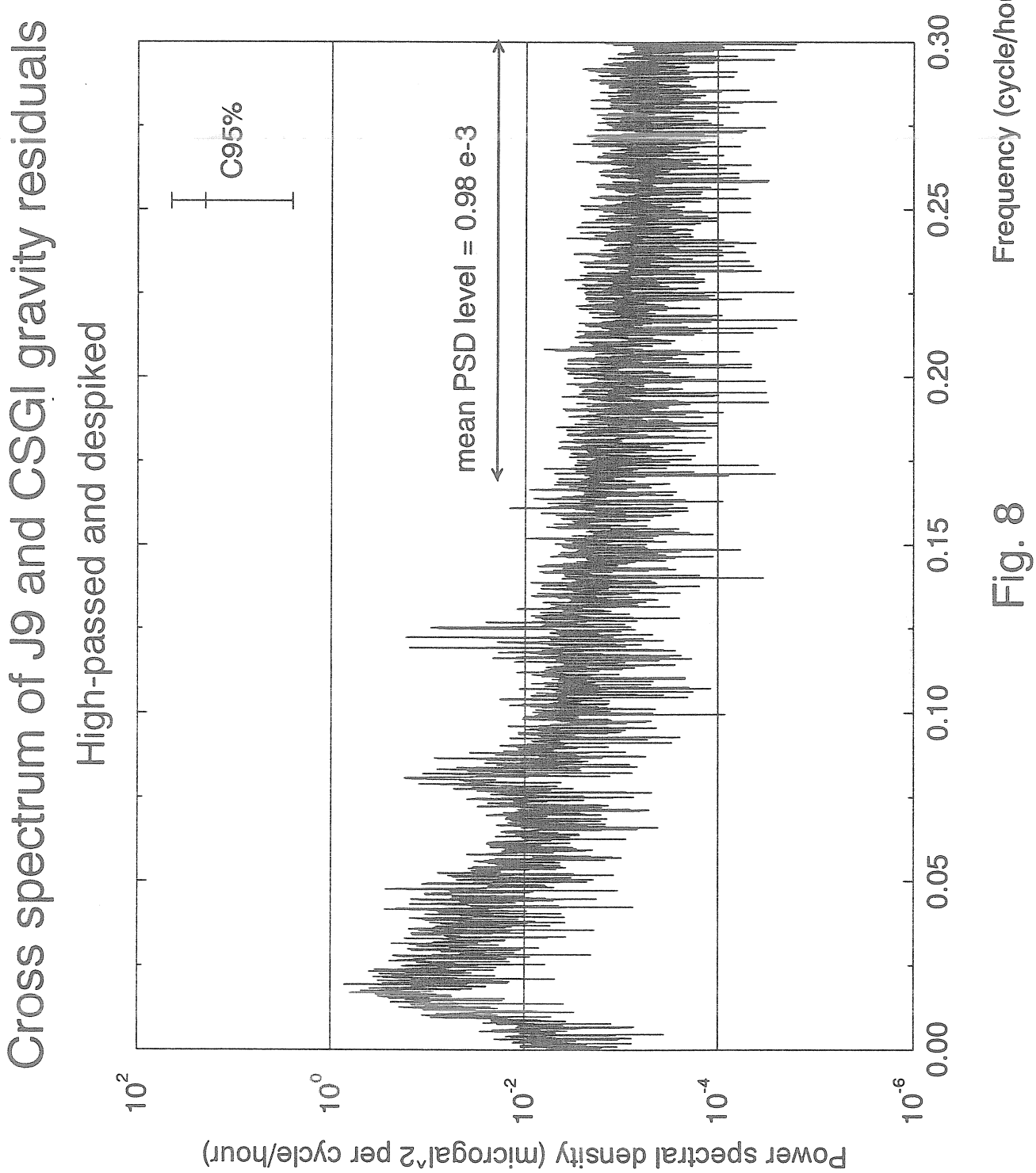
Cross spectrum of J9 and CSGI gravity residuals
High-passed and despiked
C95%
mean PSD level = 0.98 e-3
Power spectral density (microgal^2 per cycle/hour)
Frequency (cycle/hour)
10^2
10^0
10^-2
10^-4
10^-6
0.00
0.05
0.10
0.15
0.20
0.25
0.30

Fig. 8